NASA TECHNICAL NOTE

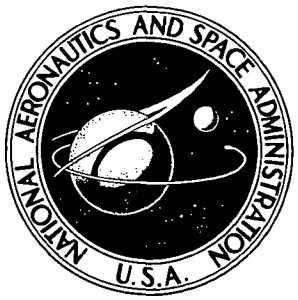

NASA TN D-7193

NASA TN D-7193

APPLICATION OF PHASE-CHANGE TECHNIQUE TO THIN SECTIONS WITH HEATING ON BOTH SURFACES

by James L. Hunt, Joan I. Pitts, and Christine B. Richie

Langley Research Center
Hampton, Va. 23665

NATIONAL AERONAUTICS AND SPACE ADMINISTRATION • WASHINGTON, D. C. • AUGUST 1973

1. Report No.	2. Government Accession No.	3. Recipient's Catalog No.
NASA TN D-7193		

4. Title and Subtitle	5. Report Date
APPLICATION OF PHASE-CHANGE TECHNIQUE TO THIN SECTIONS WITH HEATING ON BOTH SURFACES	August 1973
	6. Performing Organization Code
7. Author(s)	8. Performing Organization Report No.
James L. Hunt, Joan I. Pitts, and Christine B. Richie	L-7774
	10. Work Unit No.
9. Performing Organization Name and Address	502-37-01-10
NASA Langley Research Center Hampton, Va. 23665	11. Contract or Grant No.
	13. Type of Report and Period Covered
12. Sponsoring Agency Name and Address	Technical Note
National Aeronautics and Space Administration Washington, D.C. 20546	14. Sponsoring Agency Code

15. Supplementary Notes

16. Abstract

A numerical digital computer program has been developed to calculate the heat-transfer coefficients for both sides of a one-dimensional finite slab subject to the boundary conditions ascribed to the phase-change coating heat-transfer technique. In a typical tunnel test situation where a thin wing was exposed to heating on both sides, the data reduction procedures for a semi-infinite slab gave heat-transfer coefficients as much as 375 percent too high on the side with the lowest heating. The results from the one-dimensional finite-slab procedure are presented in the form of correction factors to the solution for a semi-infinite slab in terms of parameters normally used with the phase-change heat-transfer technique. These correlations are not restricted to slab thickness or thermophysical properties and are easily used to obtain accurate data on thin model sections.

17. Key Words (Suggested by Author(s))	18. Distribution Statement
Phase-change technique Finite slab Thin sections One dimensional Heating on both surfaces	Unclassified – Unlimited

19. Security Classif. (of this report)	20. Security Classif. (of this page)	21. No. of Pages	22. Price*
Unclassified	Unclassified	68	$3.00

*For sale by the National Technical Information Service, Springfield, Virginia 22151

APPLICATION OF PHASE-CHANGE TECHNIQUE TO THIN SECTIONS WITH HEATING ON BOTH SURFACES

By James L. Hunt, Joan I. Pitts, and Christine B. Richie
Langley Research Center

SUMMARY

A numerical digital computer program has been developed to calculate the heat-transfer coefficients for both sides of a one-dimensional finite slab subject to the boundary conditions ascribed to the phase-change coating heat-transfer technique. In a typical tunnel test situation where a thin wing was exposed to heating on both sides, the data reduction procedures for a semi-infinite slab gave heat-transfer coefficients as much as 375 percent too high on the side with the lowest heating. The results from the one-dimensional finite-slab procedure are presented in the form of correction factors to the solution for a semi-infinite slab in terms of parameters normally used with the phase-change heat-transfer technique. These correlations are not restricted to slab thickness or thermophysical properties and are easily used to obtain accurate data on thin model sections.

INTRODUCTION

Existing solutions (ref. 1) for obtaining quantitative heat-transfer data from the phase-change coating technique are restricted by the assumption of a one-dimensional semi-infinite slab. In practice this assumption requires that the depth of heat penetration into the model be small compared with the wall thickness. The depth of heat penetration has been shown to depend primarily upon the thermal properties of the model material and the test time. A simple empirical equation given in reference 1 as

$$t_{d,l} \approx \frac{0.2l^2}{\alpha} \tag{1}$$

where l is the thickness of the slab and α the thermal diffusivity, determines the maximum test time for which the assumption of a semi-infinite slab can be applied with negligible error. However, models of many configurations tested in hypersonic wind tunnels have very thin wings and tails so that practical test times exceed the allowable time given by equation (1). In addition, for many tests, heat enters at both surfaces of such thin wings. At the present time no solutions are available for determining the

magnitude of the errors incurred when the semi-infinite-slab assumption is violated. Therefore, a computer program was developed to calculate the heat-transfer coefficients for both sides of a one-dimensional finite slab subject to the boundary conditions ascribed to the phase-change coating technique (ref. 1). The results are presented in the form of correction factors to solutions for a semi-infinite slab in terms of parameters normally used with the technique. These correction factors are not restricted to slab thickness or thermophysical properties and can be easily used to obtain accurate data on thin model sections.

SYMBOLS

A	area
c	specific heat
h	aerodynamic heat-transfer coefficient
h_s	heat-transfer coefficient to stagnation point of reference sphere
k	thermal conductivity
l	thickness of slab, $\sum_{j=1}^{N} w_j$
M	free-stream Mach number
N	number of blocks upon which heat balance is performed
N_{Nu}	finite-slab heat-transfer parameter (Nusselt number), $\frac{lh}{k}$
$\dot{Q}$	heating rate
$\dot{q}$	heating rate per unit area
R	free-stream Reynolds number
T	temperature
$\bar{T}$	temperature parameter, $\frac{T_{pc} - T_i}{T_{aw} - T_i}$

t	time
$t_{d,l}$	thermal-interference diffusion time for thickness of slab
$t_{d,l/2}$	thermal-interference diffusion time for one-half thickness of slab
Δt	delta time or computing interval
V	volume of block
w	thickness of block
x,y	coordinates
Y	chord length
α	thermal diffusivity, $\frac{k}{\rho c}$
β	heat-transfer parameter for semi-infinite slab, $\frac{h\sqrt{\alpha t}}{k}$
ϵ	emissivity
θ	angle of attack
ρ	density
σ	Stefan-Boltzmann constant
ψ	time parameter for finite slab, $\frac{\alpha t}{l^2}$

Subscripts:

aw	adiabatic or recovery conditions
BG	background
c	convection surface
i	initial conditions

j	variable integer (either 1 or 2) which refers to surface of slab at which heat is entering
m	variable integer which refers to block upon which heat balance is being performed
n	variable integer which refers to any other block that affects heat balance for block m
pc	phase change
sis	semi-infinite slab
w	wall
1	front side of finite slab
2	back side of finite slab

A prime indicates the value in the previous time step.

ANALYTICAL METHOD FOR FINITE SLAB

A computer code (appendix A) which calculates the heat-transfer coefficients for both sides of a one-dimensional finite slab subject to the boundary condition ascribed to the phase-change coating was developed in the following manner. The finite slab of thickness l (fig. 1) with heat exchange at both surfaces is divided into N blocks. The block thicknesses are graduated inversely with the distribution of the temperature gradient expected in the slab. These thicknesses are given in appendix A as a percentage of the total thickness of the slab l for two values of N (20 and 30). These two thickness distributions are built into the computer code and selected according to the input value of N. A heat balance is performed on each block. In the heat-stored term, each block is assumed to be at a uniform temperature throughout its volume. In the heat-conduction term, a linear temperature variation between centers of blocks is assumed, with heat passing through an area equal to the touching surfaces.

Convection blocks (surfaces 1 and 2):

$$\dot{Q}_{convection} = \dot{q}_j A_{c,j} = h_j A_{c,j}(T_{aw,j} - T_{c,j})$$

$$\dot{Q}_{radiation} = \sigma\epsilon_j A_{c,j}\left[\left(T'_{c,j}\right)^4 - \left(T_{BG}\right)^4\right]$$

$$\dot{Q}_{stored} = \rho_m c_m V_m \frac{T_m - T'_m}{\Delta t}$$

$$\dot{Q}_{conducted} = 2k_{m,n}A_{m,n}\frac{T_m - T_n}{w_m + w_n}$$

$$\dot{Q}_{convection} - \dot{Q}_{radiation} - \dot{Q}_{stored} - \dot{Q}_{conducted} = 0$$

The surface temperatures $T_{c,j}$ are assumed to be equal to the temperature of their respective surface blocks $T_{c,m}$, which are kept extremely thin.

Conduction blocks (internal):

$$\dot{Q}_{stored} = \rho_m c_m V_m \frac{T_m - T'_m}{\Delta t}$$

$$\dot{Q}_{conducted} = 2k_{m,n}A_{m,n}\frac{T_m - T_n}{w_m + w_n}$$

$$\dot{Q}_{conducted\text{-}in} - \dot{Q}_{stored} - \dot{Q}_{conducted\text{-}out} = 0$$

The resulting system of linear equations is solved simultaneously at each successive time step with a subroutine (ref. 2) which solves the matrix equation $AZ = B$ (Z denotes the unknown variables taken as temperatures of blocks here, A denotes a square coefficient matrix, and B denotes a vector of constants). The values of specific heat and thermal conductivity are updated at the new temperatures obtained for each block after each time step. This heat-balance procedure is implicit and is therefore not bound by a stability criterion. The resulting computer program was checked against exact solutions of finite-slab problems (ref. 3) to determine the effect of the number of blocks, the distribution of the thickness of the blocks, and the computational time interval (Δt) on the accuracy of the solution for various heating rates, slab thicknesses, and thermophysical properties. (See appendix A.)

As described thus far, this program calculates the temperature-time profile in each block for a prescribed heat flux $\dot{q}_1 = h_1\left(T_{aw,1} - T_{c,1}\right)$ and $\dot{q}_2 = h_2\left(T_{aw,2} - T_{c,2}\right)$. This procedure is now incorporated into an iterative cycle which enables the determination of the heat-transfer coefficients h_1 and h_2. This iterative cycle includes (1) a method to approximate the heat-transfer coefficient at the two surfaces to be used as starting points in the cycle and (2) a method of searching for the actual heat-transfer

coefficients – defined here as that combination which produces surface temperature-time profiles that include the corresponding input points $(T_{pc,1}, t_{pc,1})$ and $(T_{pc,2}, t_{pc,2})$ ($T_{pc,1}$ not necessarily equal to $T_{pc,2}$ and $t_{pc,1}$ not necessarily equal to $t_{pc,2}$).

The solution to the one-dimensional heat-conduction equation for a semi-infinite slab with a step input in h is used to obtain the heat-transfer coefficient at both surfaces for the starting point in the iterative cycle. The solution is given in appendix B.

The approximation for a semi-infinite slab will always give a higher value for the heat-transfer coefficient at either surface of the finite slab than that which actually occurs, provided that heat is entering the slab at both surfaces (no negative heating rates). This is because the larger effective mass of the semi-infinite slab requires more heat input to reach a given surface temperature than does the finite slab. When the heat-transfer coefficient for the semi-infinite slab is imposed on the finite slab, the resulting surface temperature is higher than that which actually occurs on the surface of the finite slab (see sketch). As shown in the sketch, the heat-transfer coefficient is

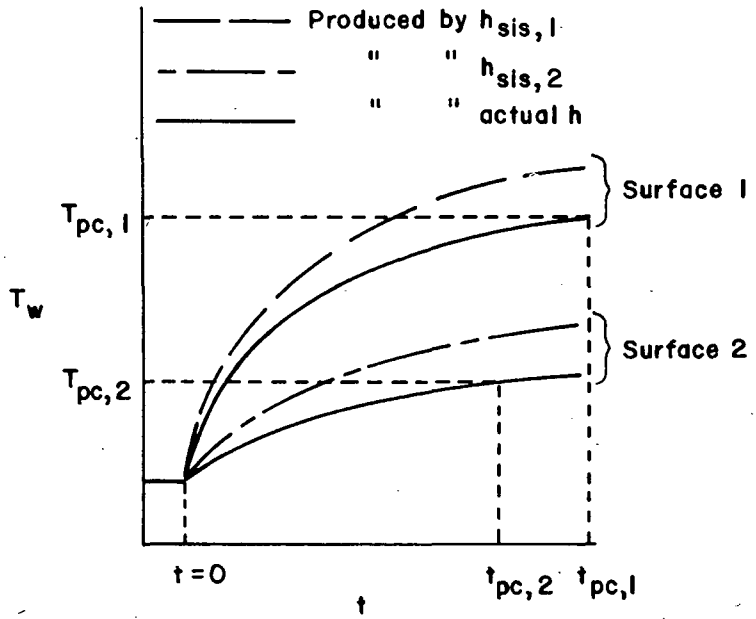

Example temperature-time profile at both surfaces of finite slab

higher for surface 1 than for surface 2. The task is to find the combination of h_1 and h_2 which corresponds to the respective set of surface temperature-time profiles (labeled "actual" in the sketch) that include the respective input points $(T_{pc,1}, t_{pc,1})$ and $(T_{pc,2}, t_{pc,2})$.

A Newton-Raphson procedure (ref. 4) is used to determine the respective amounts by which both surface heat-transfer coefficients are changed at the beginning of each successive iterative cycle in order to reach the actual set of heat-transfer coefficients for the finite slab in the fewest steps. This procedure is employed at the constant input time points $t = t_{pc,1}$ and $t = t_{pc,2}$ and proceeds until a combination of heat-transfer coefficients is found $(h_1$ and $h_2)$ that produces corresponding surface temperatures within a given ΔT of the respective input temperatures $T_{pc,1}$ and $T_{pc,2}$.

RESULTS AND DISCUSSION

Experimental Test Situation

As an example of the magnitude of errors which may occur by violating the semi-infinite-slab assumption in practical test situations, phase-change data (ref. 5) obtained in the Langley Mach 8 variable-density hypersonic tunnel (on a 0.005-scale Stycast model of a NASA Lyndon B. Johnson Space Center space shuttle launch configuration at zero degrees angle of attack) were examined. The wings of the orbiter of this configuration were very thin (midsection thickness on the order of 0.2 cm). A chordwise profile of the wing on the orbiter at 69.3 percent semispan is shown in figure 2. The time at which the phase change (339 K) occurred along the top and bottom surfaces at this span position and the thermal-interference diffusion time $\left(t_{d,l/2} = \frac{0.2(l/2)^2}{\alpha}\right)$ distribution for the center line of the wing profile are included in figure 2.

Data for the front and back surfaces of the wing were obtained from different tests at essentially the same stream Reynolds number. The stagnation pressure for both tests was 360 kN/m^2, and the stagnation temperatures were 739 K and 722 K for the front and back, respectively. Since the value of the aerodynamic heat-transfer coefficient is not a strong function of the stagnation temperature, data from different tests can be used as input conditions provided that the initial temperatures are the same. The initial temperature of the model was 300 K which with the adiabatic wall (assuming an adiabatic-to-total temperature ratio of 0.925 obtained by using a laminar recovery factor $\left(\sqrt{N_{Pr}}\right)$ and the Newtonian local condition on a flat plate) and phase-change temperatures give a $\bar{T}$ of approximately 0.1 for these tests.

The chordwise heat-transfer-coefficient distributions on the windward profile obtained by using the phase-change data reduction procedures for both the semi-infinite and finite slab (heat exchange at both surfaces) are given in figure 3. The distributions are presented in terms of the nondimensional heat-transfer-coefficient ratio h/h_s, where h_s is the theoretical heat-transfer coefficient (ref. 6, eq. (61)) for the stagnation

point of a 0.2-cm-radius sphere (a 0.3-m-radius sphere scaled by the same scale factor as the model, 0.005).

The data obtained from these two reduction procedures differ significantly in level; also, the distributions diverge for the back surface. On the front surface, the procedure for the semi-infinite slab gives heat-transfer coefficients which exceed those obtained with the procedure for the finite slab by a factor of approximately 1.25 (25 percent). For these data the time of phase change (t_{pc}) divided by the thermal-interference diffusion time for one-half the wing thickness $\left(t_{d,l/2} = \frac{0.2(l/2)^2}{\alpha}\right)$ varies from 6 to 16. On the back surface the data for the semi-infinite slab exceed the data for the finite slab by factors of 1.2 to 4.75 (20 to 375 percent). Here $t_{pc}/t_{d,l/2}$ varies from 5 to 25. However, for the same $t_{pc}/t_{d,l/2}$ variation as the front surface (6 to 16) the data for the back surface of the semi-infinite slab exceed those for the finite slab by factors of 1.23 to 2.56 (23 to 156 percent). This result indicates the influence of the time of phase change at the opposite surface and the thickness of the wing. Comparing the time of phase change and the thickness of wing distribution in figure 2 with the heat-transfer-coefficient distributions in figure 3 indicates that the difference between the results for the semi-infinite and finite slabs is much more sensitive to the differences in times of phase change at the front and back surfaces for smaller thicknesses.

The example heat-transfer-coefficient distribution on the wing illustrates the necessity of using the numerical finite-slab data reduction procedure with the phase-change heat-transfer technique on midsections of thin fins and wings. However, calculating the actual heat-transfer-coefficient distribution along a wing profile or phase-change isotherms is time consuming and expensive. Therefore, for practical engineering applications, a graphical presentation of the results from this numerical digital computer program for the finite slab with heat exchange at both surfaces which will not be restricted to a given slab thickness or set of thermophysical properties is needed.

Presentation of Solutions

Identification of independent parameters.- In order to identify the correlating parameters and to separate the influence of some of the independent variables from the influence of one convective surface on another, the simpler case for the finite slab with heat exchange at only one surface ($x = l$) is first analyzed. The closed-form solution to the differential equation for the one-dimensional flow of heat at the convective surface of this "restricted" finite slab (ref. 2) is

$$\bar{T} = 1 - \sum_{j=1}^{\infty} \frac{2N_{Nu}}{N_{Nu}(N_{Nu} + 1) + \eta_j^2} e^{-\eta_j^2 \psi} \tag{2}$$

where

$$\bar{T} = \frac{T_{pc} - T_i}{T_{aw} - T_i}$$

$$N_{Nu} = \frac{lh}{k}$$

$$\psi = \frac{\alpha t_{pc}}{l^2}$$

and η_k for $j = 1, 2, \ldots$ are the positive roots of

$$\eta \tan \eta = N_{Nu}$$

with the initial and boundary conditions of

$$T(x,0) = T_i$$

$$\frac{dT(0,t)}{dx} = 0$$

$$\frac{dT(l,t)}{dx} = \frac{h\left[T_{aw} - T(0,t)\right]}{k}$$

Equation (2) is plotted in figure 4 in terms of N_{Nu} as a function of ψ for constant values of $\bar{T}$. The range of the variables given should cover that encountered in any phase-change heat-transfer data reduction process.

In contrast to the solution for a semi-infinite slab (appendix B, eqs. (B5) and (B7)), the thermophysical properties in the "restricted" finite-slab solution (eq. (2)) are no longer coupled as $\sqrt{\rho ck}$, and time appears to the first power in the finite-slab parameter ψ, whereas the solution for a semi-infinite slab depends on $\sqrt{t}$. This is not to say that the solution for a finite slab depends linearly on t since both solutions must agree for times less than the thermal-interference diffusion time of the slab. Also, the solutions for a finite slab depend on the thickness of the slab l, whereas l does not appear in the solution for a semi-infinite slab.

In order to present the solutions for a finite slab in a manner more applicable to the phase-change heat-transfer technique, consider the independent finite-slab parameters $N_{Nu} = lh/k$ and $\psi = \alpha t_{pc}/l^2$. From equation (1), l is proportional to $\sqrt{\alpha t_{d,l}}$; therefore, N_{Nu} is proportional to $h\sqrt{t_{d,l}}/\sqrt{\rho ck}$. Comparing this parameter with the solution for a semi-infinite slab (eq. (2)) suggests a correlation parameter of the form h/h_{sis} (the heat-transfer coefficient for a surface of a finite slab divided by the

heat-transfer coefficient calculated for the same point from the solution for a semi-infinite slab). In the parameter $\psi = \alpha t_{pc}/l^2$, α/l^2 may be replaced by $0.2/t_{d,l}$ (eq. (1)); therefore, ψ is directly proportional to $t_{pc}/t_{d,l}$; thus, the parameters that define the restricted finite-slab solution are h/h_{sis}, $t_{pc}/t_{d,l}$, and $\bar{T}$.

A plot of the parameter h/h_{sis} (at surface 1) as a function of $t_{pc}/t_{d,l}$ for a finite slab with no heat exchange at surface 2 (eq. (2)) is given in figure 5 for three fixed values of $\bar{T}$. Since h_{sis} is a function of $\bar{T}$, the correction factor h/h_{sis} becomes a rather weak function of $\bar{T}$. However, for the same value of the phase-change time parameter, the correction factor decreases (below 1 – greater departure from the value for a semi-infinite slab) as $\bar{T}$ increases. Also, the ratio h/h_{sis} is unity for $t_{pc,1}/t_{d,l} \leqq 1$. This result substantiates the validity of the constant in equation (1), which was obtained by empirical means (ref. 1).

Effect of heating at both surfaces.- An example showing the effect of heat input (Nusselt number) at surface 2 on the ratio of heat-transfer coefficient for a finite slab to that for a semi-infinite slab at surface 1 is presented in figure 6. These curves were obtained from the numerical data reduction procedure for a finite slab. In figure 6 h/h_{sis} for surface 1 is plotted as a function of the time at which the phase change occurs at surface 1 nondimensionalized by the thermal-interference diffusion time of one-half the thickness of the slab $\left(t_{d,l/2}\right.$ is used because heat is entering the slab at both surfaces$\left.\right)$. Figure 6 is presented for $\bar{T}_1 = 0.348$ and $\frac{T_{aw,2} - T_i}{T_{aw,1} - T_i} = 1$ and contains lines for constant values of the Nusselt number $\left(N_{Nu} = \frac{lh}{k}\right)$ at surface 2. The influence of heat transfer at surface 2 on the heat-transfer correction factor h/h_{sis} at surface 1 is strong for $t_{pc,1}/t_{d,l/2} > 4$ and increases substantially as this parameter increases.

The effect of changing the front-surface $\bar{T}_1$ on the front-surface correction factor for a constant back-surface Nusselt number can be ascertained from figure 7. Here, the correction factors for a finite slab with a constant heat-transfer coefficient at the back surface (assuming l and k are the same for all solutions) for three values of $\bar{T}_1$ $\left(\bar{T}_1 = 0.239, 0.348, \text{and } 0.455\right)$ are shown, along with the correction factors for a finite slab with no heat exchange at the back surface for the same three values of $\bar{T}_1$. The finite-slab correction factor solutions for $N_{Nu,2} > 0$ depend on $\bar{T}_1$ in an inverse manner to that of the restricted $\left(N_{Nu,2} = 0\right)$ solutions. For no heat exchange at the back surface $\left(N_{Nu,2} = 0\right)$ and for a given phase-change time, the solutions for a finite slab move away (clockwise in fig. 7) from those of the semi-infinite slab $\left(h/h_{sis} = 1\right)$ as $\bar{T}_1$ increases. This is because the heat transfer to the front surface increases as $\bar{T}_1$ increases and the higher the heat load the greater the front-surface temperature, and thus the heat-transfer coefficient for this inverse method feels the effects of the finite

dimension of the slab. For heat exchange at the back surface (fig. 7, $N_{Nu,2} = 0.139$) and for a given phase-change time, the solution for a finite slab moves toward (counterclockwise) the solution for a semi-infinite slab ($h/h_{sis} = 1$) as $\bar{T}_1$ increases.

At first glance there seems to be a contradiction, since the $N_{Nu,2} = 0$ solutions are a limit of the solutions with heat exchange at the back surface ($N_{Nu,2} = \text{Constant}$) and figure 7 indicates that they have an opposite $\bar{T}_1$ dependence. Actually, the solutions with the heat exchange at the back surface ($N_{Nu,2} = \text{Constant}$) are moving toward the solution for a finite slab (for the same $\bar{T}_1$) with no heat exchange ($N_{Nu,2} = 0$) as $\bar{T}_1$ increases. As $\bar{T}_1$ increases, the heat-transfer coefficient at the front surface increases, while for these solutions ($N_{Nu,2} = \text{Constant}$) the heat-transfer coefficient at the back surface remains constant. Therefore, the ratio of the heat transfer at the front surface to that at the back surface for the same initial driving potential is increasing with $\bar{T}_1$ which is in the direction of the front- to back-surface heating ratio (∞) for the finite slab with no heat exchange at the back surface. Thus, as $\bar{T}_1$ increases, the two solutions ($N_{Nu,2} = 0$ and $N_{Nu,2} = \text{Constant}$) converge.

Solutions for large angles of attack.- In tunnel tests of models at large angles of attack, the flow on the leeward surface of a wing or horizontal stabilizer is separated, and the heat-transfer coefficient is less than 20 percent of that on the windward side. The approximate regions where $h_2 = h_1/5$ and $h_2 = h_1$ are shown as bands in figure 6 because of the wide spacing of the limited number of calculated points. For the condition ($h_2 \leq h_1/5$) and for the set of temperature parameters given in figure 6, the heat-transfer coefficient on the windward side is within 10 percent of the value for a semi-infinite slab for $t_{pc,1}/t_{d,l/2} \leq 9$. However, since the $h_2 = h_1/5$ band is essentially parallel to the $h_2 = 0$ ($N_{Nu,2} = 0$) solution for the finite slab with no heat exchange at surface 2, the heat-transfer coefficient ratio on the windward side of the section is within 10 percent of the $h_2 = 0$ solution for $t_{pc,1}/t_{d,l/2} \leq 20$. The similar slopes of these two lines ($h_2 = 0$ and $h_2 = h_1/5$) indicate that much larger values of $t_{pc,1}/t_{d,l/2}$ can be attained with little increase in the error band.

The question of the influence of $\bar{T}_1$ on the spread of the error band now arises. Correction factors for surface 1 of a finite slab are given in figure 8 for constant values of the Nusselt number at surface 2 as in figure 6 ($\bar{T}_1 = 0.348$) but for a $\bar{T}_1$ of 0.174. A comparison of these two plots shows the downward rotation of the constant Nusselt number lines as $\bar{T}_1$ decreases (discussed previously). However, a comparison of the $h_2 = h_1/5$ lines in the two plots indicates that these two lines are essentially independent of $\bar{T}_1$. This, along with the fact that the $h_2 = 0$ lines are a weak function of $\bar{T}_1$ (fig. 5), means that the spread in the error band (between the $h_2 = 0$ and $h_2 = h_1/5$ solutions for $t_{pc,1}/t_{d,l/2} \leq 20$) is also a weak function of $\bar{T}_1$. As an example, for

$t_{pc,1}/t_{d,\ell/2} = 20$ the error spread is approximately 10 percent for a $\bar{T}_1$ of 0.348 (fig. 6) and 15 percent for a $\bar{T}_1$ of 0.174 (fig. 8). This $\bar{T}_1$ range covers that which will occur in most wind-tunnel tests. Also, the magnitude of the initial temperature potential on the leeward surface compared with that on the windward surface $(T_{aw,2} - T_i)/(T_{aw,1} - T_i)$ will affect the error band quoted (10 to 15 percent or less) for $t_{pc,1}/t_{d,\ell/2} \leqq 20$ even though it does not enter into the $N_{Nu,2} = 0$ solutions. For values of $T_{aw,2} - T_i$ smaller than that of the windward surface (fig. 9), which is realistic for practical test situations, the lines of $N_{Nu,2}$ rotate upward toward the $N_{Nu,2} = 0$ solution, as a comparison of figures 8 and 9 shows. This comparison also shows that decreasing the initial temperature potential also rotates the $h_2 = h_1/5$ and $h_2 = h_1$ solutions upward. This upward rotation of the $h_2 = h_1/5$ line toward the $N_{Nu,2} = 0$ solution (independent of $T_{aw,2} - T_i$) decreases the error band from approximately 15 percent (fig. 8) at $t_{pc,1}/t_{d,\ell/2} = 20$ to 10 percent (fig. 9) for a $\bar{T}$ of 0.174.

Thus, the heat-transfer-coefficient distribution on the windward surface of the midsection of wings and fins at large angles of attack can be determined within 15 percent for $t_{pc,1}/t_{d,\ell/2} \leqq 20$ by using the distribution of the time of the phase change and thickness of the section in conjunction with the restricted finite-slab solution (fig. 4) for the appropriate windward surface temperature parameter. This is restrained by the provisions that $\bar{T}_1$ be greater than or equal to 0.174 and the initial temperature potential for the heating rate of the leeward surface $(T_{aw,2} - T_i)$ be less than or equal to that of the windward surface. The rate at which the error band widens as these restraints are violated has not yet been determined. However, the $\bar{T}_1$ restraint has been shown to be extremely weak, and for wind-tunnel tests the initial temperature potential for the heating rate of the leeward surface $T_{aw,2} - T_i$ is always less than that for the windward surface $T_{aw,1} - T_i$. Therefore, there is little practical need for determining the spread of the error band with an increasing violation of these two restraints.

General solutions for low angles of attack.- At low angles of attack the heat-transfer coefficients on opposite sides of a wing or fin are of the same order of magnitude. In this situation, time of phase-change distributions must be obtained on both sides of the section as given for the example wing profile in figure 2. Results of example calculations of the heat-transfer parameters for a finite slab for this more general test situation are presented in figures 10 and 11. These figures are presented for fixed values of the correlating parameter $\bar{T}$ ($\bar{T}_1$ not necessarily equal to $\bar{T}_2$) and an initial temperature potential ratio $(T_{aw,2} - T_i)/(T_{aw,1} - T_i)$ of 1. This equal initial temperature potential restraint is generally not violated or at most violated to very little extent on wings or fins at zero to low angles of attack. These correlations are not restricted to a given slab thickness or set of thermophysical properties.

Figure 10 is presented for $\bar{T}_1 = 0.45$ and $\bar{T}_2 = 0.24$. In figure 10(a), h/h_{sis} for surface 1 is plotted as a function of $t_{pc,1}/t_{d,l/2}$. This figure contains lines for various constant values of the correlating parameter that specifies the time at which the phase change occurs at surface 2 $\left(t_{pc,2}/t_{d,l/2}\right)$. In figure 10(b), h/h_{sis} for surface 2 is plotted as a function of $t_{pc,2}/t_{d,l/2}$ for various values of $t_{pc,1}/t_{d,l/2}$. Figure 10(b) can also be used to determine the heat-transfer coefficient at surface 1 if $\bar{T}_1 = 0.24$ and $\bar{T}_2 = 0.45$. Thus, these two plots (figs. 10(a) and (b)) specify the heat-transfer coefficients at surfaces 1 and 2 for $\bar{T}_1 = 0.45$ and $\bar{T}_2 = 0.24$ provided that the thermophysical properties of the slab, the thickness of the slab, and the time at which the phase change occurs on each surface are known. For example, with $\bar{T}_1 = 0.45$ and $\bar{T}_2 = 0.24$, suppose $\alpha/l^2 = 0.2$ per second, $t_{d,l/2} = 0.25$ second, and the phase change on surface 1 occurs in 4 seconds and that on surface 2 occurs in 3 seconds. Thus, $t_{pc,1}/t_{d,l/2}$ for surface 1 is 16 and $t_{pc,2}/t_{d,l/2}$ for surface 2 is 12. Entering these values into figure 10(a) gives a heat-transfer-coefficient ratio h/h_{sis} of 0.765 for surface 1. Again, $t_{pc,2}/t_{d,l/2}$ for surface 2 is 12 and $t_{pc,1}/t_{d,l/2}$ for surface 1 is 16. Entering these values into figure 10(b) gives a heat-transfer-coefficient ratio h/h_{sis} for surface 2 of 0.212. The large differences in the front- and back-surface correction factors (figs. 10(a) and (b)) are caused by the influence of the $\bar{T}$ of the opposite surface. Thus, for a complete solution of all test conditions likely to occur, a set of plots similar to those of figure 10 is needed for a range of $\bar{T}_1$ and $\bar{T}_2$ parameters.

Figure 11 is presented in the same format as figure 10 with $\bar{T}_1 = \bar{T}_2 = 0.1$. Since $\bar{T}_1$ and $\bar{T}_2$ are equal in this figure, the (a) and (b) versions as described for figure 10 are identical; therefore, only one plot for each set of values of $\bar{T}$ is needed in the correlations where the values of $\bar{T}$ are equal. For example, consider the $y/Y = 0.45$ position on the wing profile in figure 2. The temperature parameter $\bar{T}$ is approximately 0.1 for both sides, $\alpha/l^2 = 0.0863$ per second, $t_{d,l/2} = 0.579$ second, and the phase change on surface 1 (front) occurred in 4.4 seconds and that on surface 2 (back) in 6.2 seconds. Therefore, $t_{pc,1}/t_{d,l/2}$ for surface 1 is 7.6 and $t_{pc,2}/t_{d,l/2}$ for surface 2 is 10.7. Entering these values into figure 11 gives a coefficient ratio $\left(h/h_{sis}\right)_1$ of approximately 0.82. For $t_{pc,1} = 4.4$ seconds, h_{sis} is calculated from equation (B7) to be 61 W/m^2-K, and h_s is given in figure 3 as 776 W/m^2-K. This gives an h/h_s of 0.06 for the front surface, which corresponds closely to that plotted in figure 3. Again, $t_{pc,2}/t_{d,l/2}$ for surface 2 (back) is 10.7 and $t_{pc,1}/t_{d,l/2}$ is 7.6. Switching the surface designation subscripts in figure 8 and entering these values give an $\left(h/h_{sis}\right)_2$ of approximately 0.5. For $t_{pc,2} = 6.2$ seconds, $h_{sis} = 50$ W/m^2-K (eq. (2)), and h/h_s is calculated to be 0.033, which matches that given for the back surface in figure 3 at $y/Y = 0.45$.

A compilation of the results from the numerical calculations is presented in figure 12. The correction factor h/h_{sis} for a finite slab is given for a $\bar{T}_1$ and $\bar{T}_2$ combination range from 0.05 to 0.45 and for an initial temperature potential ratio $(T_{aw,2} - T_i)/(T_{aw,1} - T_i)$ of 1. This range of $\bar{T}$ should cover most test conditions likely to be encountered in phase-change heat-transfer wind-tunnel tests. Instead of giving the correction factor at surfaces 1 and 2 for a $\bar{T}$ combination as in figure 10, these plots are given in terms of only the correction factor at surface 1. The correction factor at surface 1 (h/h_{sis}) becomes larger than 1 (fig. 12) when heat is lost from surface 2. To obtain the correction factor at surface 2, one considers the plot for the reverse set of $\bar{T}$, as previously stated, and treats surface 2 as if it were surface 1 in both the abscissa and ordinate; also, the lines of constant phase-change time at surface 2 should be treated as if it were surface 1.

In using these plots, one should be aware that errors associated with small mismatches in either T_{pc} or t_{pc} increase as the thermal interference diffusion time decreases and as the difference in the time of phase change at opposite surfaces increases.

Analysis of Restraints and Variable System

In the previous section the need for determining the exact error incurred in the finite-slab correction factor correlation for a specific restraint violation was stated to be of little value. This assessment was made on the premise that the specified boundaries of the restraints are seldom violated in phase-change heat-transfer tests on thin surfaces. (See table I.) However, the limit within which a restraint must be contained in order to remain within a given error band is of interest.

TABLE I.- BOUNDARIES OF RESTRAINTS

Type of surface	Solution
Thick sections (any θ)	Semi-infinite slab
Thin sections (zero to small θ)	Finite-slab solution with heat exchange on both surfaces Figures 9 to 13 $\bar{T}$ combination range from 0.05 to 0.45 $(T_{aw,2} - T_i)/(T_{aw,1} - T_i) \approx 1$
Thin sections (moderate to large θ)	Finite-slab solution with heat exchange at only one surface Figure 4 $\bar{T} \geq 0.174$ (weak restraint) $(T_{aw,1} - T_i) \geq (T_{aw,2} - T_i)$

The heat-transfer-coefficient correction factor correlation for a finite slab with a phase change on both sides showing the change in the correction factor for a given change in the initial temperature potential ratio $(T_{aw,2} - T_i)/(T_{aw,1} - T_i)$ and $\bar{T}$ is given in figure 13. This figure was initially for $\bar{T}_1 = \bar{T}_2 = 0.45$ and $(T_{aw,2} - T_i)/(T_{aw,1} - T_i) = 1$ (case A). The initial temperature potential ratio was changed from 1 (case A) to 0.870 (case B) to 0.773 (case C) with the values of $\bar{T}$ remaining at 0.45 to illustrate the possible error in relaxing this restraint. For example, for $t_{pc,1}/t_{d,l/2} = 8$, the difference between h/h_{sis} for values of $(T_{aw,2} - T_i)/(T_{aw,1} - T_i)$ of 1 and 0.773 (using h/h_{sis} for the initial temperature potential ratio of 1 as the standard) is approximately 37 percent for $t_{pc,2}/t_{d,l/2} = 2$ and 24 percent for $t_{pc,2}/t_{d,l/2} = 4$. This type of percent deviation is shown in figure 14 as a function of initial temperature potential ratio. The percent deviation from the h/h_{sis} value for an initial temperature potential ratio of 1 decreases linearly to zero as the initial temperature potential ratio increases to 1 for constant values of the time of phase-change parameter at surfaces 1 and 2. For a given initial temperature potential ratio, the percent deviation at surface 1 increases substantially with an increase in the time-of-phase-change parameter at surface 1 and decreases substantially with an increase in the time-of-phase-change parameter at surface 2. Thus, figure 14 indicates that the unit initial temperature potential ratio restraint is rather strict in the sense that if it is violated by as much as 10 percent in certain time-of-phase-change parameter regimes $(t_{pc,1}/t_{d,l/2} < 8,\ t_{pc,2}/t_{d,l/2} < 4)$, the errors which are incurred will be extremely large. This is modified somewhat by the fact that for wings at high angles of attack in hypersonic flows the lower limit of the initial temperature potential ratio is in the vicinity of 0.87. Also, the correlation of the type given in figure 13 should be used for zero to moderate angles of attack, where the initial temperature potential ratio is near unity. For large angles of attack, the solution for a finite slab with heat exchange at only one surface (fig. 4) should be used. In this situation, the error was shown to decrease as the initial temperature ratio decreased from unity.

To assess the strength of the $\bar{T}$ restraint, the values of $\bar{T}$ were changed from 0.45 (case C) to 0.59 (case E) while the initial temperature ratio was kept at 0.773. The effect of these changes on the correction factor is shown in figure 13. There is very little difference in the lines for $\bar{T}_1 = \bar{T}_2 = 0.45$, $(T_{aw,2} - T_i)/(T_{aw,1} - T_i) = 0.773$ (case C) and the lines for $\bar{T}_1 = \bar{T}_2 = 0.59$, $(T_{aw,2} - T_i)/(T_{aw,1} - T_i) = 0.773$ (case E). This result confirms the weakness of the $\bar{T}$ restraint for the correlations at zero to moderate angles of attack.

To insure that h/h_{sis} is a function only of $\bar{T}_1$, $\bar{T}_2$, $(T_{aw,2} - T_i)/(T_{aw,1} - T_i)$, $t_{pc,1}/t_{d,l/2}$, and $t_{pc,2}/t_{d,l/2}$, calculations were made for $\bar{T}_1 = 0.45$, $\bar{T}_2 = 0.45$,

and $(T_{aw,2} - T_i)/(T_{aw,1} - T_i) = 0.773$ (case D) as in case C but with different values of $(T_{pc,1} - T_i)$, $(T_{pc,2} - T_i)$, $(T_{aw,1} - T_i)$, and $(T_{aw,2} - T_i)$. The results (identical curves for cases C and D in fig. 14) verify that the five variables mentioned completely specify the one-dimensional finite-slab system. Also, many cases which included differences in thickness and thermophysical properties were calculated. Each correlated with the $t_{pc}/t_{d,l/2}$ parameter.

CONCLUDING REMARKS

A numerical computer program has been developed to calculate the heat-transfer coefficients for both sides of a one-dimensional finite slab subject to the boundary conditions ascribed to the phase-change coating heat-transfer technique.

The data reduction procedures for a semi-infinite slab used with the phase-change coating technique can give large errors in heat-transfer coefficients on thin sections. In a typical tunnel test situation where a thin wing was exposed to heating on both sides, the data reduction procedures for a semi-infinite slab gave heat-transfer coefficients as much as 375 percent too high on the side with the lowest heating. The error at the opposite surface position, where the level of heating was approximately 5 times higher, was 29 percent.

The results from the procedure for a finite slab are presented in the form of correction factors to the solution for a semi-infinite slab in terms of parameters normally used with the phase-change heat-transfer technique. These correlations are not restricted to slab thickness or thermophysical properties and are easily used to obtain data on thin model sections.

At large angles of attack the heat-transfer-coefficient distribution on the windward surface of the midsection of a wing or fin (where lateral conduction is small) may be determined within 15 percent for nominal wind-tunnel test conditions by using the solution for a finite slab with no heat exchange on the leeward surface. This is restrained by the provisions that the finite-slab temperature parameter on the windward surface $\bar{T}_1$ be greater than or equal to 0.174 and the initial temperature potential for the heating rate of the leeward surface be less than or equal to that of the windward surface. The $\bar{T}_1$ restraint is extremely weak, and the initial temperature potential restraint is practically never violated.

Langley Research Center,
National Aeronautics and Space Administration,
Hampton, Va., May 8, 1973.

APPENDIX A

COMPUTER PROGRAM FOR FINITE SLAB

The heat-transfer computer program described in the section entitled "Analytical Method for Finite Slab" calculates the heat-transfer coefficients for both sides of a one-dimensional finite slab subject to the boundary conditions ascribed to the phase-change coating technique (ref. 1).

Program Input

FORTRAN IV NAMELIST with the name NAM1 is used to load the input data. The following list contains the input variables with the dimensions used in the program:

FORTRAN variable	Symbol	Description
TIMEØ	t_i	initial time, sec
TØ (30)	T_i	initial temperatures, ^{o}R
SIGMA	σ	Stefan-Boltzmann constant, $Btu/ft^2\text{-}sec\text{-}^{o}R^4$
EMS	ϵ	emissivity
RHØ	ρ_m	density, lbm/ft^3
NKPTS		number of entries in conductivity table (KMTAB)
TKMTAB (10)		temperature table for KMTAB, ^{o}R
KMTAB (10)	k	conductivity table, a function of temperature (TKMTAB), $Btu/ft\text{-}sec\text{-}^{o}R$
NCPTS		number of entries in specific-heat table (CPTAB)
TCPTAB (10)		temperature table for CPTAB, ^{o}R
CPTAB (10)	c	specific-heat table, a function of temperature (TCPTAB), $Btu/lbm\text{-}^{o}R$

FORTRAN variable	Symbol	Description
LEN	l	thickness of slab
NØ		number of blocks or divisions in chord length (either 20 or 30)
PRFREQ		print frequency
T1FIN	$T_{pc,1}$	phase-change temperature for surface 1, ^{o}R
TNFIN	$T_{pc,2}$	phase-change temperature for surface 2, ^{o}R
DELTAT	Δt	delta time or computing interval, sec
DELH1	Δh_1	value used to increment or decrement h_1, Btu/ft^2-sec-^{o}R
DELH2	Δh_2	value used to increment or decrement h_2, Btu/ft^2-sec-^{o}R
TEST		closeness test for values of delta temperatures, ^{o}R
NTTPTS		number of entries in total-temperature table (TTØTAB)
TTTTAB (10)		time table for TTØTAB
TTØTAB (10)		total-temperature table, a function of time (TTTTAB)
TAW1RAT		ratio of adiabatic to total temperature at surface 1
TAW2RAT		ratio of adiabatic to total temperature at surface 2
RN		nose radius of reference sphere, ft
CPG	c	specific heat of test gas, Btu/lbm-^{o}R
PTØT		stagnation pressure of flow
PT2PT		total pressure ratio across normal shock

FORTRAN variable	Symbol	Description
P1PT2		ratio of static pressure to total pressure behind normal shock
STIME1	$t_{pc,1}$	time of phase change at surface 1, sec
STIME2	$t_{pc,2}$	time of phase change at surface 2, sec

The only restriction on these inputs imposed by the programing procedure is that STIME1 must be greater than or equal to STIME2. The size of the time step (Δt) and the thickness of the slab (l) along with the block thickness distribution dictate the accuracy of this program for a given thermal diffusivity of the slab. Time step sizes of up to 0.025 second were used with slab thicknesses of up to 0.015 feet to obtain heat-transfer coefficients accurate to within 1 percent of restricted finite-slab solutions (ref. 3) for a material with a thermal diffusivity of 5×10^{-6} ft^2/sec. The distributions of the thickness of the blocks through the finite slab (built into the program) are as follows:

If $N\emptyset = 20$ (used for $l < 0.005$ ft with $\alpha = 5 \times 10^{-6}$ ft^2/sec):

Block number	Thickness, w
1,20	$0.005l$
2,19	$.01l$
3,18	$.02l$
4,17	$.03l$
5,16	$.04l$
6,15	$.05l$
7,14	$.06l$
8,13	$.085l$
9,12	$.10l$
10,11	$.10l$

If $N\emptyset = 30$ (used for $l \geq 0.005$ ft with $\alpha = 5 \times 10^{-6}$ ft^2/sec):

Block number	Thickness, w
1,30	$0.001l$
2,29	$.0025l$
3,28	$.005l$
4,27	$.0075l$
5,26	$.01l$
6,25	$.0125l$
7,24	$.015l$
8,23	$.02l$
9,22	$.03l$
10,21	$.04l$
11,20	$.05l$
12,19	$.06l$
13,18	$.07l$
14,17	$.08l$
15,16	$.0965l$

Program Output

FORTRAN name	Symbol	Description
BETA1	β_1	semi-infinite-slab heat-transfer parameter at surface 1
BETA2	β_2	semi-infinite-slab heat-transfer parameter at surface 2
H1CØMP	$h_{sis,1}$	semi-infinite-slab heat-transfer coefficient at surface 1, $Btu/ft^2\text{-}sec\text{-}^oR$
H2CØMP	$h_{sis,2}$	semi-infinite-slab heat-transfer coefficient at surface 2, $Btu/ft^2\text{-}sec\text{-}^oR$
TAW1	$T_{aw,1}$	adiabatic wall temperature at surface 1, ^oR
TAWNQ	$T_{aw,2}$	adiabatic wall temperature at surface 2, ^oR
TIME	t	time, sec
DELTA TIME	Δt	delta time, sec
H(FRONT)	h_1	finite-slab heat-transfer coefficient at surface 1, $Btu/ft^2\text{-}sec\text{-}^oR$
TAW(FRONT)	$T_{aw,1}$	adiabatic wall temperature at surface 1, ^oR
H(BACK)	h_2	finite-slab heat-transfer coefficient at surface 2, $Btu/ft^2\text{-}sec\text{-}^oR$
TAW(BACK)	$T_{aw,2}$	adiabatic wall temperature at surface 2, ^oR
BLØCK NØ		block number (refers to block distribution through slab, fig. 1)
TEMPERATURE	T	temperature of block, ^oR

```
      PROGRAM MAIN(INPUT,OUTPUT,TAPE5=INPUT,TAPE6=OUTPUT)
      COMMON TBAR
      DIMENSION TO(30),TEMP(30),X(30),TAB1(20),TAB2(30),B(30),C(30),
     1D(30),TTAWTB(10),TAW1TAB(10),TAW2TAB(10),TKMTAB(10),KMTAB(10),
     2TCPTAB(10),CPTAB(10),THOLD1(5),THOLD2(5),
     3TMUTAB(33),MUTAB(33),TPRN(11),PRNO(11),TTTTAB(10),TTOTAB(10)
      EQUIVALENCE(TTTTAB,TTAWTB)
      EQUIVALENCE (NTTPTS,NTAWPT)
      REAL LEN,KM,KMTAB,KMT,KMAV,KM1,KMN
      REAL MUTAB,MUS,MUW
      DATA TAB1/.005,.01,.02,.03,.04,.05,.06,.085,4*.10,.085,.06,.05,
     1.04,.03,.02,.01,.005/
      DATA TAB2/.001,.0025,.005,.0075,.01,.0125,.015,.02,.03,.04,.05,
     1.06,.07,.08,2*.0965,.08,.07,.06,.05,.04,.03,.02,.015,.0125,.01,
     2.0075,.005,.0025,.001/
      DATA F,G,DELTX,E1,E2/0.0,10.,.2,2*.1E-6/
      DATA TMUTAB/400.,450.,500.,550.,600.,650.,700.,750.,800.,850.,
     1900.,950.,1000.,1050.,1100.,1150.,1200.,1250.,1300.,1350.,1400.,
     21450.,1500.,1550.,1600.,1650.,1700.,1750.,1800.,1850.,1900.,1950.,
     32000./
      DATA  MUTAB/9.75E-6,10.74E-6,11.7E-6,12.6E-6,13.46E-6,14.28E-6,
     115.05E-6,15.82E-6,16.57E-6,17.29E-6,17.975E-6,18.65E-6,19.30E-6,
     219.92E-6,21.16E-6,21.75E-6,22.325E-6,22.88E-6,23.45E-6,23.98E-6,
     323.98E-6,24.50E-6,25.025E-6,25.53E-6,26.03E-6,26.53E-6,27.02E-6,
     427.05E-6,27.97E-6,28.43E-6,28.88E-6,29.33E-6,29.78E-6/
      DATA TPRN/400.,450.,500.,550.,600.,650.,700.,750.,800.,850.,900./
      DATA PRNO/.7305,.7215,.7135,.706,.7,.694,.69,.686,.6835,.682,.681/
*
      INTEGER PRFREQ
      NAMELIST /NAM1/ TIMEO,TO,SIGMA,EMS,RHO,NKPTS,TKMTAB,KMTAB,NCPTS,
     1TCPTAB,CPTAB,LEN,NO,PRFREQ, TIFIN,TNFIN,DELTAT,DELH1,DELH2,TEST
     3,NTTPTS,TTTTAB,TTOTAB,TAW1RAT,TAW2RAT,RN,CPG,PTOT,PT2PT,P1PT2
     4,STIME1,STIME2
      NAMELIST/DEBG1/ BETA1,BETA2,H1COMP,H2COMP,TAW1,TAWNO
      NAMELIST/DEBG2/ H1,H2,THOLD1,THOLD2,TEMP
      NAMELIST /DEBG3/ THOLD1,THOLD2,PT1H1,PT1H2,PT2H1,PT2H2,DT1,DT2,
     1DET,DELH1,DELH2
      EXTERNAL FOFB
*
    1 READ(5,NAM1)
      IF (EOF,5)5,10
    5 STOP
   10 CONTINUE
      WRITE (6,NAM1)
      IPFCT=0
      DO  11  I=1,NTTPTS
      TAW1TAB(I)= TAW1RAT* TTOTAB(I)
   11 TAW2TAB(I)= TAW2RAT* TTOTAB(I)
      IF (NO.GT.20) GO TO 20
      DO  15  I=1,NO
   15 X(I)= LEN * TAB1(I)
      GO TO 30
   20 DO 25   I=1,NO
   25 X(I)= LEN * TAB2(I)
   30 CONTINUE
*
* COMPUTE H1 AND H2 FROM SEMI-INFINITE SLAB APPROXIMATION
*
```

```
      CALL FTLUP(STIME1 ,TAW1,1,NTAWPT,TTAWTB,TAW1TAB)
      CALL FTLUP(STIME2 ,TAWNO,1,NTAWPT,TTAWTB,TAW2TAB)
      TBAR =(T1FIN-TO(1))/(TAW1 -TO(1))
      CALL ITR2(BETA1,F,G,DELTX,FOFB,E1,E2,50,ICODE)
      TBAR =(TNFIN-TO(NO))/(TAWNO-TO(NO))
      CALL ITR2(BETA2,F,G,DELTX,FOFB,E1,E2,50,ICODE)
      CALL FTLUP(T1FIN,KM1,1,NKPTS,TKMTAB,KMTAB)
      CALL FTLUP(TNFIN,KMN,1,NKPTS,TKMTAB,KMTAB)
      CALL FTLUP(T1FIN,CP1,1,NCPTS,TCPTAB,CPTAB)
      CALL FTLUP(TNFIN,CPN,1,NCPTS,TCPTAB,CPTAB)
      H1COMP= BETA1 * SQRT(RHO*CP1*KM1/STIME1)
      H2COMP= BETA2 * SQRT(RHO*CPN*KMN/STIME2)
      H1 =H1COMP
      H2 =H2COMP
      WRITE (6,DEBG1)
   40 DO  130  K=1,5
      DO  50   J=1,NO
   50 TEMP(J)= TO(J)
      TIME= TIMEO
*
* GO HERE TO UPDATE TIME AND RECOMPUTE
*
   60 TIME=TIME+ DELTAT
      DO  70   J=1,NO
      B(J)=0.0
      C(J)=0.0
   70 D(J)=0.0
*
* DIAGONAL ELEMENTS ARE STORED IN B ARRAY
* UPPER DIAGONAL ELEMENTS ARE STORED IN C ARRAY
* THE ARRAYOFLOWER DIAGONAL ELEMENTS ARE EQUIVALENT TO C ARRAY
* CONSTANT PART OF EQ. IS STORED I D ARRAY
* SAVE1 CONTAINS HEAT STORED COMPUTATION
* SAVE2 CONTAINS CONDUCTION COMPUTATION
*
      B(1)= -H1
      CALL FTLUP(TIME,TAW1,1,NTAWPT,TTAWTB,TAW1TAB)
      CALL FTLUP(TIME,TAWNO,1,NTAWPT,TTAWTB,TAW2TAB)
      D(1)=-H1*TAW1 +SIGMA*EMS*TEMP(1)**4
      D(NO)=-H2*TAWNO+SIGMA*EMS*TEMP(NO)**4
      CALL FTLUP(TEMP(1),KM,1,NKPTS,TKMTAB,KMTAB)
      NSTOP=NO-1
      DO 80    I=1,NSTOP
      CALL FTLUP(TEMP(I+1),KMT,1,NKPTS,TKMTAB,KMTAB)
      KMAV=(KM+KMT)*.5
      KM=KMT
      CALL FTLUP(TEMP(I),CP,1,NCPTS,TCPTAB,CPTAB)
      SAVE1 =RHO*CP*X(I)/DELTAT
      SAVE2 =2.0*KMAV/(X(I)+X(I+1))
      B(I)= B(I)-SAVE1-SAVE2
      B(I+1)= -SAVE2
      C(I)= SAVE2
   80 D(I)=D(I) -SAVE1*TEMP(I)
      CALL FTLUP(TEMP(NO),CP,1,NCPTS,TCPTAB,CPTAB)
      SAVE1= RHO*CP*X(NO)/DELTAT
      B(NO)= B(NO)-SAVE1 - H2
      D(NO)= D(NO)-SAVE1*TEMP(NO)
      CALL TRIDMAT(C,B,C,D,TEMP,NO)
      IF (ABS(TIME-STIME2) .GT. .00001)  GO TO 85
      THOLD2(K)= TEMP(NO)
```

```
      GO TO 60
   85 IF (ABS(TIME-STIME1) .GT. .00001)  GO TO 60
      THOLD1(K)=TEMP(1)
*
      GO TO (90,100,110,120,130) K
   90 H1 =H1COMP+DELH1
      GO TO 130
  100 H1 =H1COMP-DELH1
      GO TO 130
  110 H1 =H1COMP
      H2 =H2COMP+DELH2
      GO TO 130
  120 H2 =H2COMP-DELH2
  130 CONTINUE
*
* THOLD1(1)AND THOLD2(1) CONTAIN TEMPERATURES COMPUTED AS  F(H1,H2)
* THOLD1(2)AND THOLD2(2) CONTAIN TEMPERATURES COMPUTED AS  F(H1+DELH1,H2)
* THOLD1(3)AND THOLD2(3) CONTAIN TEMPERATURES COMPUTED AS  F(H1-DELH1,H2)
* THOLD1(4)AND THOLD2(4) CONTAIN TEMPERATURES COMPUTED AS  F(H1,H2+DELH2)
* THOLD1(5)AND THOLD2(5) CONTAIN TEMPERATURES COMPUTED AS  F(H1,H2-DELH2)
*
      PT1H1= (THOLD1(2)-THOLD1(3))/(2.0*DELH1)
      PT1H2= (THOLD1(4)-THOLD1(5))/(2.0*DELH2)
      PT2H1= (THOLD2(2)-THOLD2(3))/(2.0*DELH1)
      PT2H2= (THOLD2(4)-THOLD2(5))/(2.0*DELH2)
*
      DT1   = T1FIN - THOLD1(1)
      DT2   = TNFIN - THOLD2(1)
*
      DET = PT1H1* PT2H2 +PT1H2*PT2H1
*
      DELH1 = -(DT1*PT2H2 -DT2*PT1H2)/DET
      DELH2 = (DT2*PT1H1 -DT1*PT2H1)/DET
*
      IF (ABS(DT1).LE.TEST.AND.ABS(DT2).LE.TEST) GO TO 150
      H1COMP = H1COMP +DELH1
      H2COMP = H2COMP +DELH2
      H1 = H1COMP
      H2 = H2COMP
      GO TO 40
*
  150 DO 160  J=1,NO
  160 TEMP(J)=TO(J)
      TIME=TIMEO
      H1= H1COMP
      H2= H2COMP
  170 TIME =TIME +DELTAT
      DO 180  J=1,NO
      B(J)=0.0
      C(J)=0.0
  180 D(J)=0.0
      B(1)= -H1
      CALL FTLUP(TIME,TAW1,1,NTAWPT,TTAWTB,TAW1TAB)
      CALL FTLUP(TIME,TAWNO,1,NTAWPT,TTAWTB,TAW2TAB)
      D(1)=-H1 *TAW1+SIGMA*EMS* TEMP(1)**4
      D(NO) =-H2*TAWNO +SIGMA*EMS*TEMP(NO)**4
      CALL FTLUP(TEMP(1),KM,1,NKPTS,TKMTAB,KMTAB)
      NSTOP= NO-1
      DO 190  I=1,NSTOP
```

```
      CALL FTLUP(TEMP(I+1),KMT,1,NKPTS,TKMTAB,KMTAB)
      KMAV=.5 *(KM +KMT)
      KM =KMT
      CALL FTLUP(TEMP(I),CP,1,NCPTS,TCPTAB,CPTAB)
      SAVE1 = RHO *CP* X(I)/DELTAT
      SAVE2 = 2.0* KMAV/(X(I)+X(I+1))
      B(I) = B(I)-SAVE1-SAVE2
      B(I+1) = -SAVE2
      C(I)= SAVE2
  190 D(I)= D(I)-SAVE1 *TEMP(I)
      CALL FTLUP(TEMP(NO),CP,1,NCPTS,TCPTAB,CPTAB)
      SAVE1 = RHO*CP* X(NO)/DELTAT
      B(NO)= B(NO) -SAVE1 -H2
      D(NO)= D(NO) -SAVE1 *TEMP(NO)
      CALL TRIDMAT(C,B,C,D,TEMP,NO)
      IPFCT=IPFCT+1
      IF (IPFCT.NE.PRFREQ)  GO TO 195
      IPFCT=0
      WRITE (6,1000)TIME,DELTAT,H1,H2,TAW1,TAWNO
 1000 FORMAT(1X///6X6HTIME =F10.4,6X13HDELTA TIME = F6.4//7X9HH(TOP)  =
     1E16.8,5X12HH(BOTTOM)  =E16.8/7X9HTAW(TOP)=E16.8,5X12HTAW(BOTTOM)=
     2E16.8//6X8HBLOCK NO11X11HTEMPERATURE//)
      WRITE (6,2000)(I,TEMP(I),I=1,NO)
 2000 FORMAT(9X,I3,6X,E20.8)
  195 IF (ABS(TIME-STIME1) .GT. .00001)  GO TO 170
      R=53.35
      G=32.2
      HOLD= 2.7*PTOT * PT2PT
      CALL FTLUP(STIME1 ,TTOT,1,NTTPTS,TTTTAB,TTOTAB)
      CALL FTLUP(TTOT,PRN,1,11,TPRN,PRNO)
      SAVE1 =.768*CPG*(PRN**-.6)
      CALL FTLUP(TTOT,MUS,1, 33  ,TMUTAB,MUTAB)
      RHOS= HOLD/TTOT
      DUEDX=SQRT(2.0*R*G *TTOT*(1.0-P1PT2))/RN
      SAVE2=((RHOS *MUS)**.4)* SQRT(DUEDX)
*
      CALL FTLUP(T1FIN,MUW,1, 33  ,TMUTAB,MUTAB)
      RHOW= HOLD/T1FIN
      HRS1= SAVE1*SAVE2*((RHOW*MUW)**.1)
      CALL FTLUP(STIME2 ,TTOT,1,NTTPTS,TTTTAB,TTOTAB)
      CALL FTLUP(TTOT,PRN,1,11,TPRN,PRNO)
      SAVE1 =.768*CPG*(PRN**-.6)
      CALL FTLUP(TTOT,MUS,1, 33  ,TMUTAB,MUTAB)
      RHOS= HOLD/TTOT
      DUEDX=SQRT(2.0*R*G *TTOT*(1.0-P1PT2))/RN
      SAVE2=((RHOS *MUS)**.4)* SQRT(DUEDX)
*
      CALL FTLUP(TNFIN,MUW,1, 33  ,TMUTAB,MUTAB)
      RHOW= HOLD/TNFIN
      HRSN= SAVE1 * SAVE2 * ((RHOW*MUW)**.1)
*
      H1RAT = H1/HRS1
      H2RAT = H2/HRSN
*
      WRITE (6,3000) H1,HRS1,H1RAT,H2,HRSN,H2RAT
 3000 FORMAT(1X///5X3HH1=E14.6,4X15HH1(REF.SPHERE)=E14.6,4X10HH1(RATIO)=
     1E14.6/5X3HH2=E14.6,4X15HH2(REF.SPHERE)=E14.6,4X10HH2(RATIO)=E14.6)
      GO TO 1
      END
```

```
      FUNCTION  FOFB(BETA)
      COMMON TBAR
      Y = ERF(BETA)
      C =1.0 - Y
      FOFB=(1.0-EXP(BETA**2)*C)- TBAR
      RETURN
      END
```

```
      SUBROUTINE TRIDMAT(A,B,C,D,T,N)
      DIMENSION A(1),B(1),C(1),D(1),T(1),W(30),SV(30),G(30)
*
*   THIS ROUTINE SOLVES A TRIDIAGONAL MATRIX
*
      W(1)=B(1)
      SV(1)= C(1) / B(1)
      G(1)= D(1)/W(1)
      NM1=N-1
      DO 100 K=2,N
      KM1 = K-1
      W(K) = B(K) - A(KM1)*SV(KM1)
      IF (K.EQ.N)  GO TO 5
    4 SV(K)= C(K)/W(K)
    5 G(K) = (D(K)- A(KM1)*G(KM1))/W(K)
  100 CONTINUE
      T(N)=G(N)
      DO 200 K=1,NM1
      KK= N-K
      T(KK)= G(KK)- SV(KK)*T(KK+1)
  200 CONTINUE
      RETURN
      END
```

APPENDIX B

SOLUTION FOR SEMI-INFINITE SLAB

In the phase-change data reduction method (ref. 1) for the semi-infinite slab, the heat-transfer coefficient depends on the time required for the phase change to occur (t_{pc}), the temperature of the phase change (T_{pc}), the initial and adiabatic wall temperatures $(T_i$ and $T_{aw})$, and the thermophysical properties of the model wall $(\sqrt{\rho ck})$. The relationship between the heat-transfer coefficient and the other parameters is determined from the solution to the equation governing the transient one-dimensional flow of heat. This equation is

$$\frac{\partial T}{\partial t} = \frac{\partial^2 T}{\partial x^2} \tag{B1}$$

with the following initial and boundary conditions which most nearly describe the actual tunnel transient test:

$$T(x,0) = T_i \tag{B2}$$

$$T(\infty,t) = T_i \tag{B3}$$

$$\frac{\partial T(0,t)}{\partial x} = \frac{h}{k}\left[T_{aw} - T(0,t)\right] \tag{B4}$$

It is assumed (ref. 1) that the phase-change coating is at the surface temperature $T(0,t)$ and the time t_{pc} is required when $T(0,t) = T_{pc}$. Other assumptions are as follows (ref. 1):

1. The depth of heat penetration into the wall is small compared with the wall thickness and surface radius of curvature so that the wall acts like a semi-infinite slab (eq. (B3)).

2. The model is isothermal before injection into the airstream (eq. (B2)).

3. The surface experiences an instantaneous step in aerodynamic heat-transfer coefficient at time zero, and this coefficient is invariant with time (eq. (B4)).

4. The thermal diffusivity α of the wall is invariant with temperature.

The solution to equation (B1) with the specified boundary conditions is (ref. 3)

$$\bar{T} = 1 - e^{\beta^2}\operatorname{erfc}(\beta) \tag{B5}$$

where

$$\bar{T} = \frac{T_{pc} - T_i}{T_{aw} - T_i} \tag{B6}$$

$$h_{sis} = \frac{\beta\sqrt{\rho ck}}{\sqrt{t_{pc}}} \tag{B7}$$

$$\operatorname{erfc}(\beta) = \frac{2}{\sqrt{\pi}} \int_{\beta}^{\infty} e^{-\lambda^2} d\lambda \tag{B8}$$

Equation (B5) is plotted in figure 15 in terms of the parameter β as a function of $\bar{T}$. The heat-transfer coefficient is then determined from equation (B7).

REFERENCES

1. Jones, Robert A.; and Hunt, James L.: Use of Fusible Temperature Indicators for Obtaining Quantitative Aerodynamic Heat-Transfer Data. NASA TR R-230, 1966.

2. Garrett, L. Bernard; and Pitts, Joan I.: A General Transient Heat-Transfer Computer Program for Thermally Thick Walls. NASA TM X-2058, 1970.

3. Carslaw, H. S.; and Jaeger, J. C.: Conduction of Heat in Solids. Second ed., Oxford Univ. Press, Inc., 1959.

4. Scarborough, James B.: Numerical Mathematical Analysis. Fifth ed., Johns Hopkins Press, 1962, pp. 199-222.

5. Connor, L. E.; Sparks, V. W.; and Bhadsavle, A. G.: Heat Transfer Tests of the NASA-MSC Space Shuttle Configuration at the Langley Research Center Mach 8 Variable Density Facility. TM 54/20-291, LMSC/HREC D162761 (Contract NAS 9-10506). Lockheed Missiles & Space Co., Dec. 1970.

6. Beckwith, Ivan E.; and Cohen, Nathaniel B.: Application of Similar Solutions to Calculation of Laminar Heat Transfer on Bodies With Yaw and Large Pressure Gradient in High-Speed Flow. NASA TN D-625, 1961.

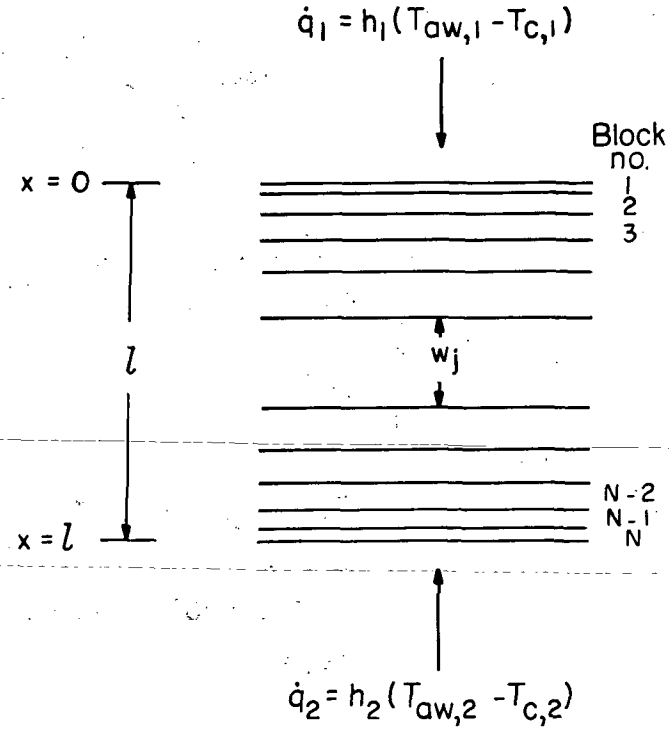

Figure 1.- Geometry of finite slab.

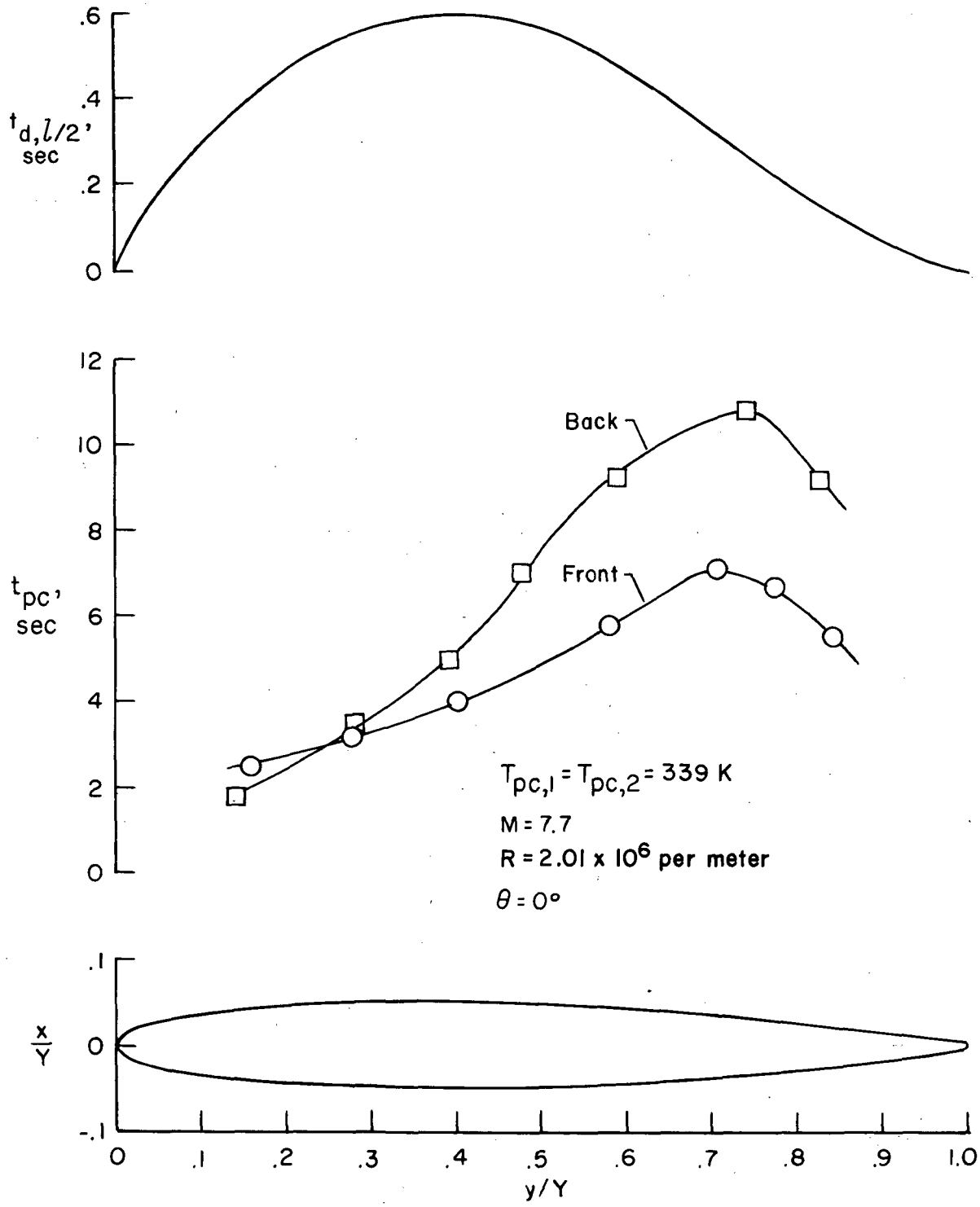

Figure 2.- Chordwise profile of wing on straight-wing orbiter at 69.3 percent semispan with time of phase-change and thermal diffusion distribution. Y = 2.042 cm.

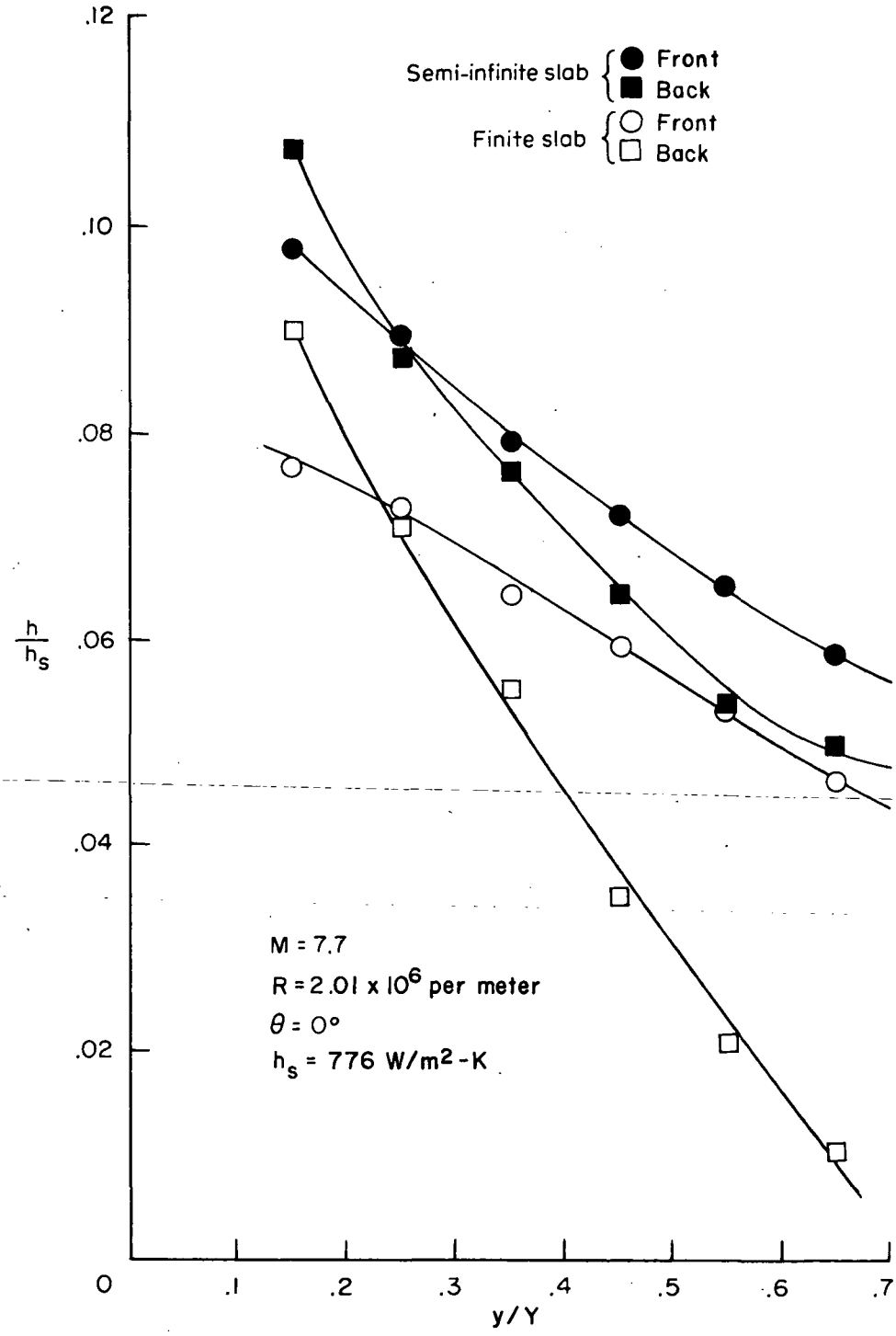

Figure 3.- Result from finite- and semi-infinite-slab heat-transfer coefficient procedures for wing on straight-wing orbiter at 69.3 percent semispan. Y = 2.042 cm.

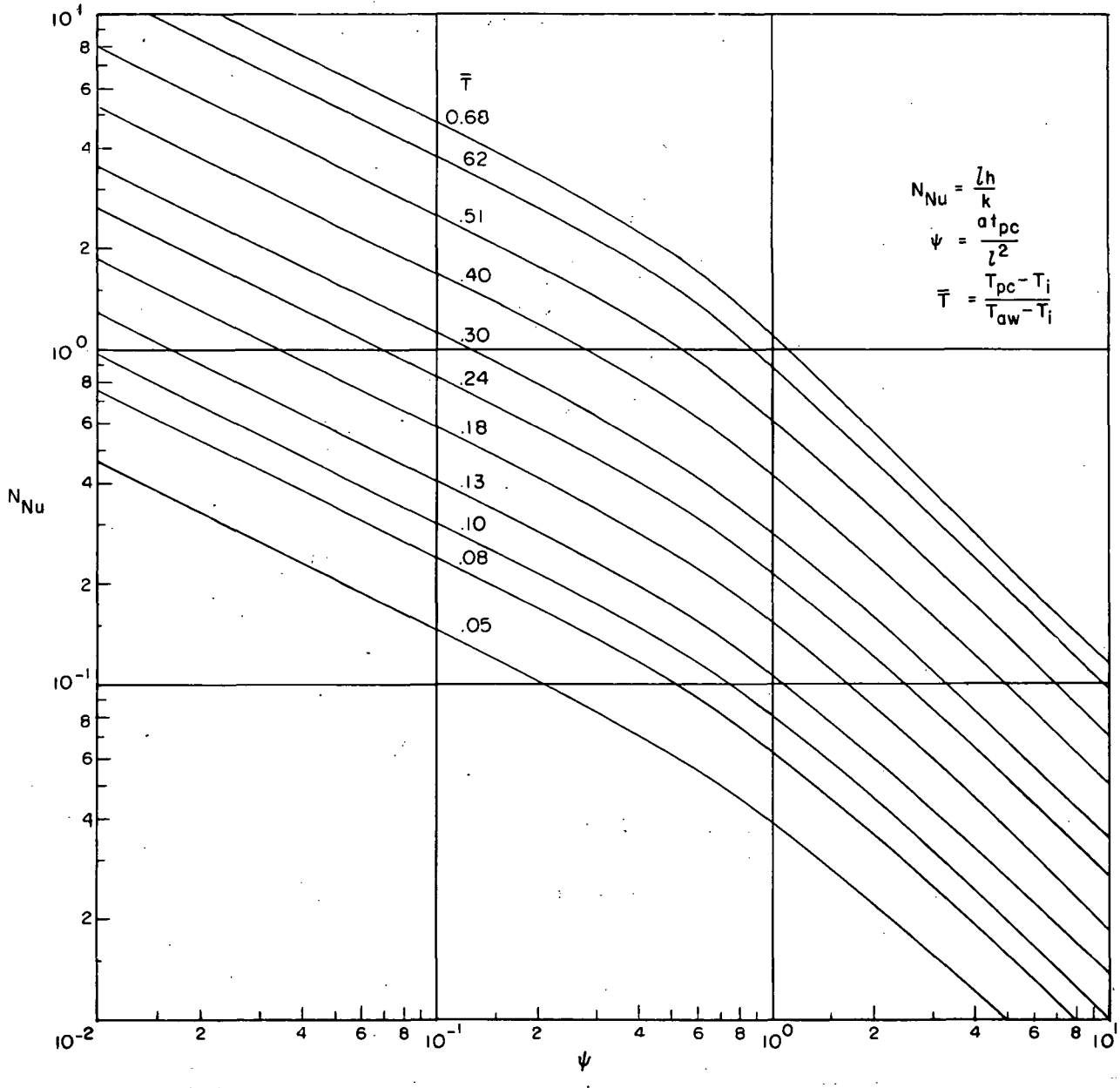

Figure 4.- Heat-transfer solution at convecting surface of finite slab with no heat exchange at back surface (plot of eq. (2)).

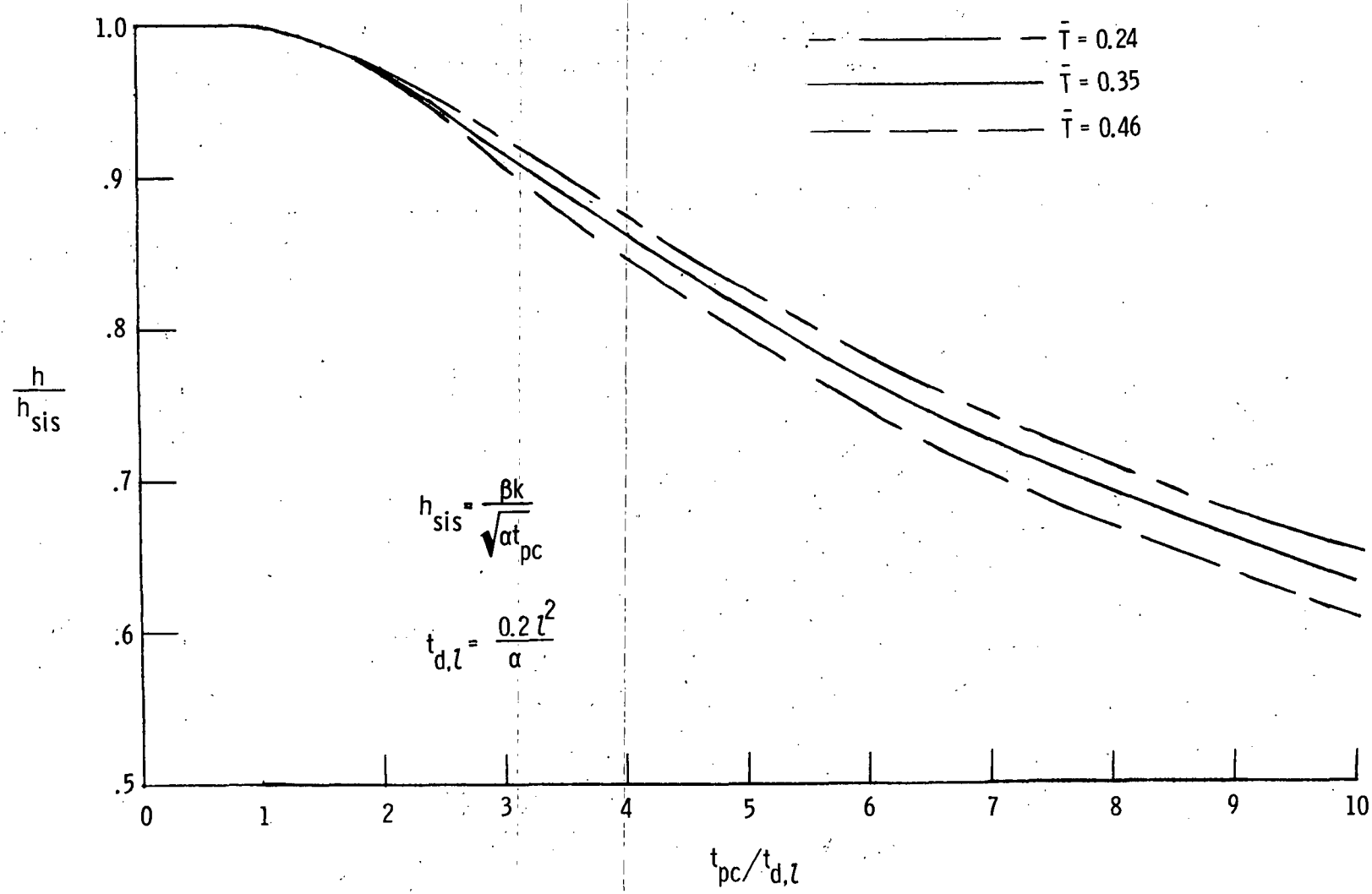

Figure 5.- Heat-transfer correction factor at convecting surface of finite slab with no heat exchange at back surface.

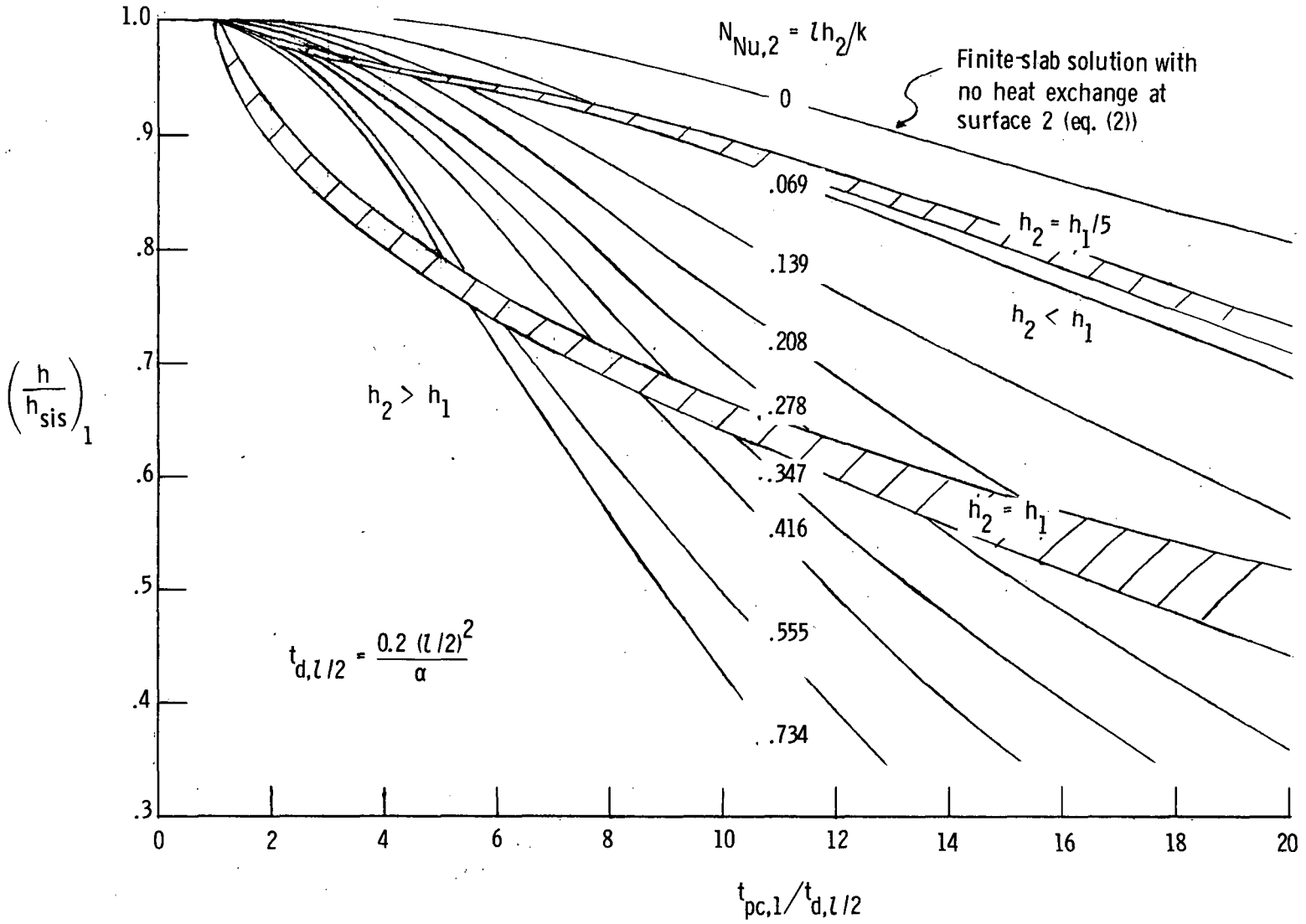

Figure 6.- Front-surface correction factor for finite slab with heat exchange at back surface. $\bar{T}_1 = 0.348$; $(T_{aw,2} - T_i)/(T_{aw,1} - T_i) = 1$.

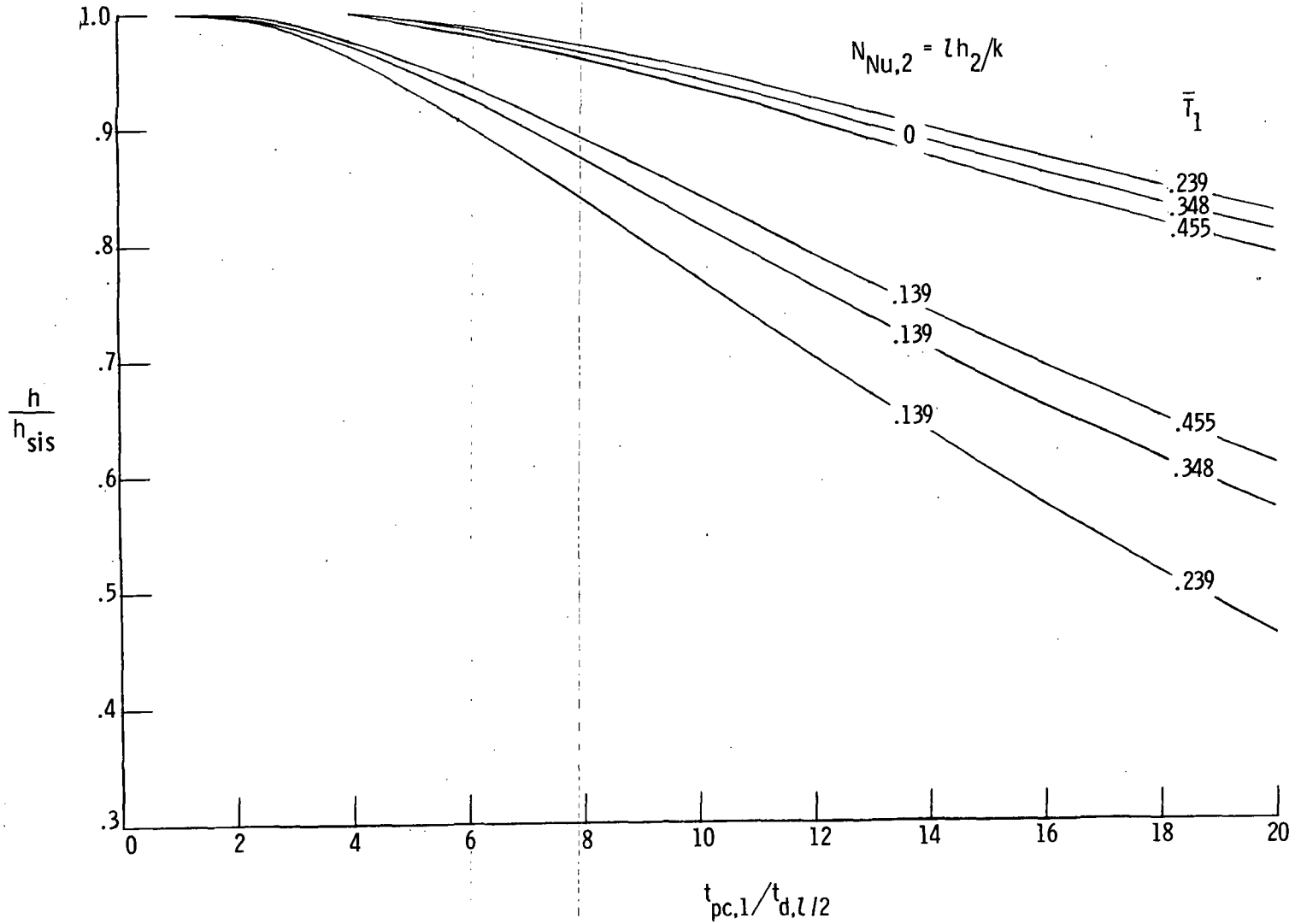

Figure 7.- Effect of $\bar{T}_1$ on front-surface correction factor for a finite slab with heat exchange at back surface. $(T_{aw,2} - T_i)/(T_{aw,1} - T_i) = 1$.

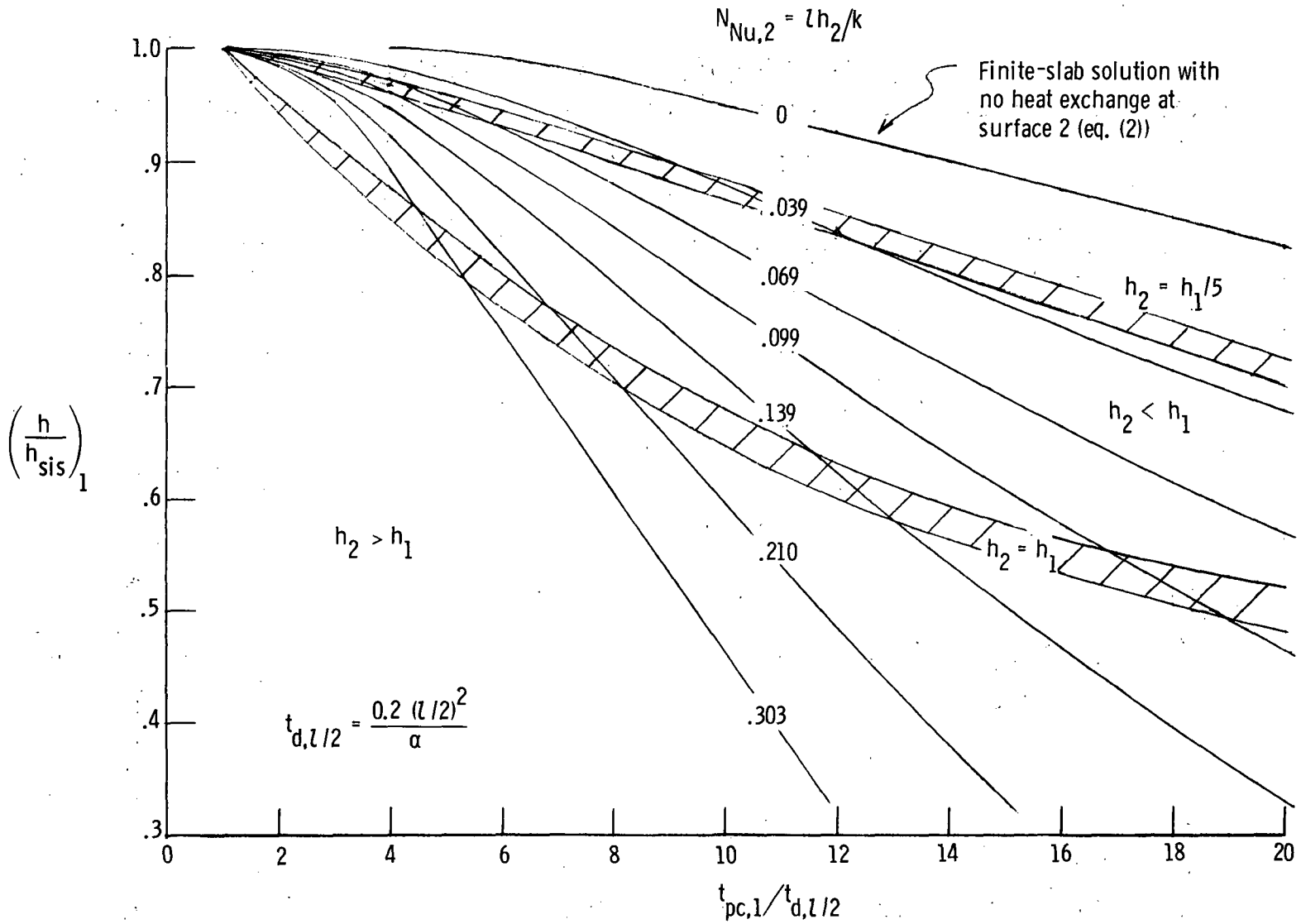

Figure 8.- Front-surface correction factor for finite slab with heat exchange at back surface. $\bar{T}_1 = 0.174$, $(T_{aw,2} - T_i)/(T_{aw,1} - T_i) = 1$.

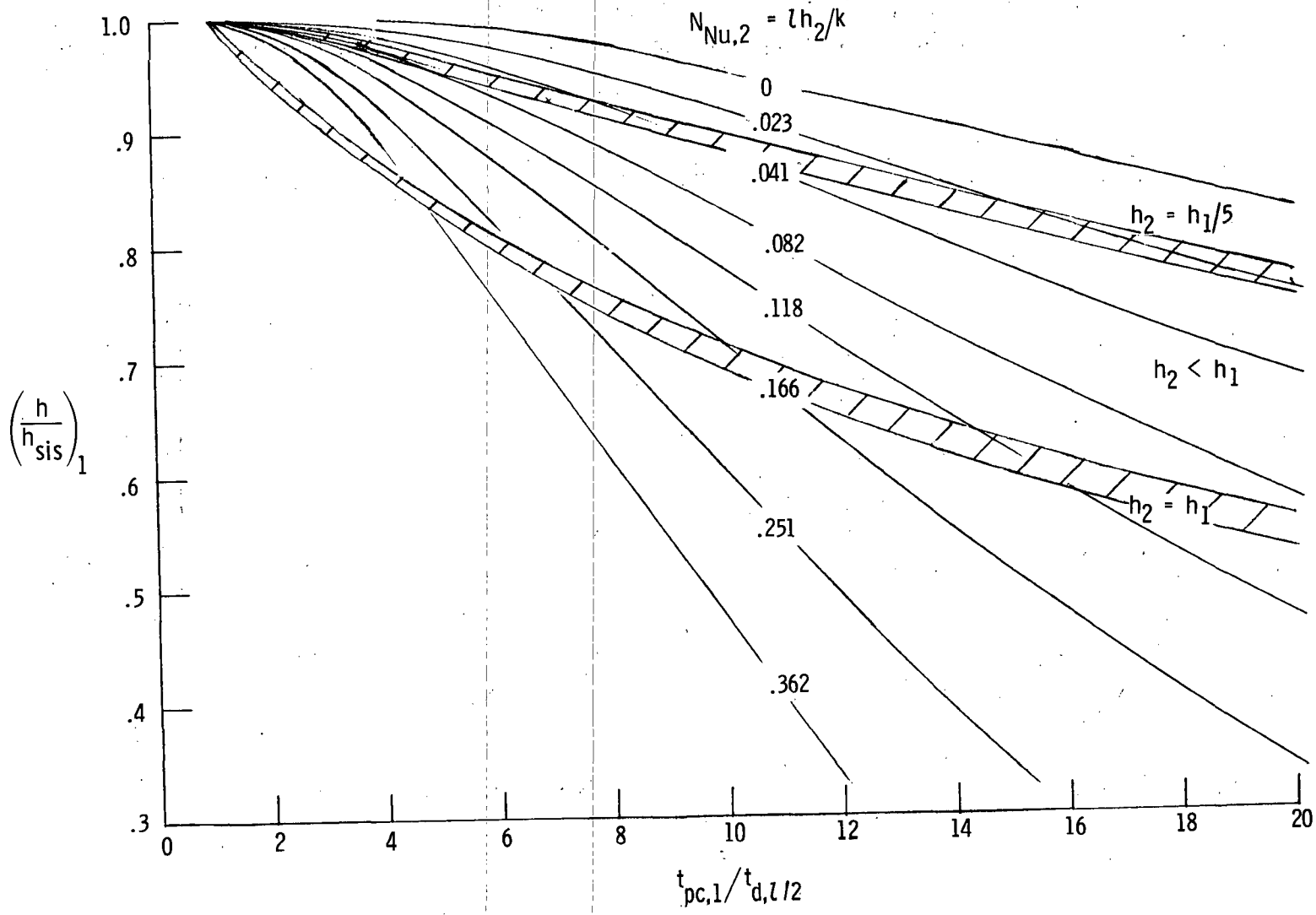

Figure 9.- Front-surface correction factor for finite slab with heat exchange at back surface. $\bar{T}_1 = 0.174$, $(T_{aw,2} - T_i)/(T_{aw,1} - T_i) = 0.9$.

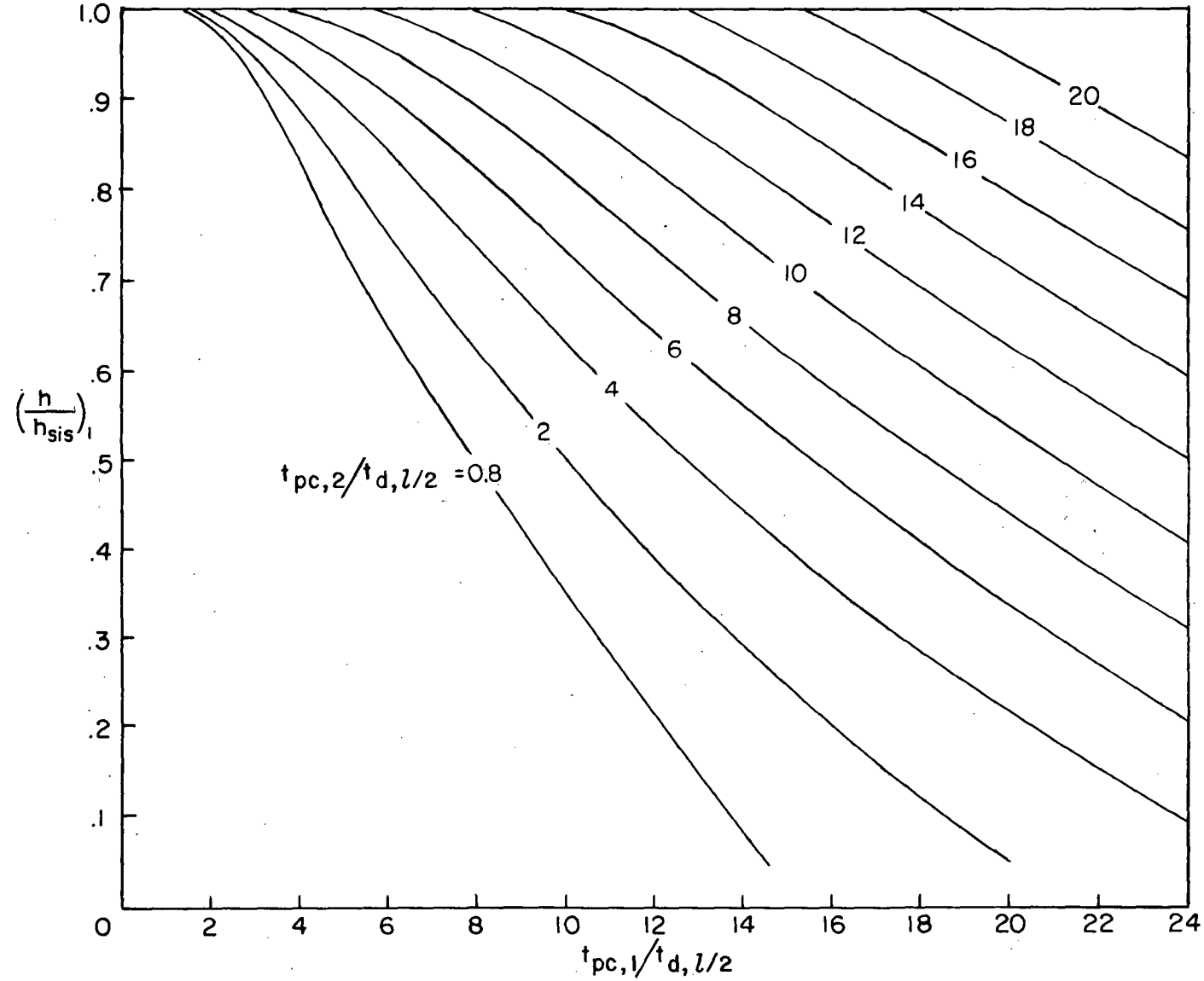

(a) Surface 1.

Figure 10.- Heat-transfer-coefficient correction factor for finite slab with phase change on both sides. $\bar{T}_1 = 0.45$; $\bar{T}_2 = 0.24$; $(T_{aw,2} - T_i)/(T_{aw,1} - T_i) = 1$.

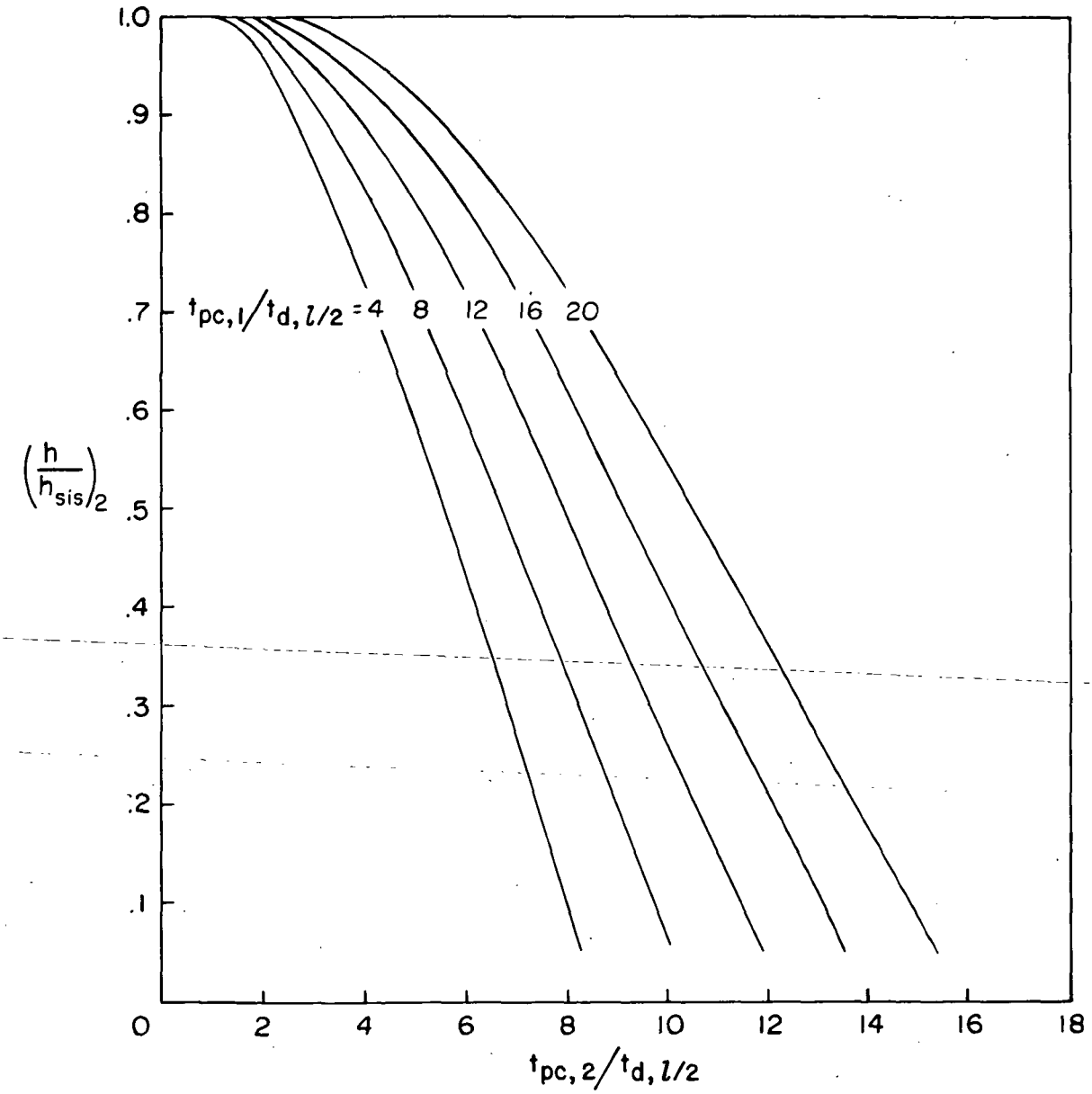

(b) Surface 2.

Figure 10.- Concluded.

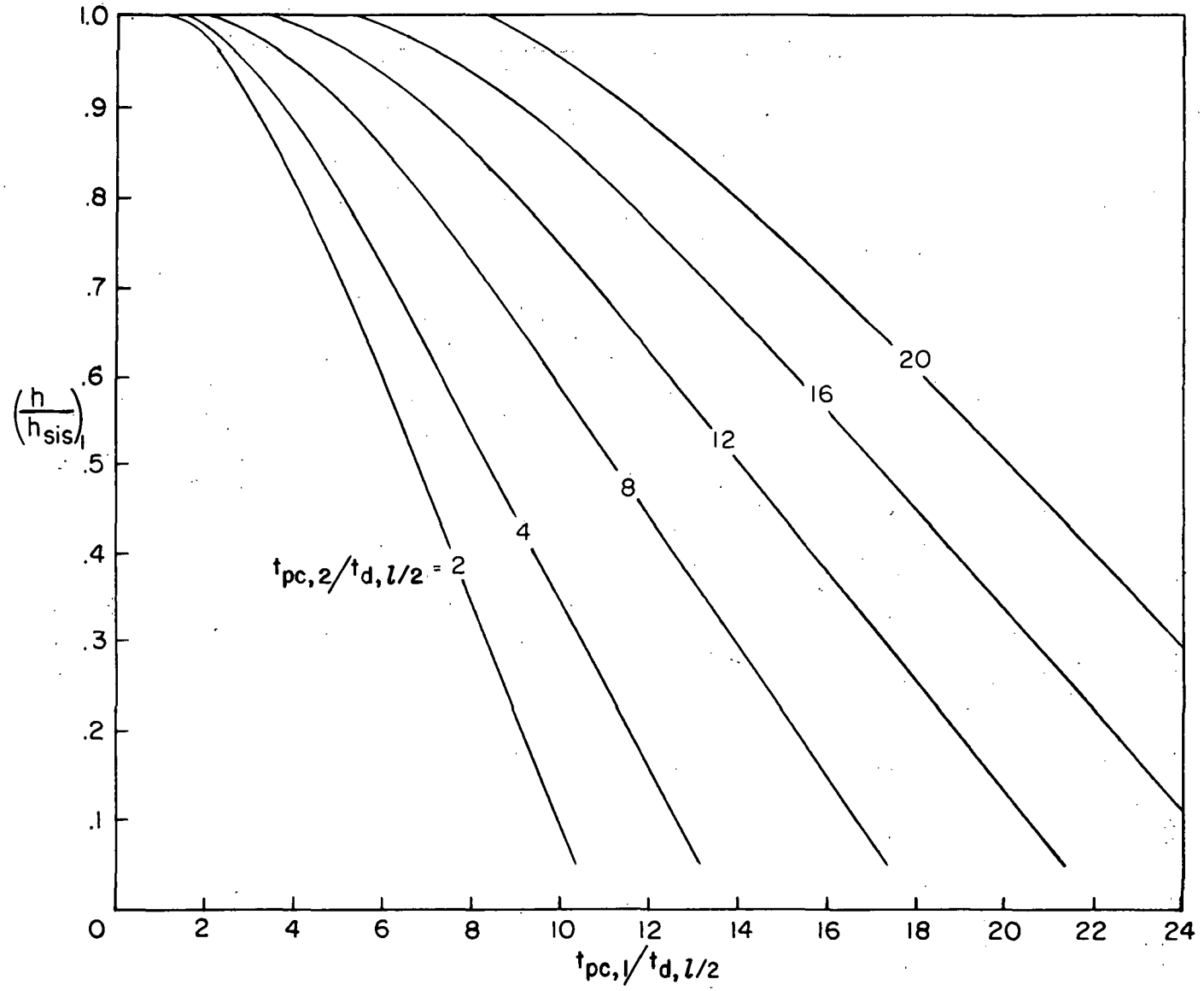

Figure 11.- Heat-transfer-coefficient correction factor for finite slab with phase change on both sides. $\bar{T}_1 = \bar{T}_2 = 0.1$; $(T_{aw,2} - T_i)/(T_{aw,1} - T_i) = 1$.

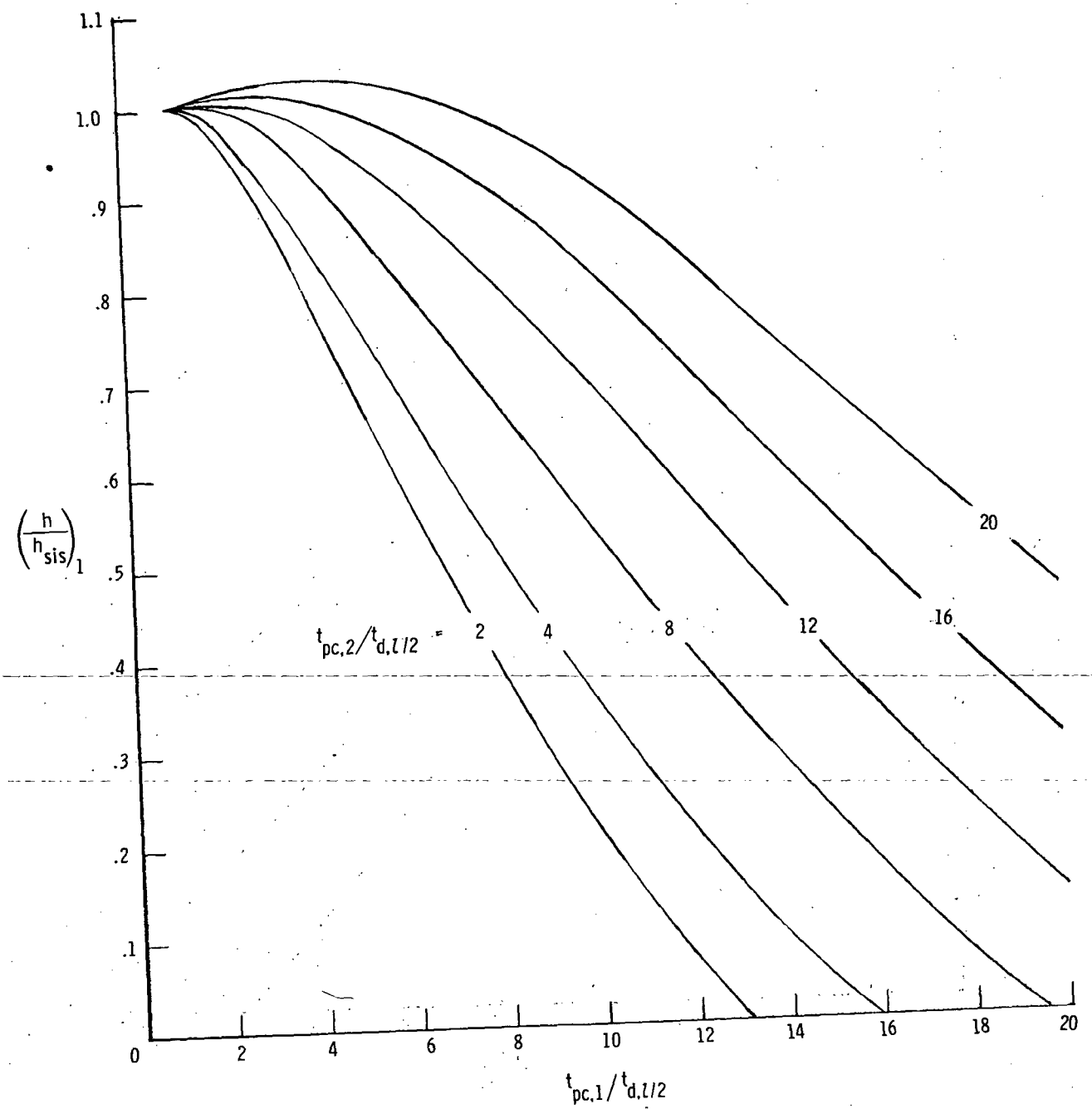

(a) $\bar{T}_1 = \bar{T}_2 = 0.45$.

Figure 12.- Heat-transfer-coefficient correction factor for finite slab with phase change on both sides. $(T_{aw,2} - T_i)/(T_{aw,1} - T_i) = 1$.

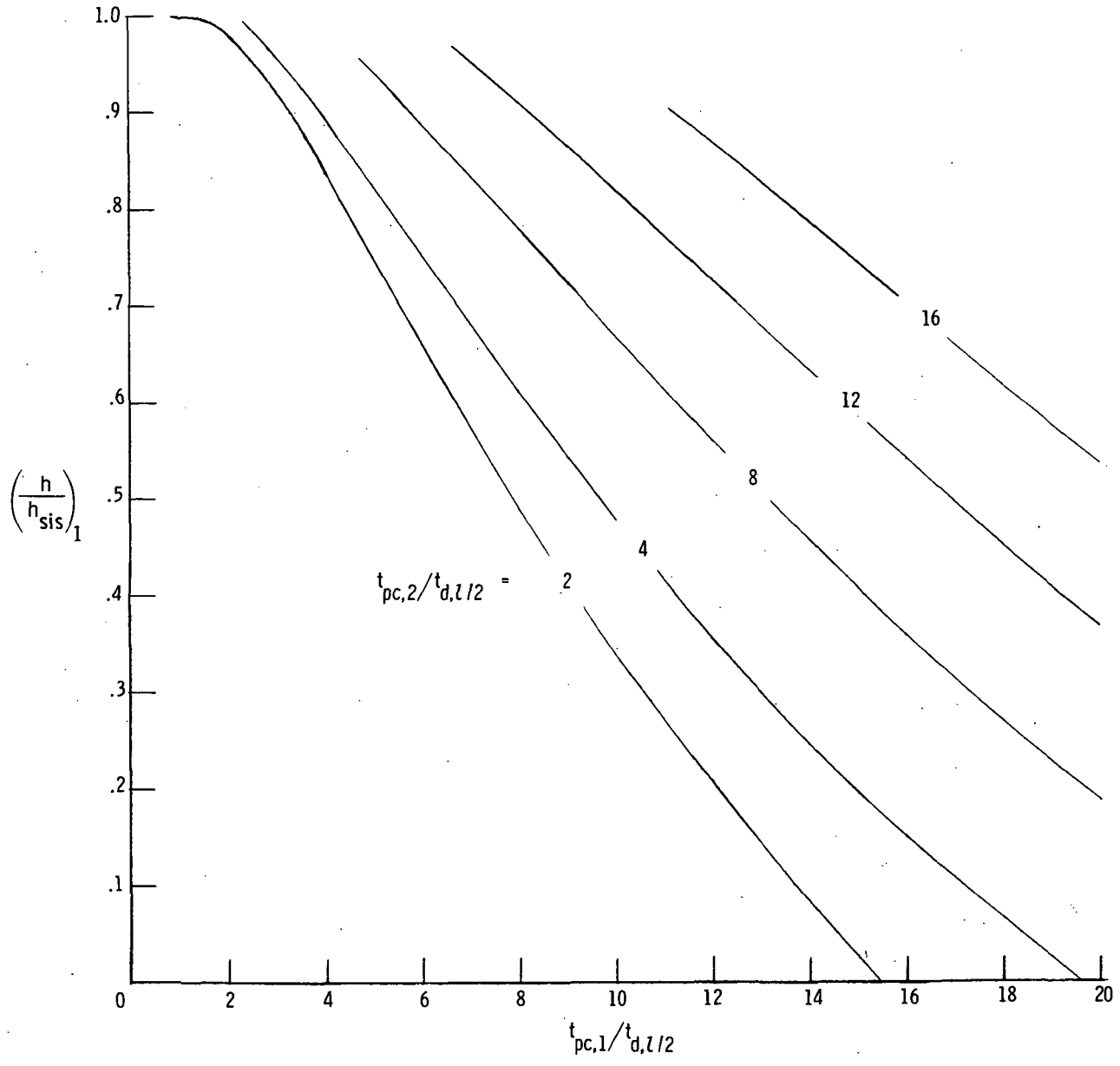

(b) $\bar{T}_1 = 0.45$; $\bar{T}_2 = 0.35$.

Figure 12.- Continued.

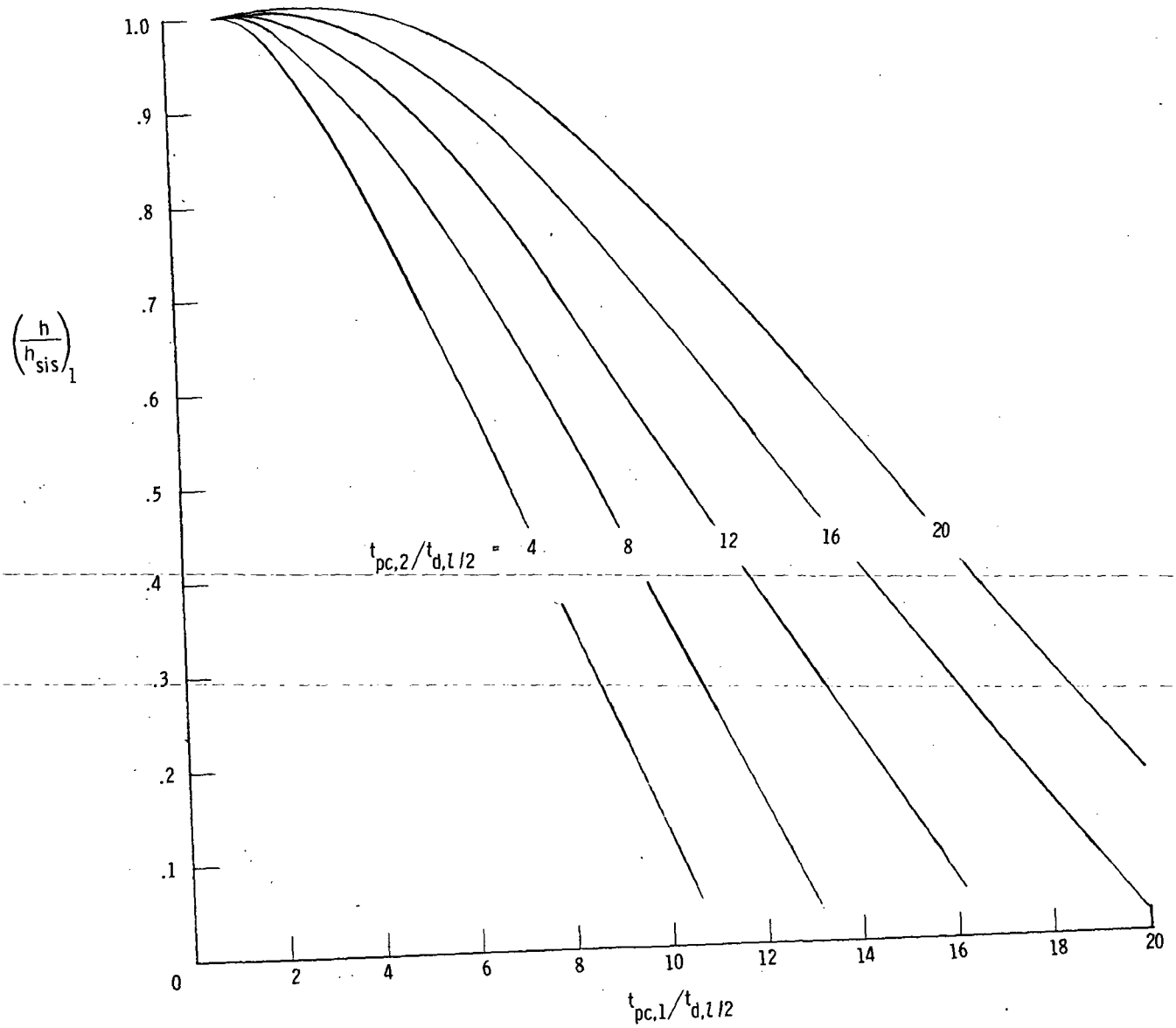

(c) $\bar{T}_1 = 0.35$; $\bar{T}_2 = 0.45$.

Figure 12.- Continued.

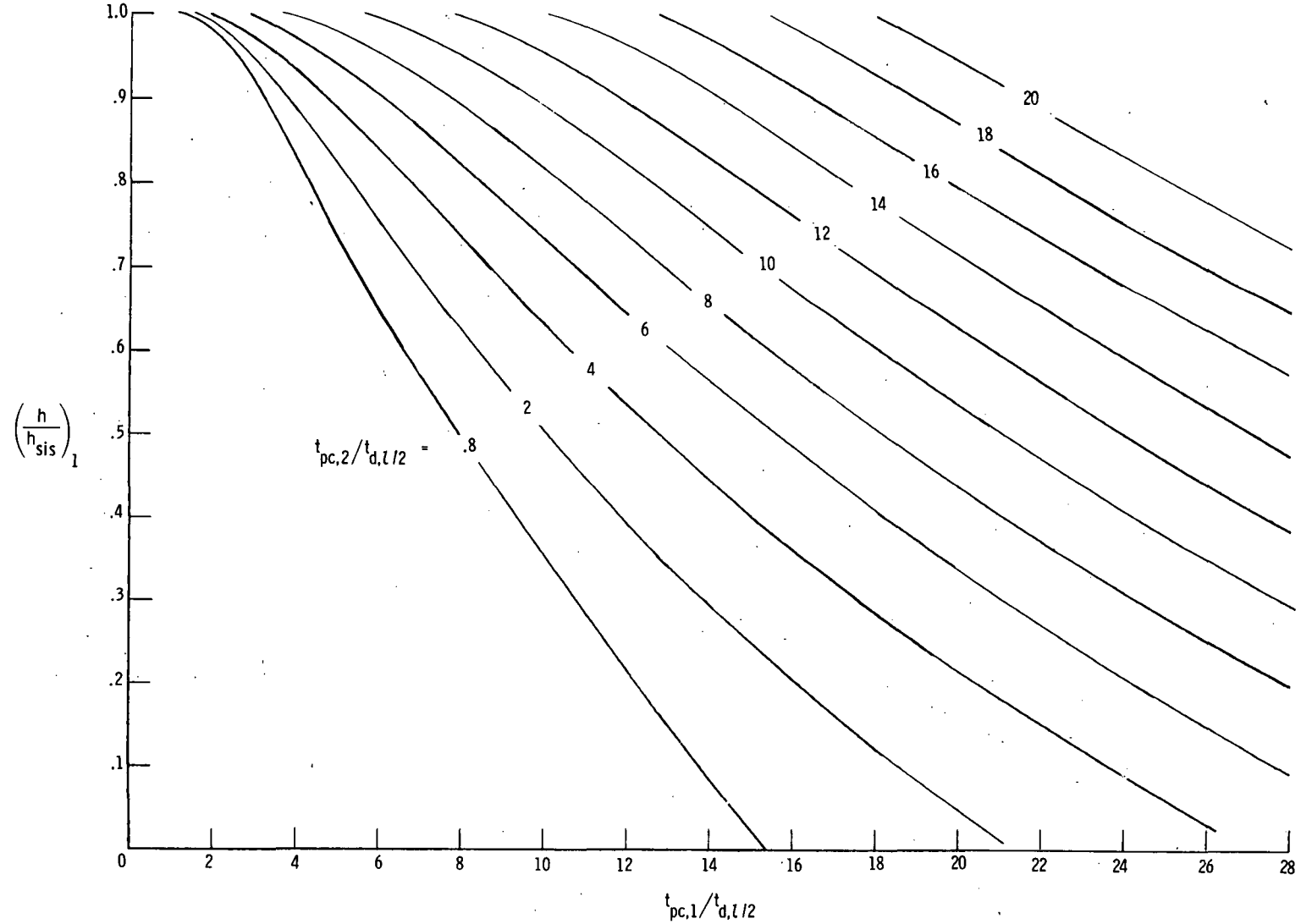

(d) $\bar{T}_1 = 0.45$; $\bar{T}_2 = 0.24$.

Figure 12.- Continued.

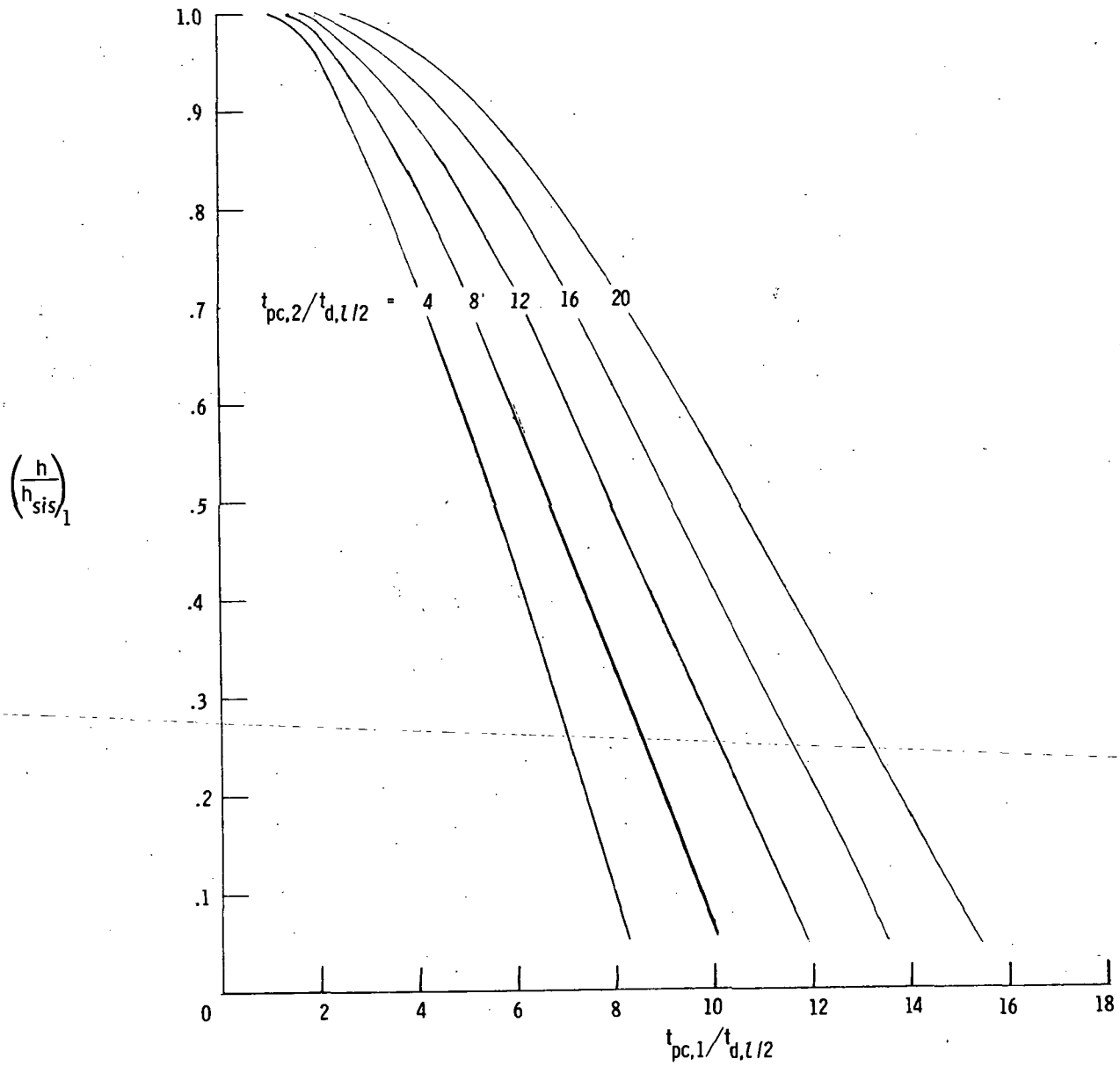

(e) $\bar{T}_1 = 0.24$; $\bar{T}_2 = 0.45$.

Figure 12.- Continued.

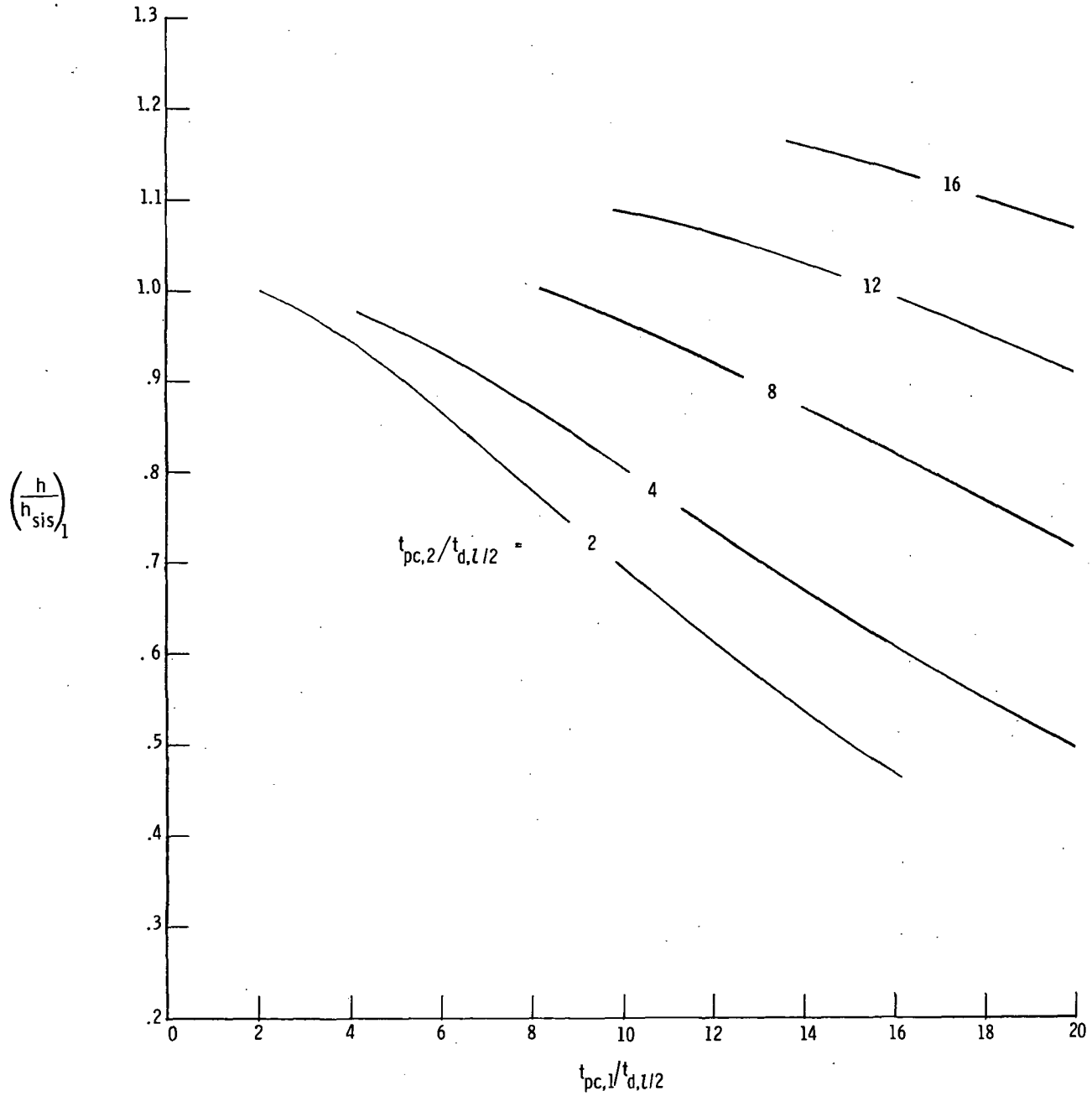

(f) $\bar{T}_1 = 0.45$; $\bar{T}_2 = 0.13$.

Figure 12.- Continued.

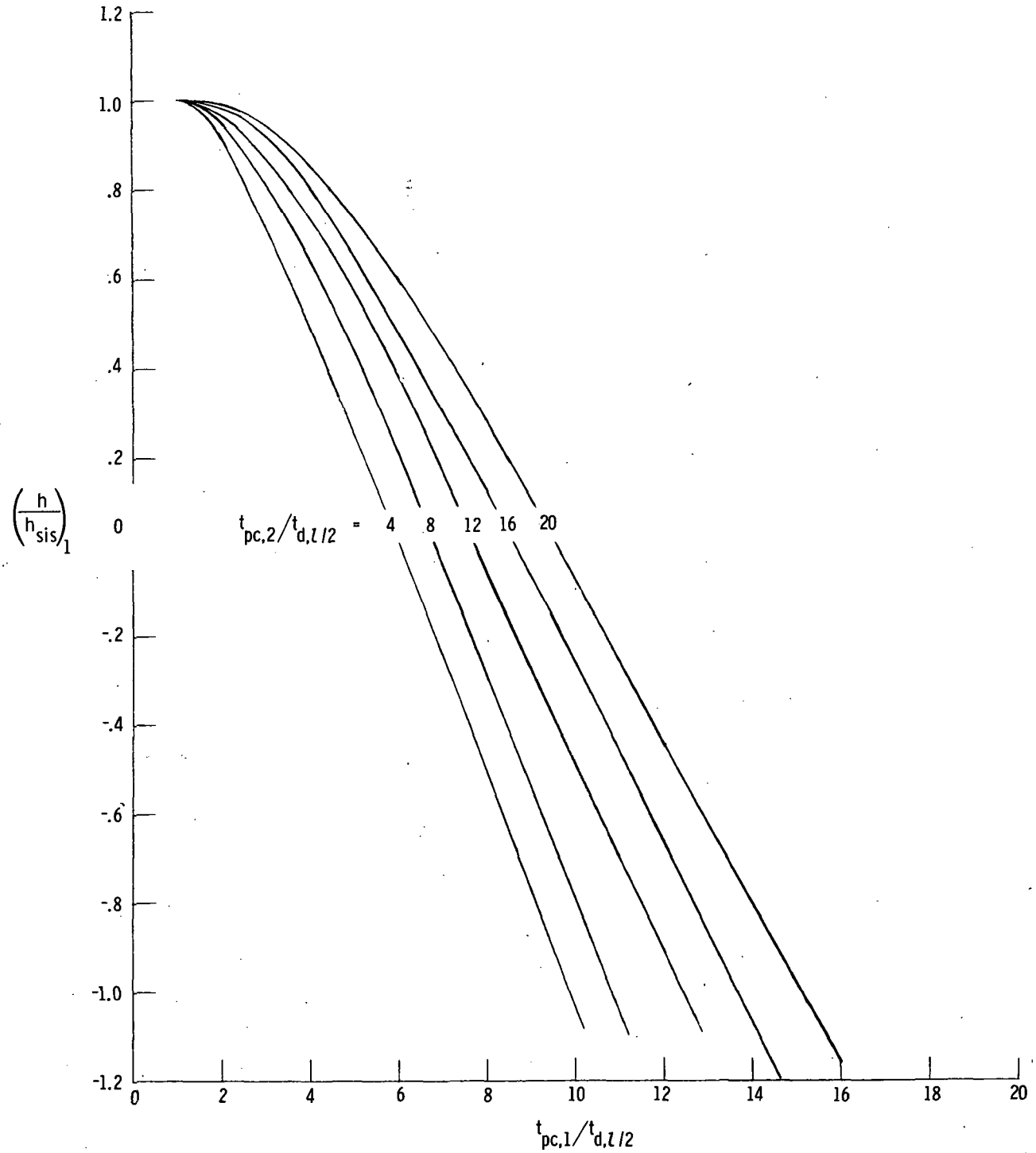

(g) $\bar{T}_1 = 0.13$; $\bar{T}_2 = 0.45$.

Figure 12.- Continued.

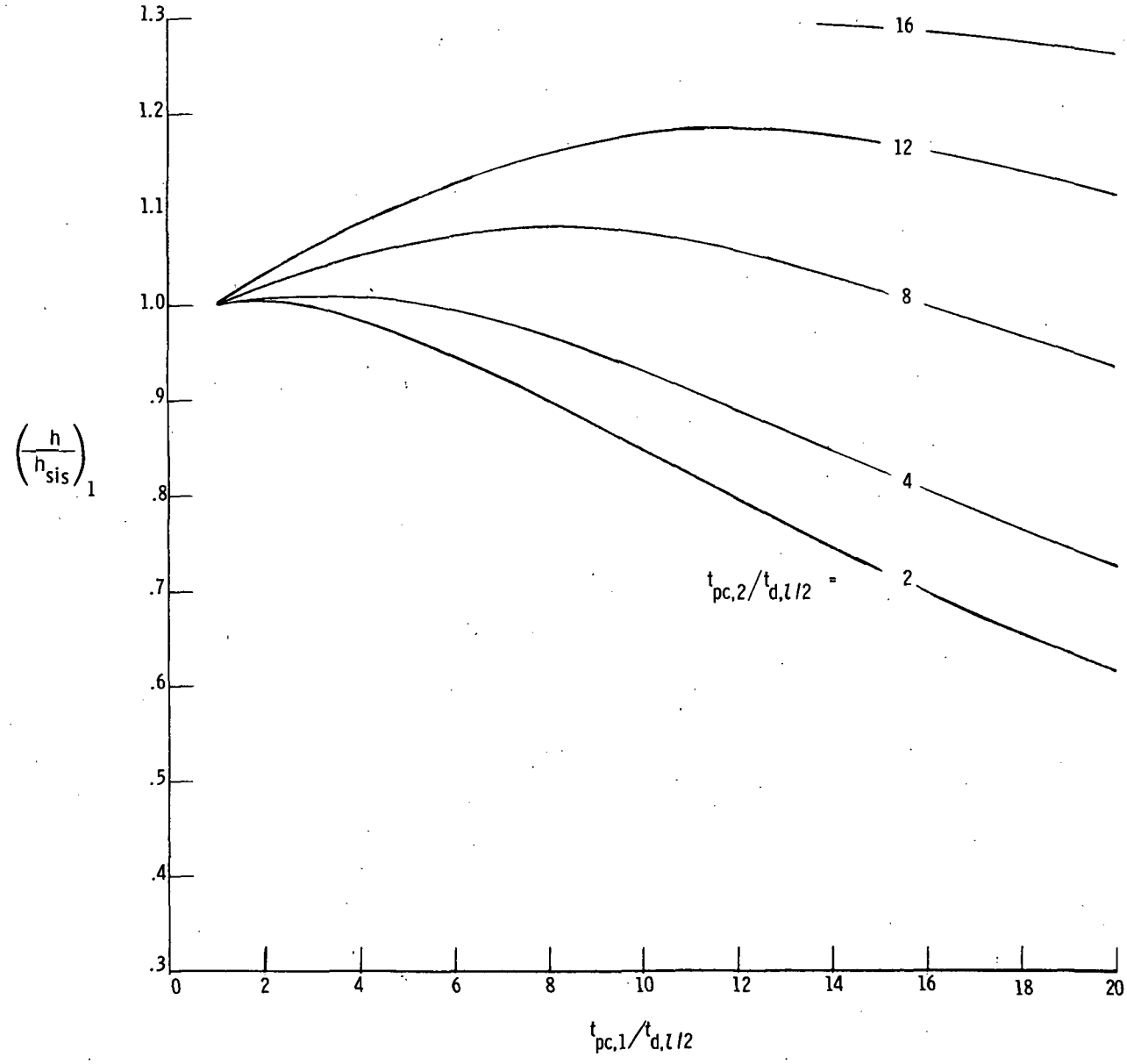

(h) $\bar{T}_1 = 0.45$; $\bar{T}_2 = 0.05$.

Figure 12.- Continued.

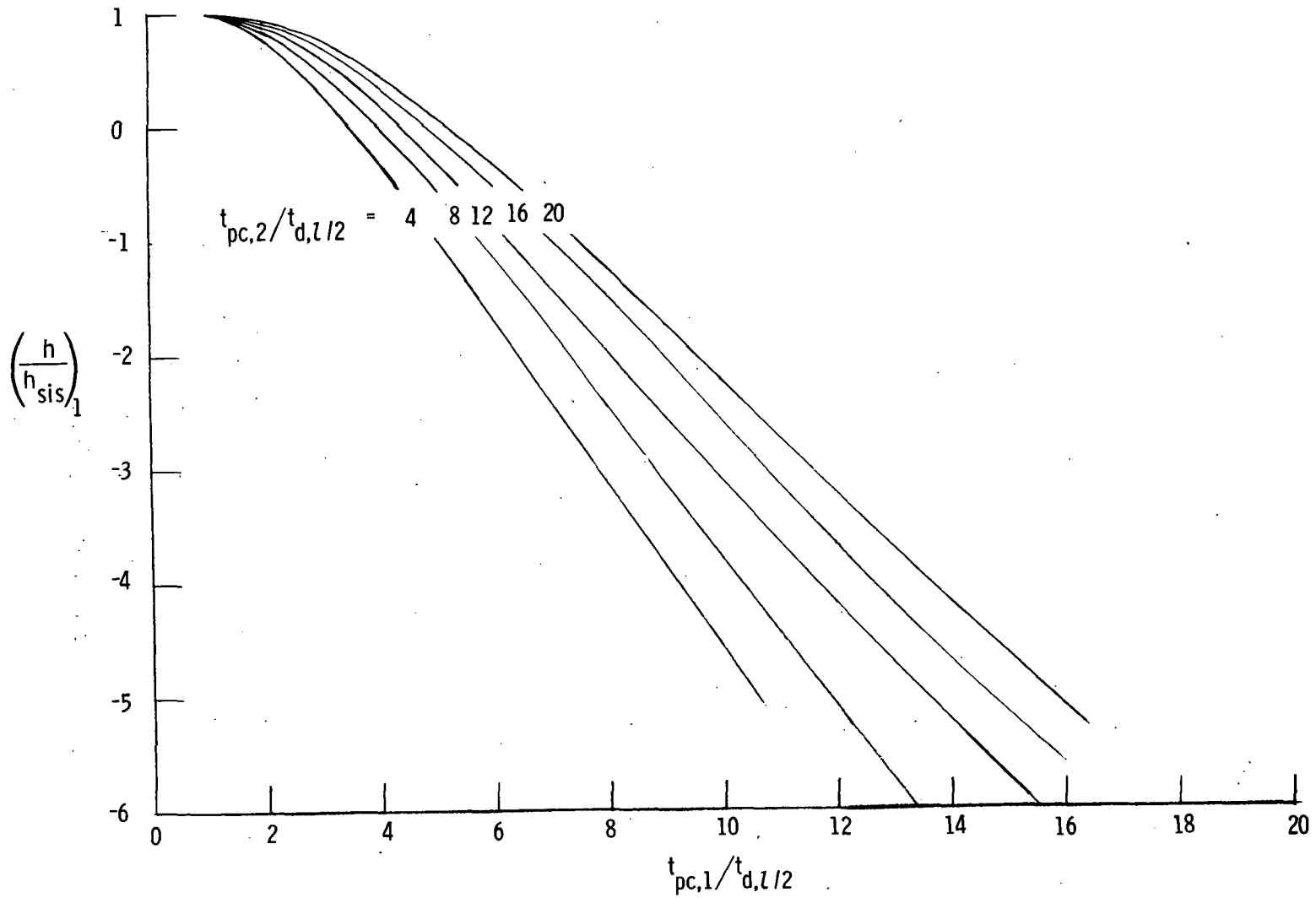

(i) $\bar{T}_1 = 0.05$; $\bar{T}_2 = 0.45$.

Figure 12.- Continued.

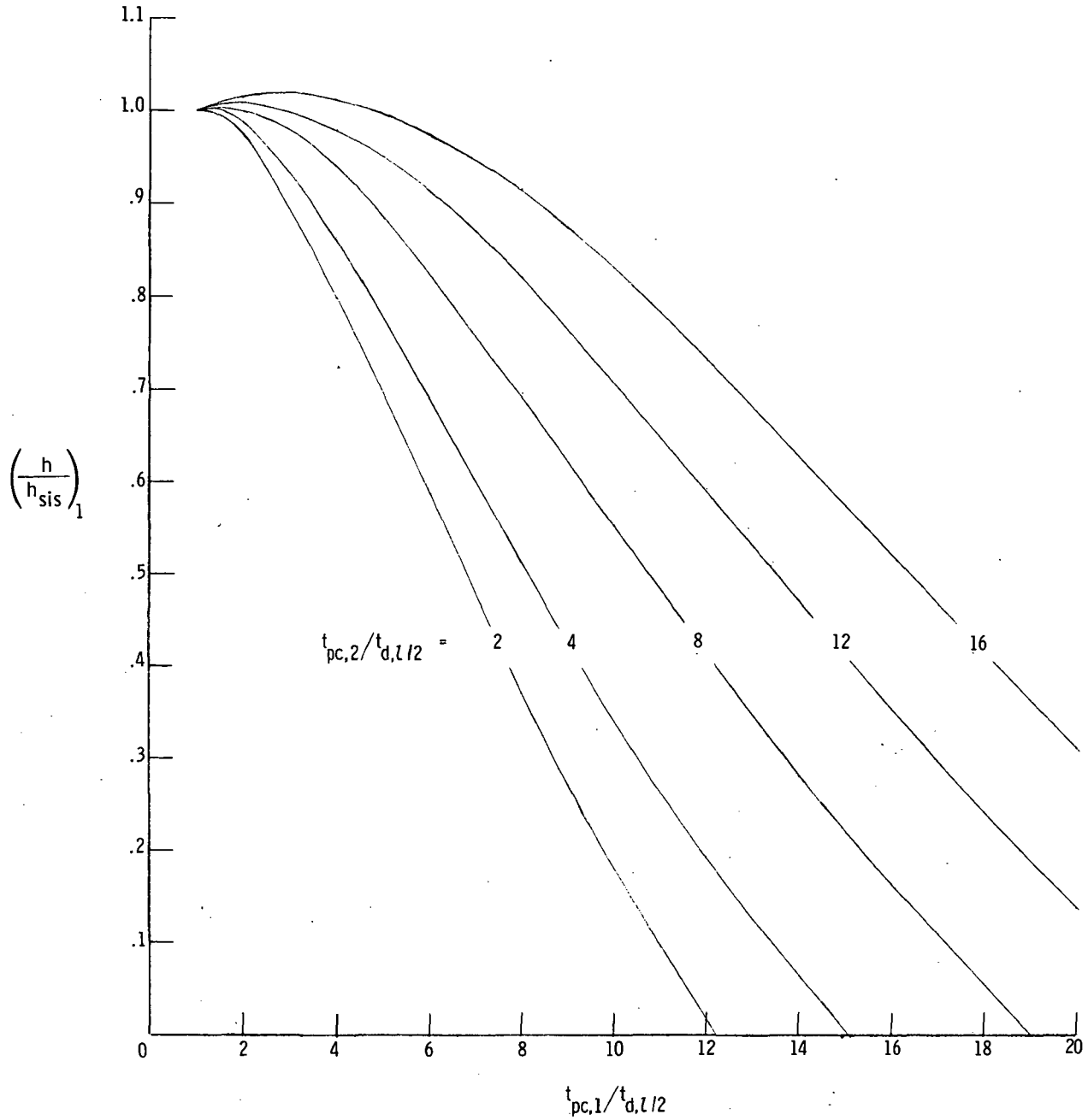

(j) $\bar{T}_1 = \bar{T}_2 = 0.35$.

Figure 12.- Continued.

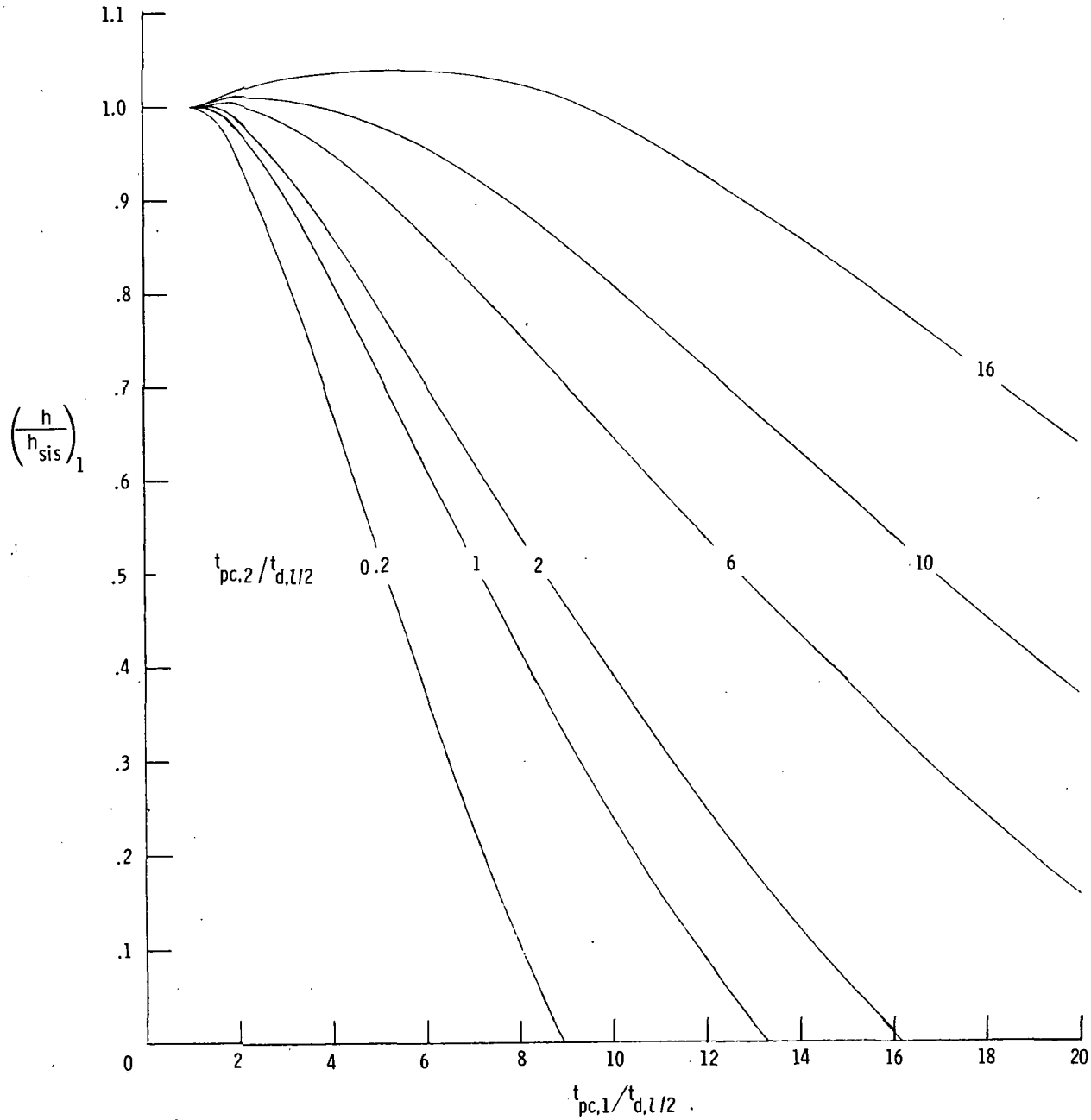

(k) $\bar{T}_1 = 0.35$; $\bar{T}_2 = 0.24$.

Figure 12.- Continued.

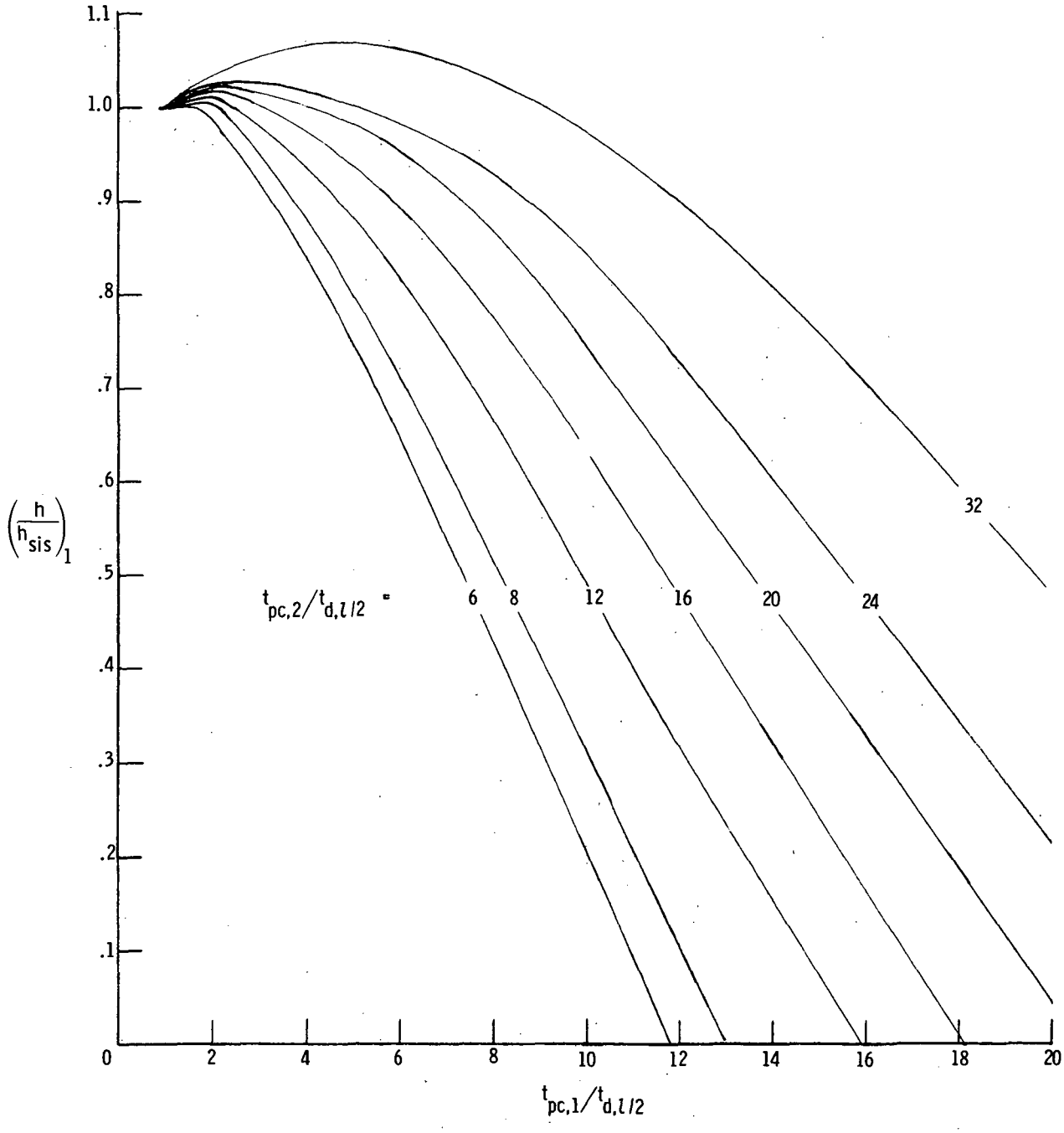

(l) $\bar{T}_1 = 0.24$; $\bar{T}_2 = 0.35$.

Figure 12.- Continued.

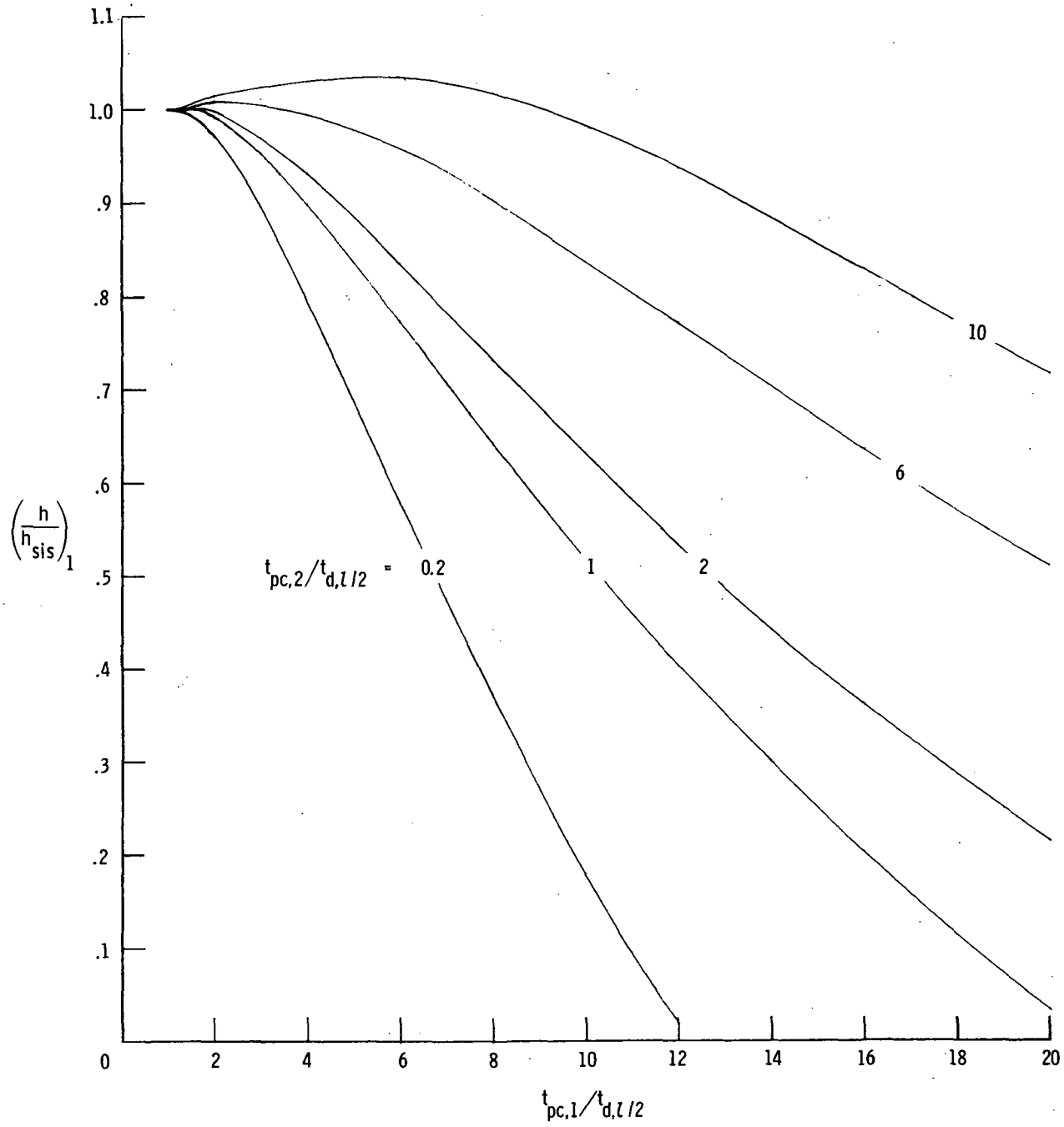

(m) $\bar{T}_1 = 0.35$; $\bar{T}_2 = 0.13$.

Figure 12.- Continued.

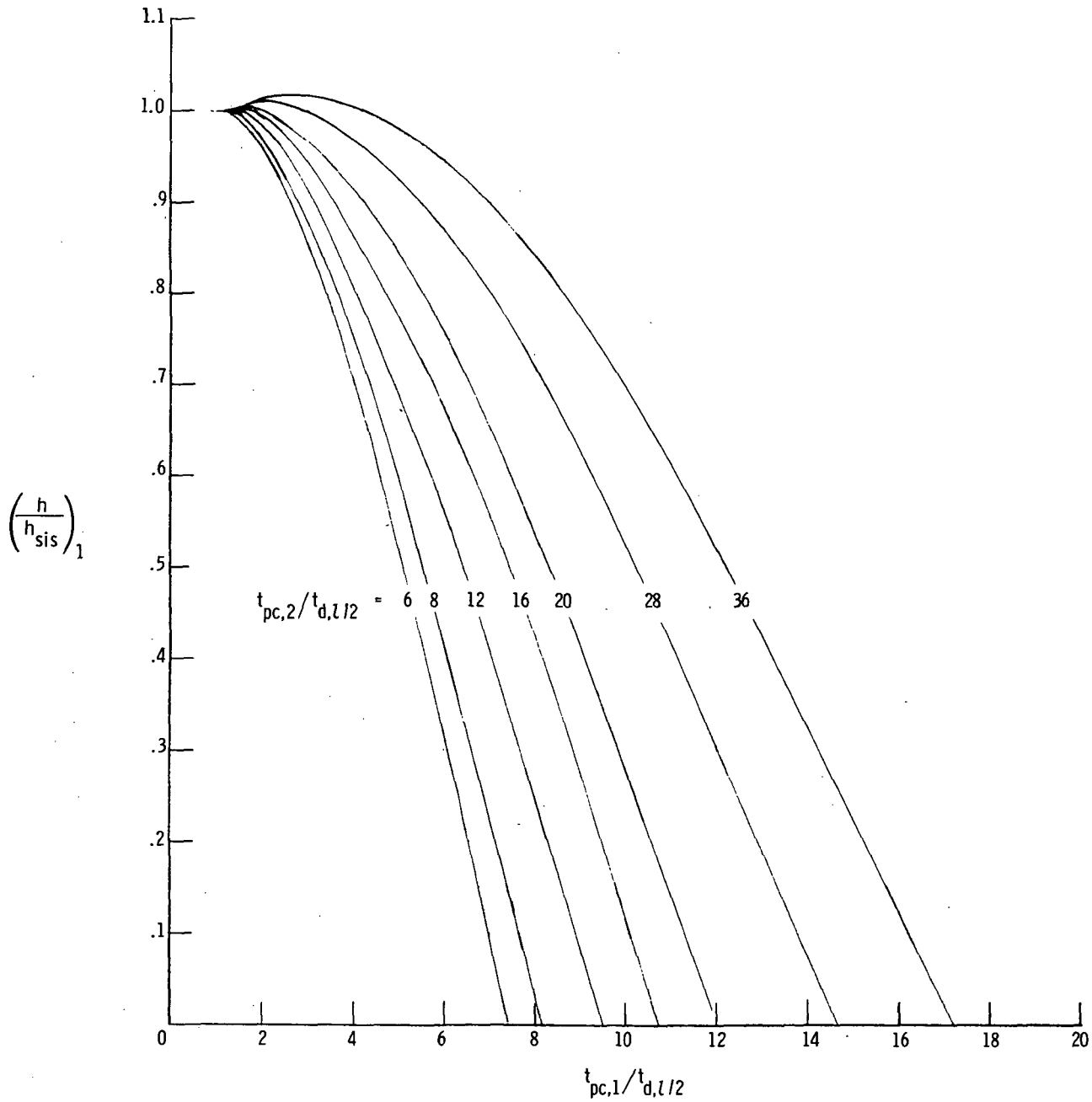

(n) $\bar{T}_1 = 0.13$; $\bar{T}_2 = 0.35$.

Figure 12.- Continued.

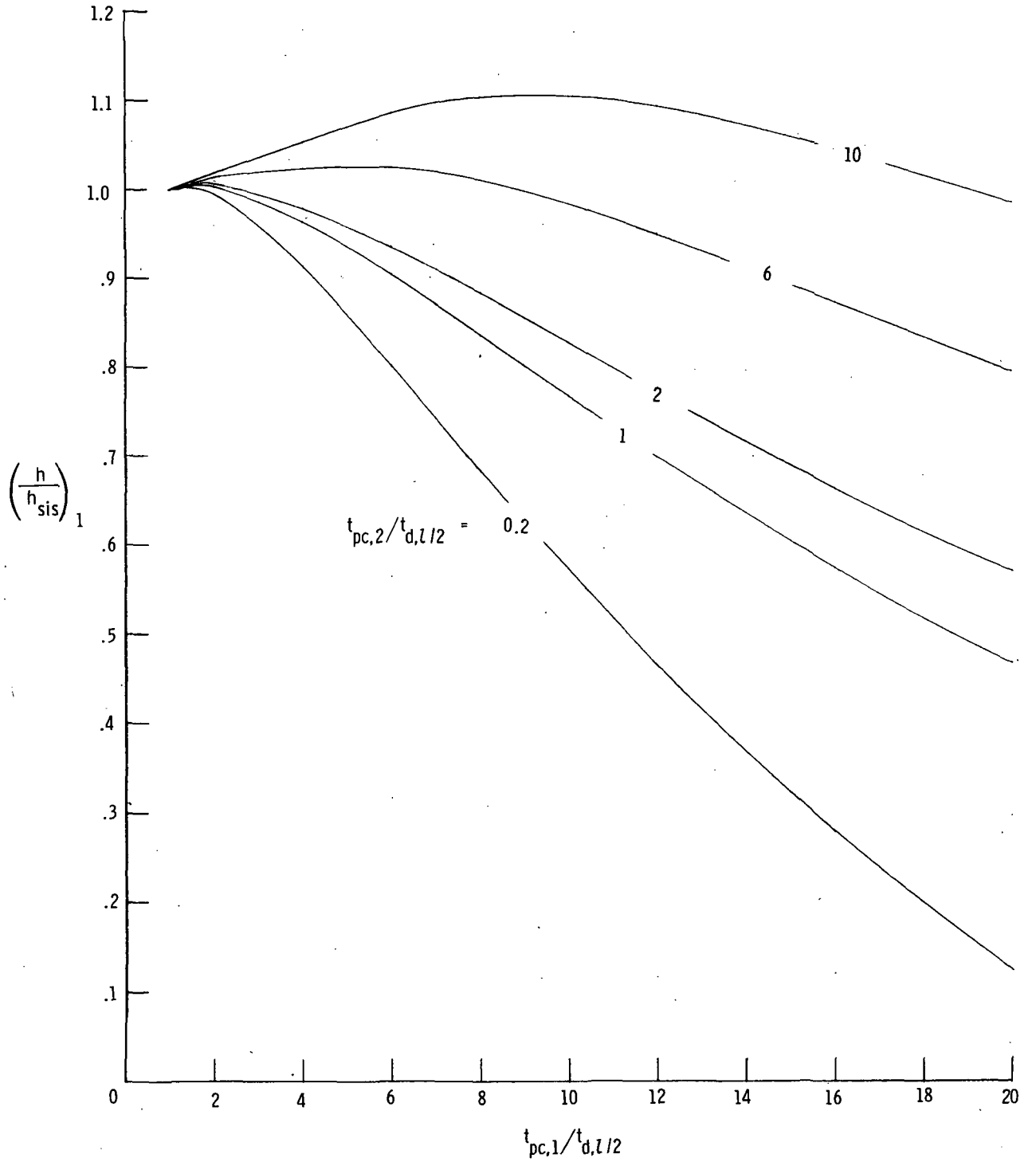

(o) $\bar{T}_1 = 0.35$; $\bar{T}_2 = 0.05$.

Figure 12.- Continued.

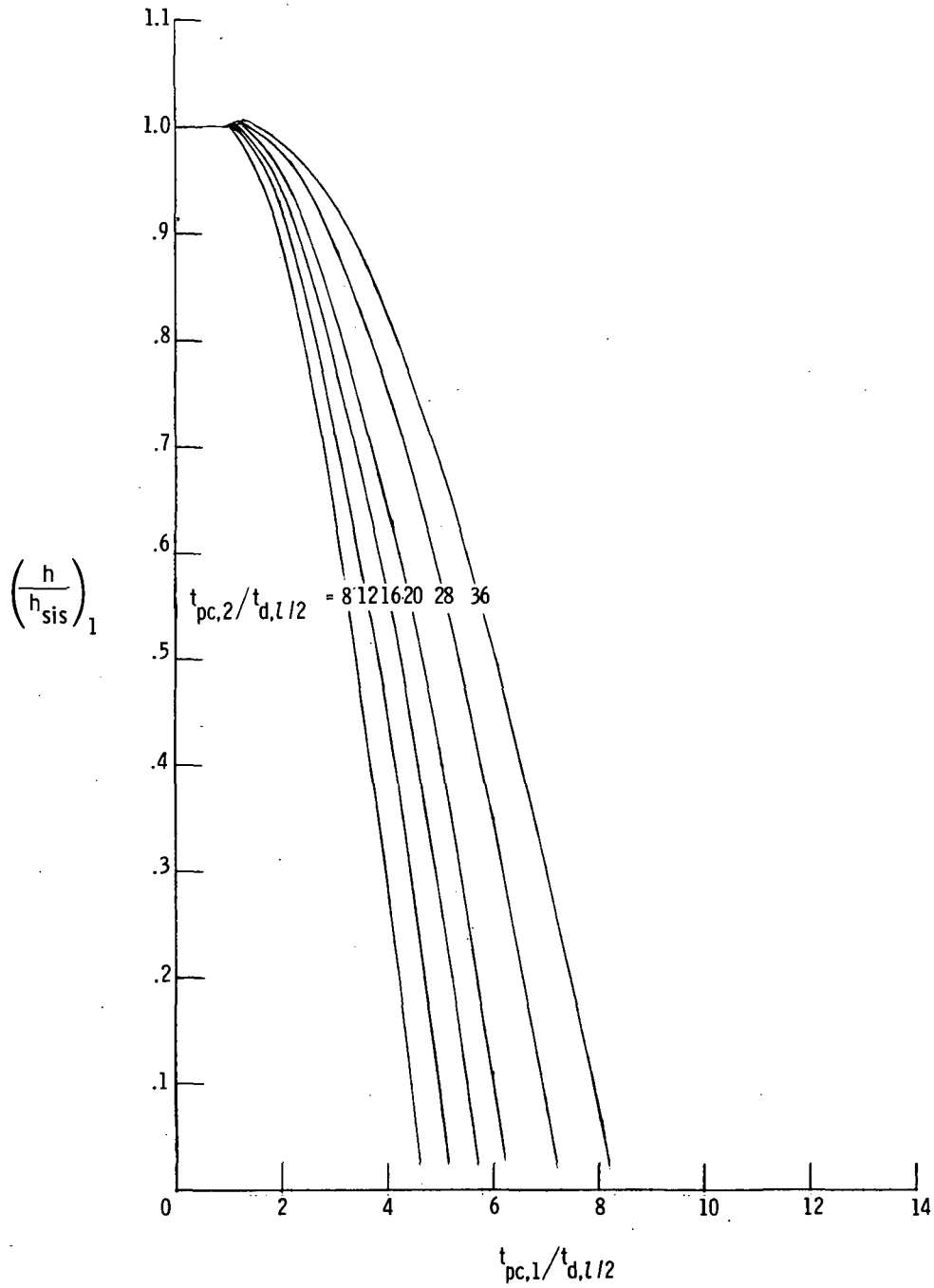

(p) $\bar{T}_1 = 0.05$; $\bar{T}_2 = 0.35$.

Figure 12.- Continued.

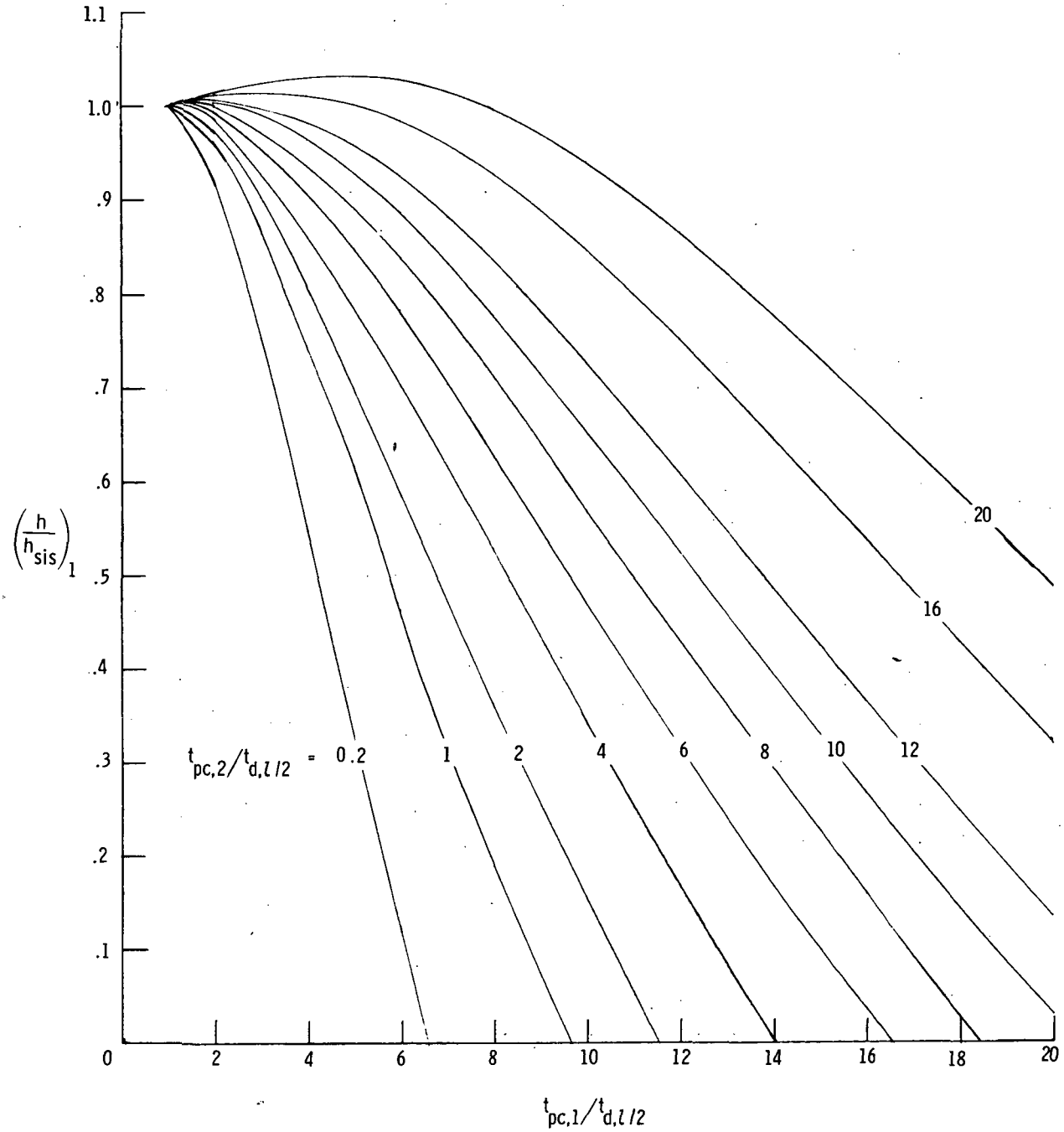

(q) $\bar{T}_1 = \bar{T}_2 = 0.24$.

Figure 12.- Continued.

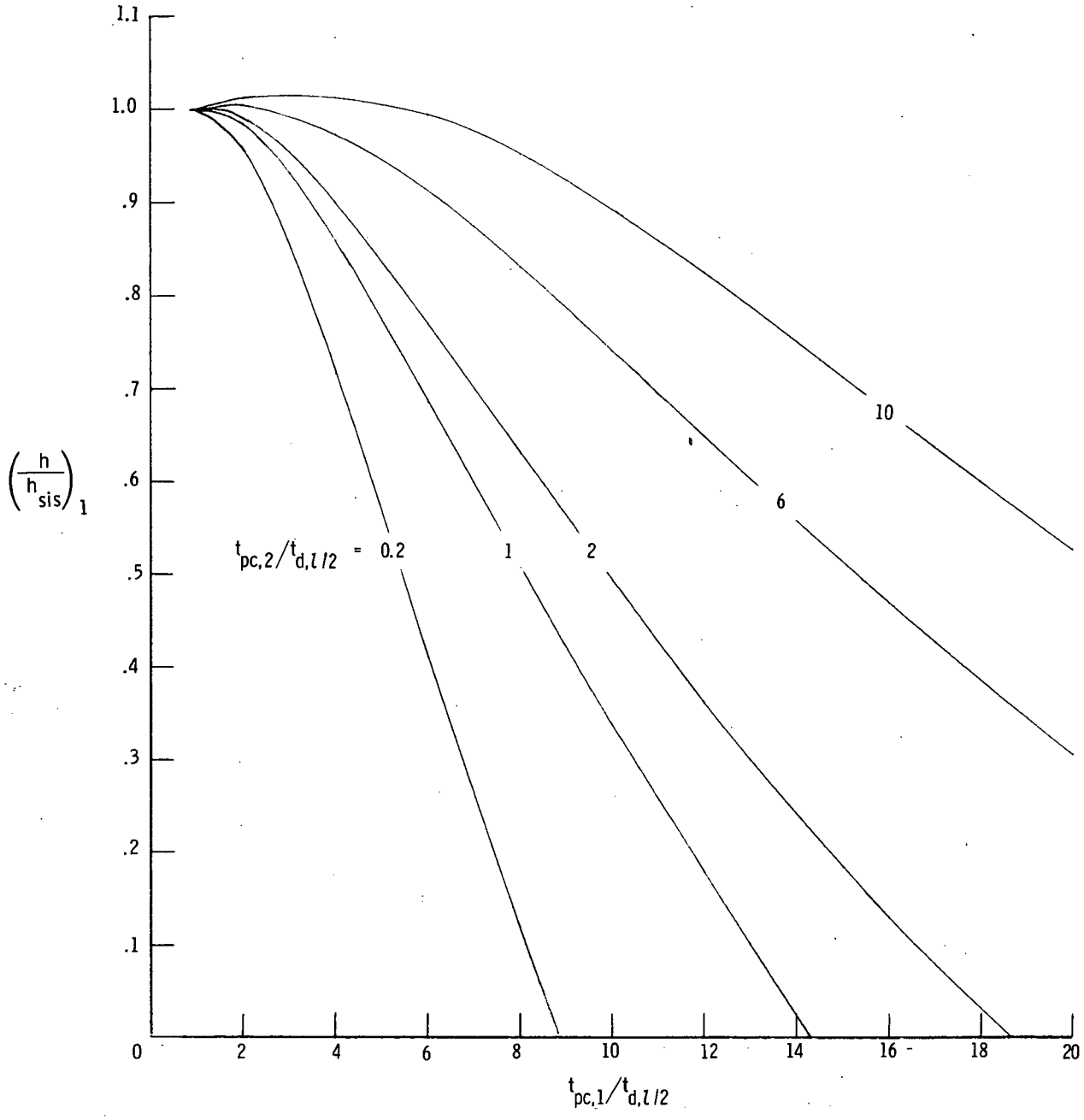

(r) $\bar{T}_1 = 0.24$; $\bar{T}_2 = 0.13$.

Figure 12.- Continued.

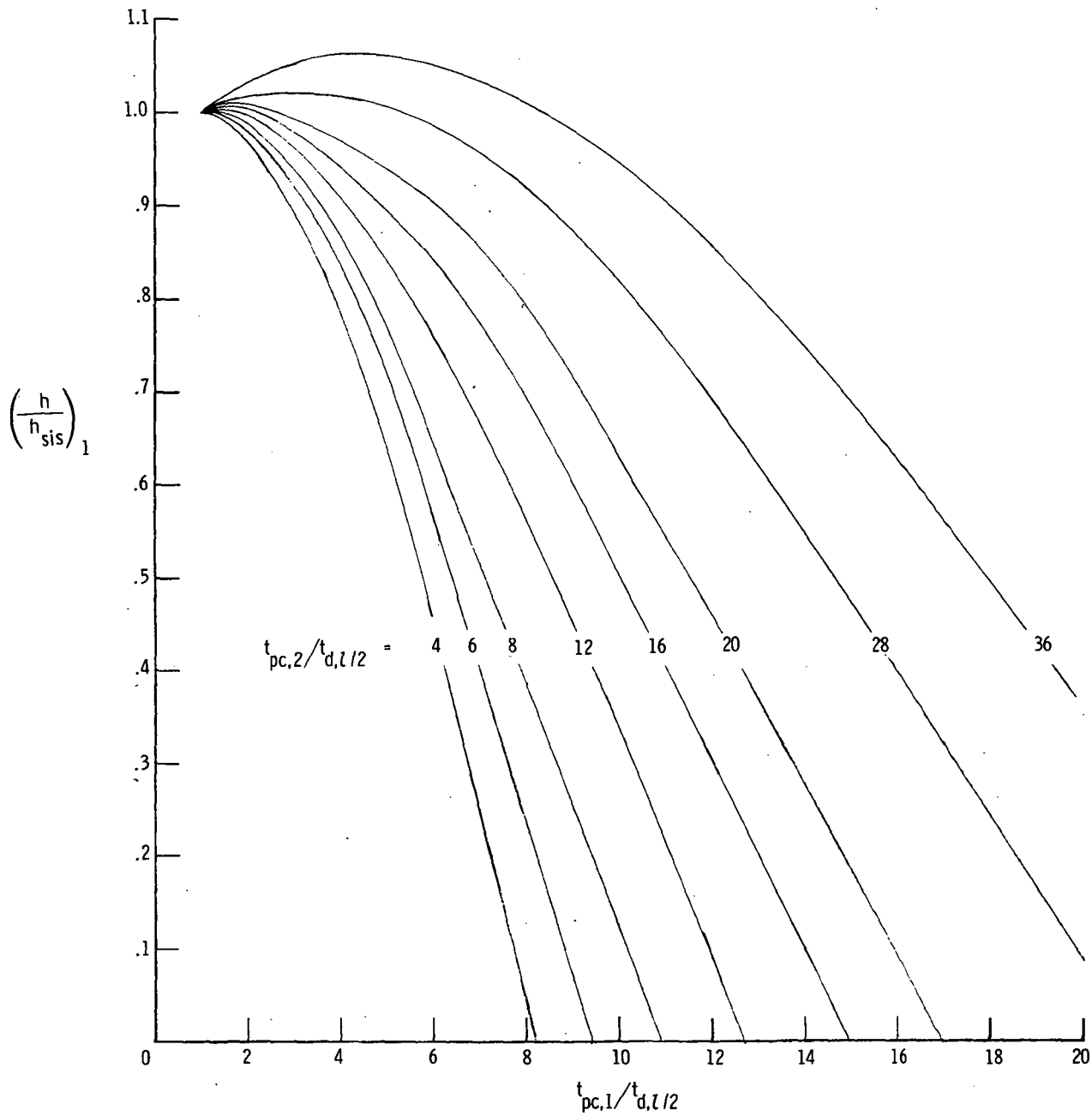

(s) $\bar{T}_1 = 0.13$; $\bar{T}_2 = 0.24$.

Figure 12.- Continued.

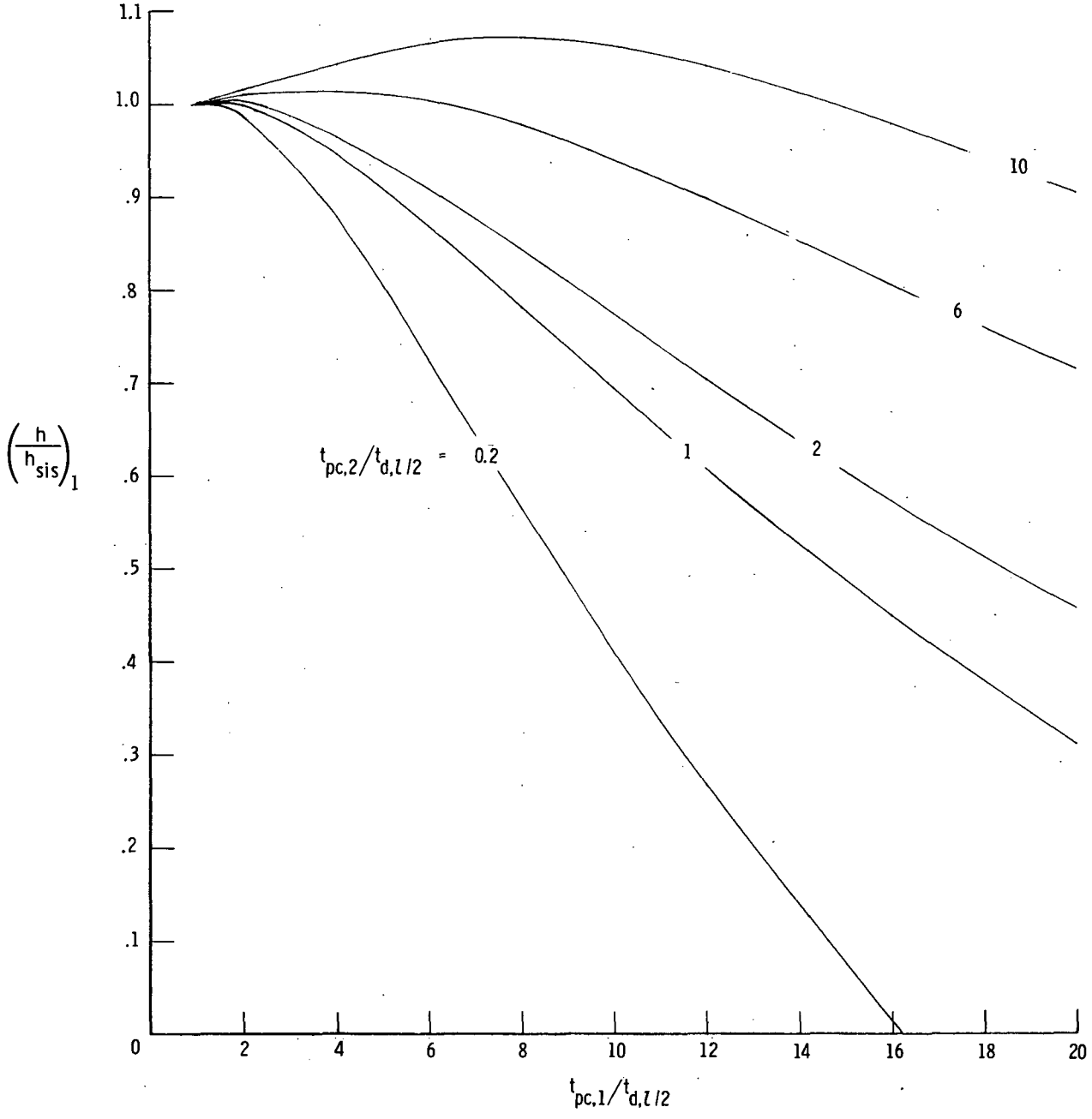

(t) $\bar{T}_1 = 0.24$; $\bar{T}_2 = 0.05$.

Figure 12.- Continued.

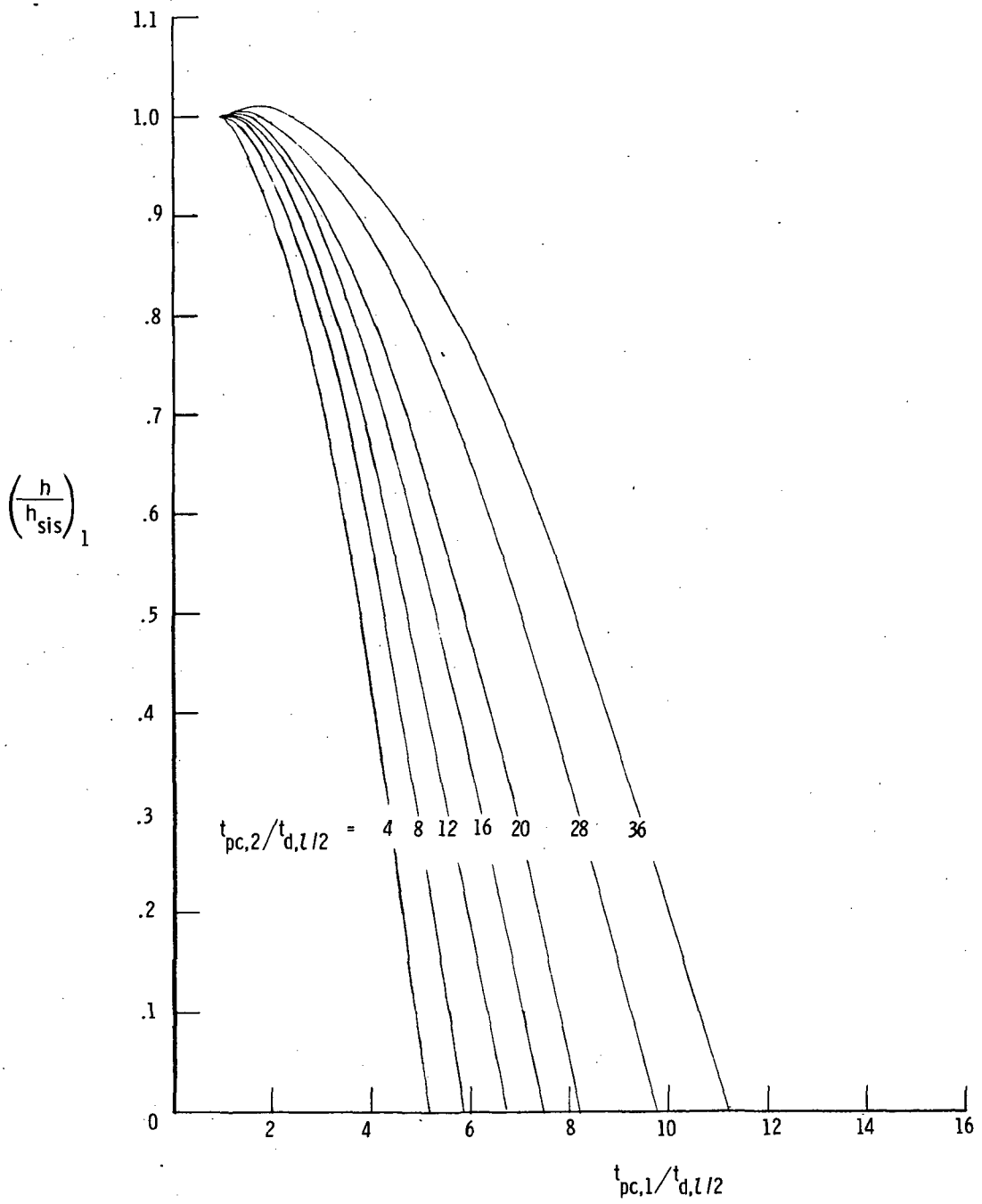

(u) $\bar{T}_1 = 0.05$; $\bar{T}_2 = 0.24$.

Figure 12.- Continued.

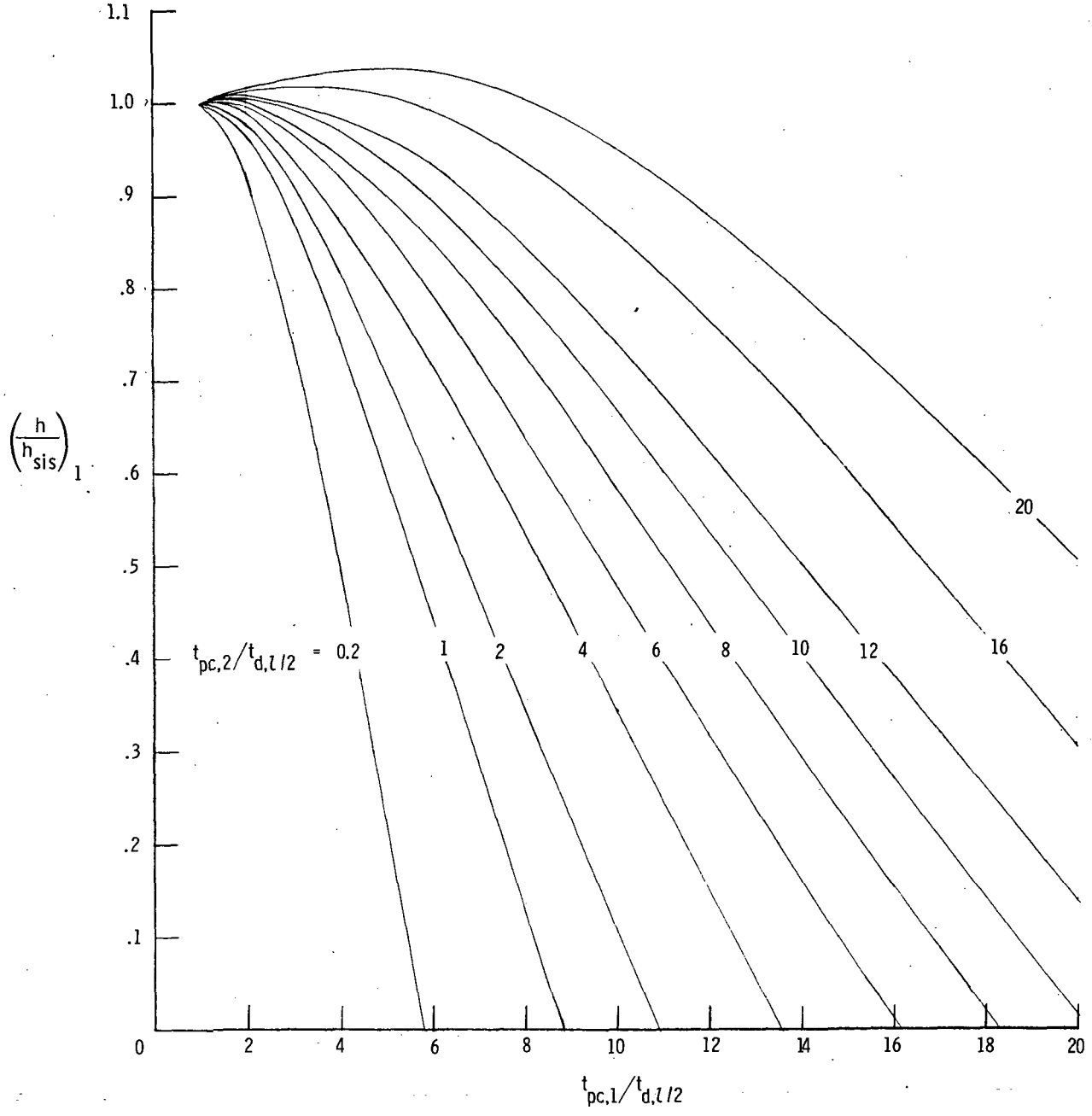

(v) $\bar{T}_1 = \bar{T}_2 = 0.13$.

Figure 12.- Continued.

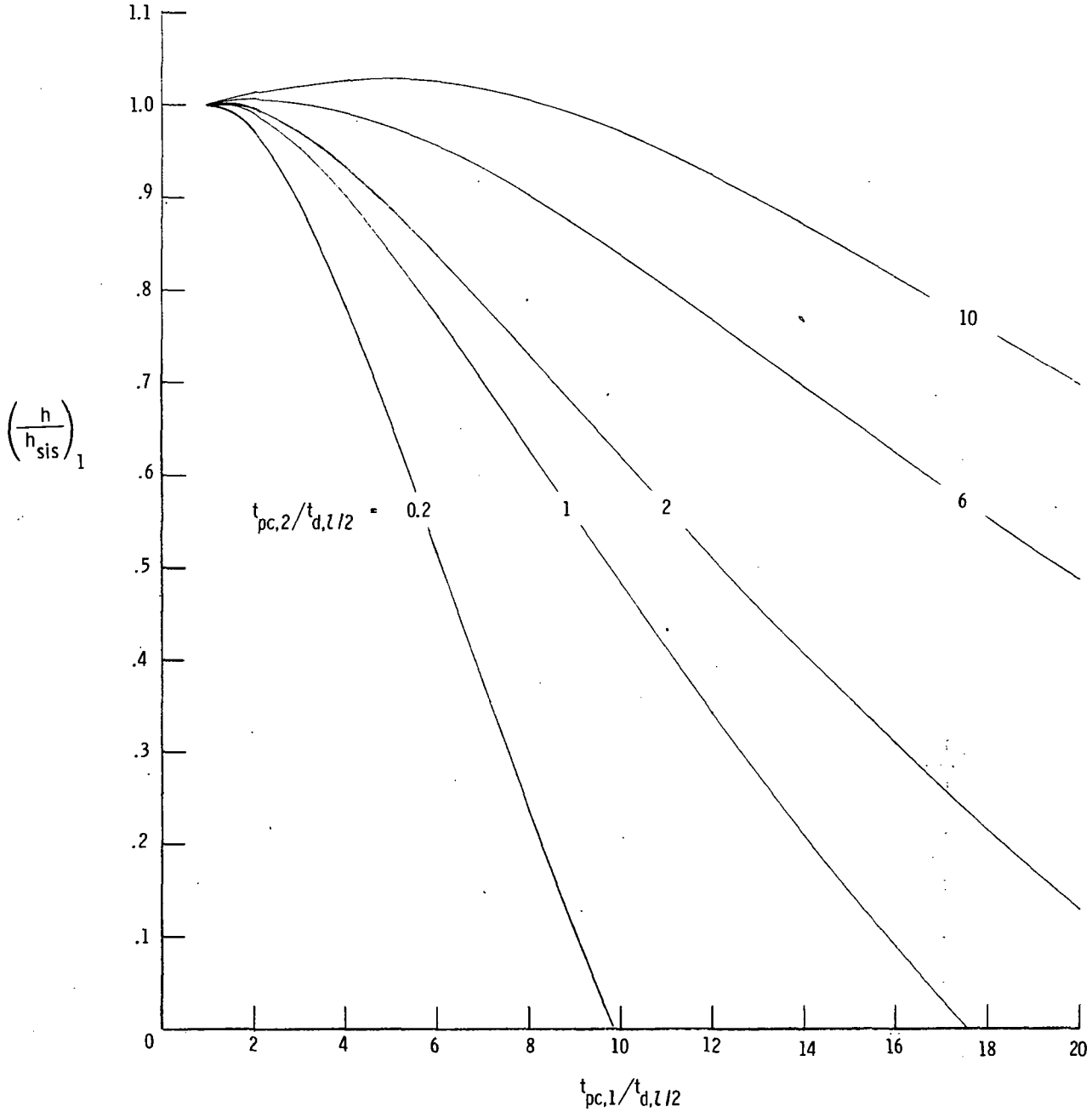

(w) $\bar{T}_1 = 0.13$; $\bar{T}_2 = 0.05$.

Figure 12.- Continued.

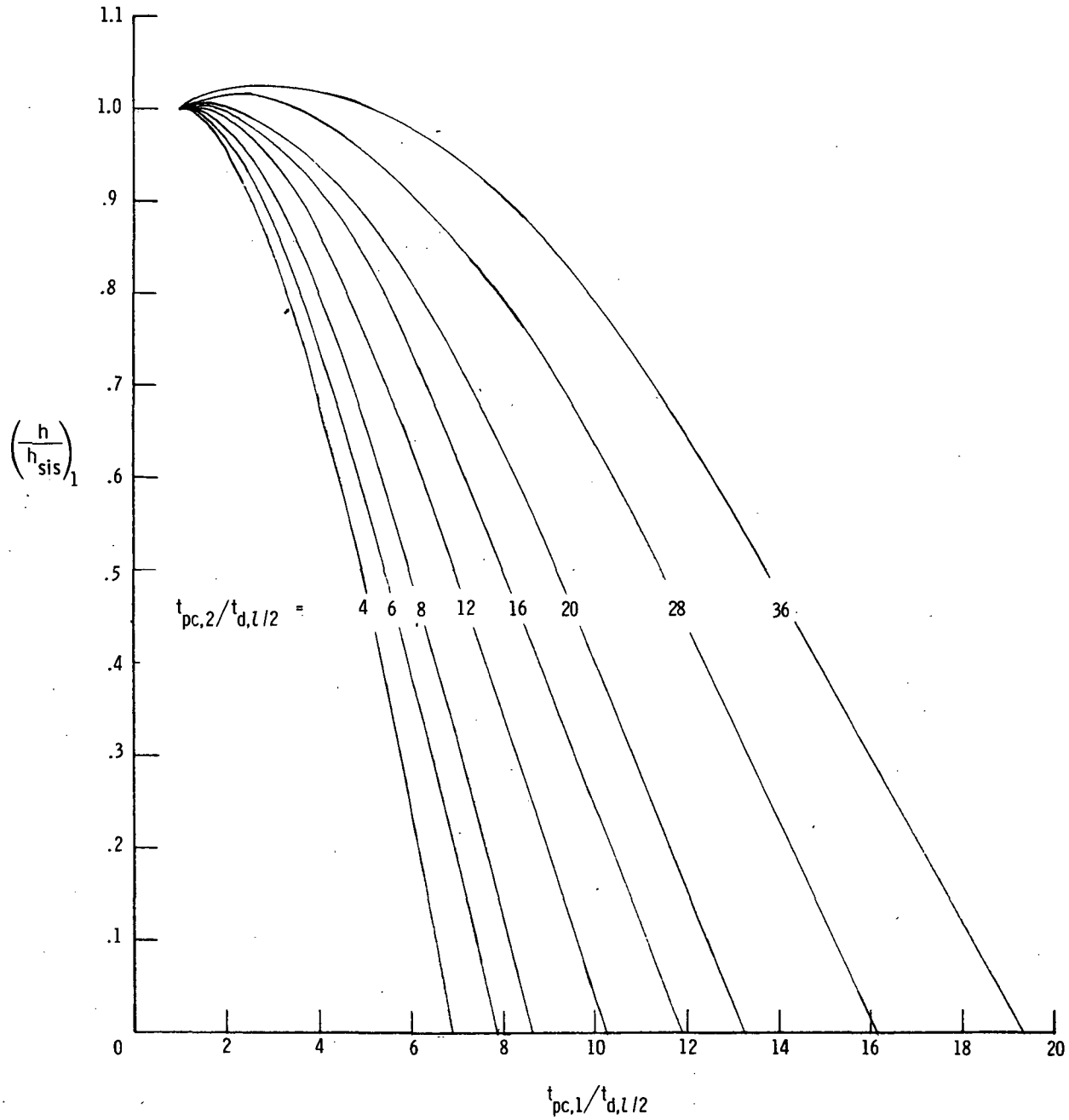

(x) $\bar{T}_1 = 0.05$; $\bar{T}_2 = 0.13$.

Figure 12.- Continued.

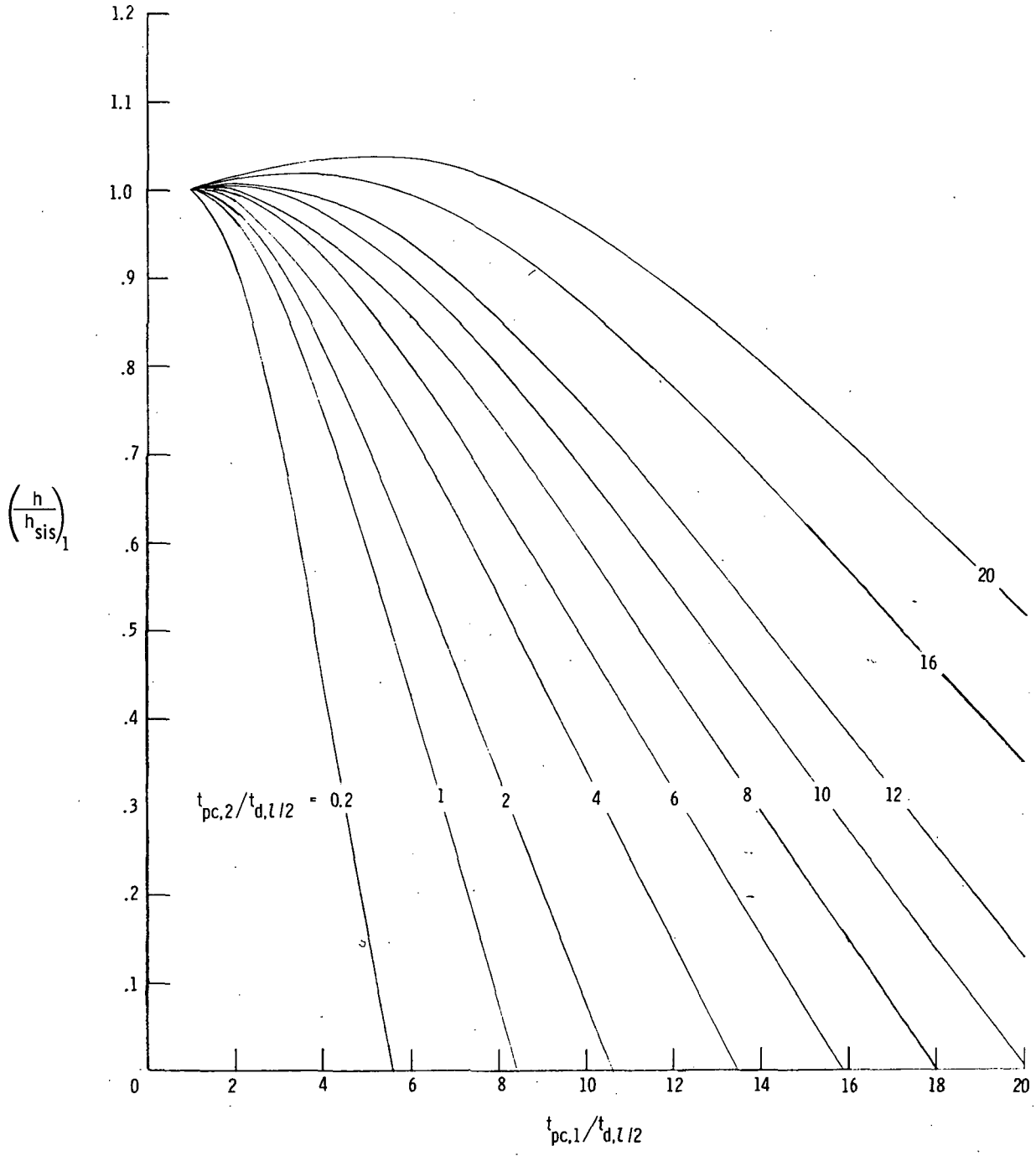

(y) $\bar{T}_1 = \bar{T}_2 = 0.05$.

Figure 12.- Concluded.

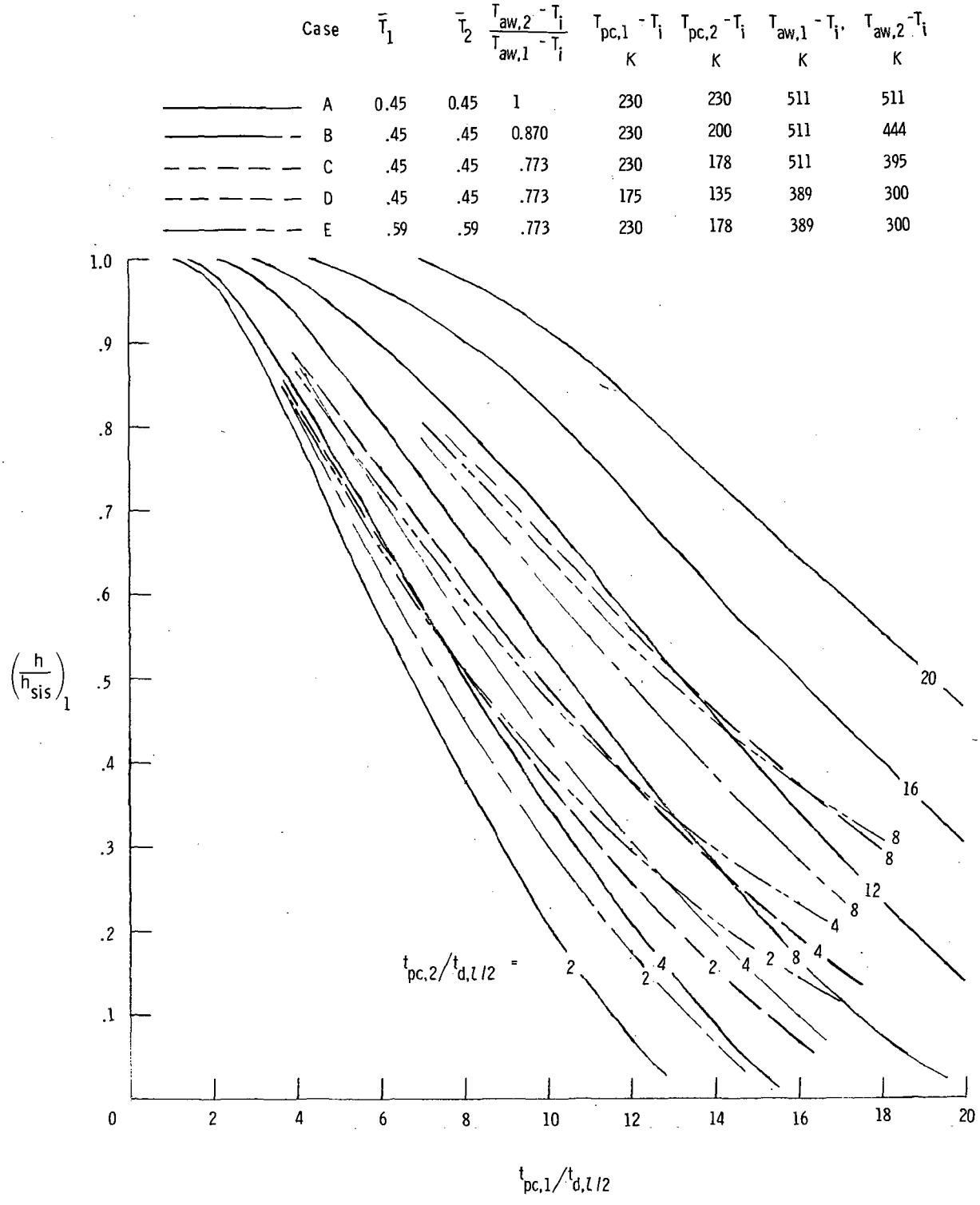

Figure 13.- Heat-transfer-coefficient correction factor for finite slab with phase change on both sides showing variations of restraints.

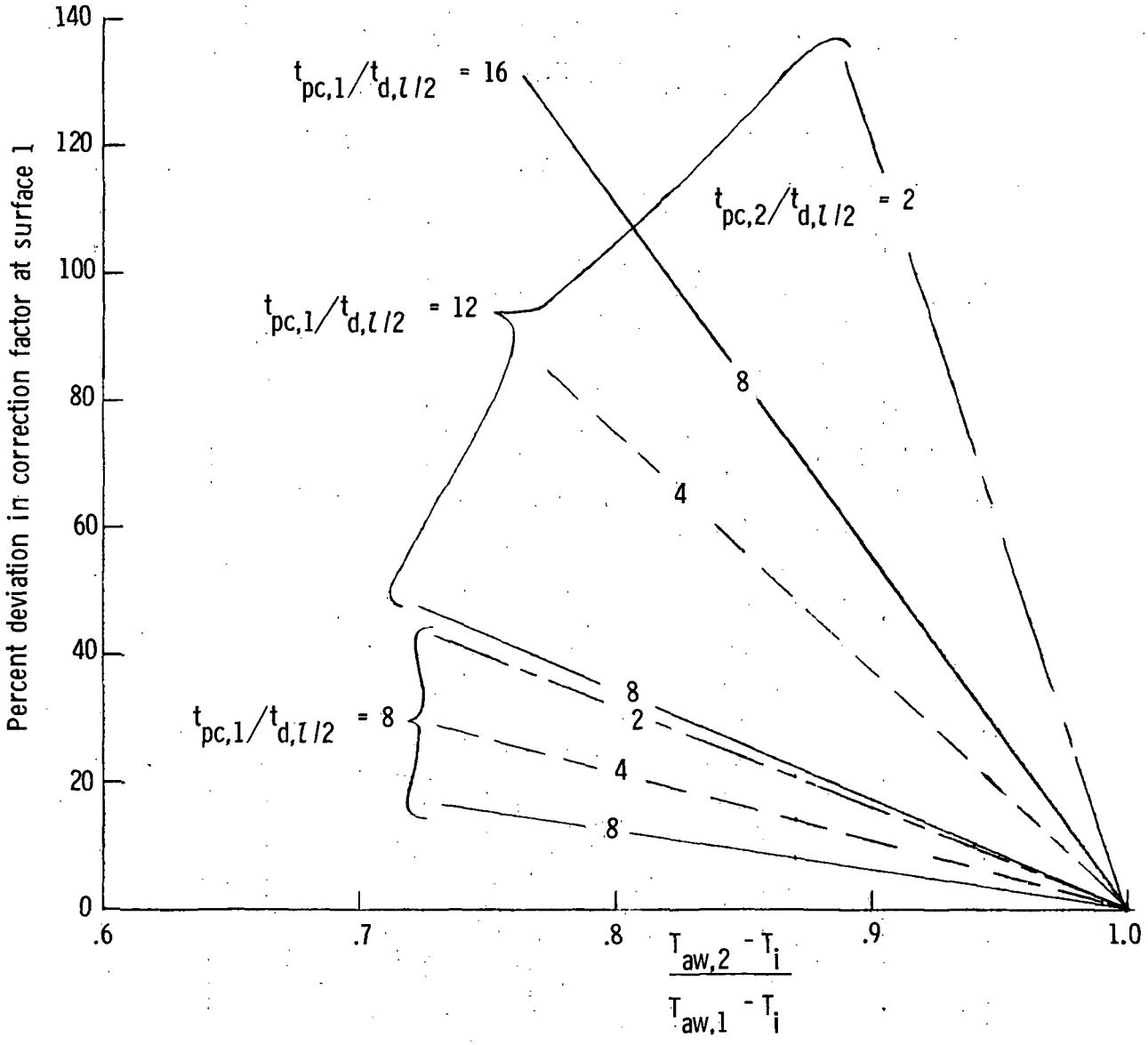

Figure 14.- Percent deviation in correction factor as initial temperature potential ratio is increased to 1. $\bar{T}_1 = \bar{T}_2 = 0.45$.

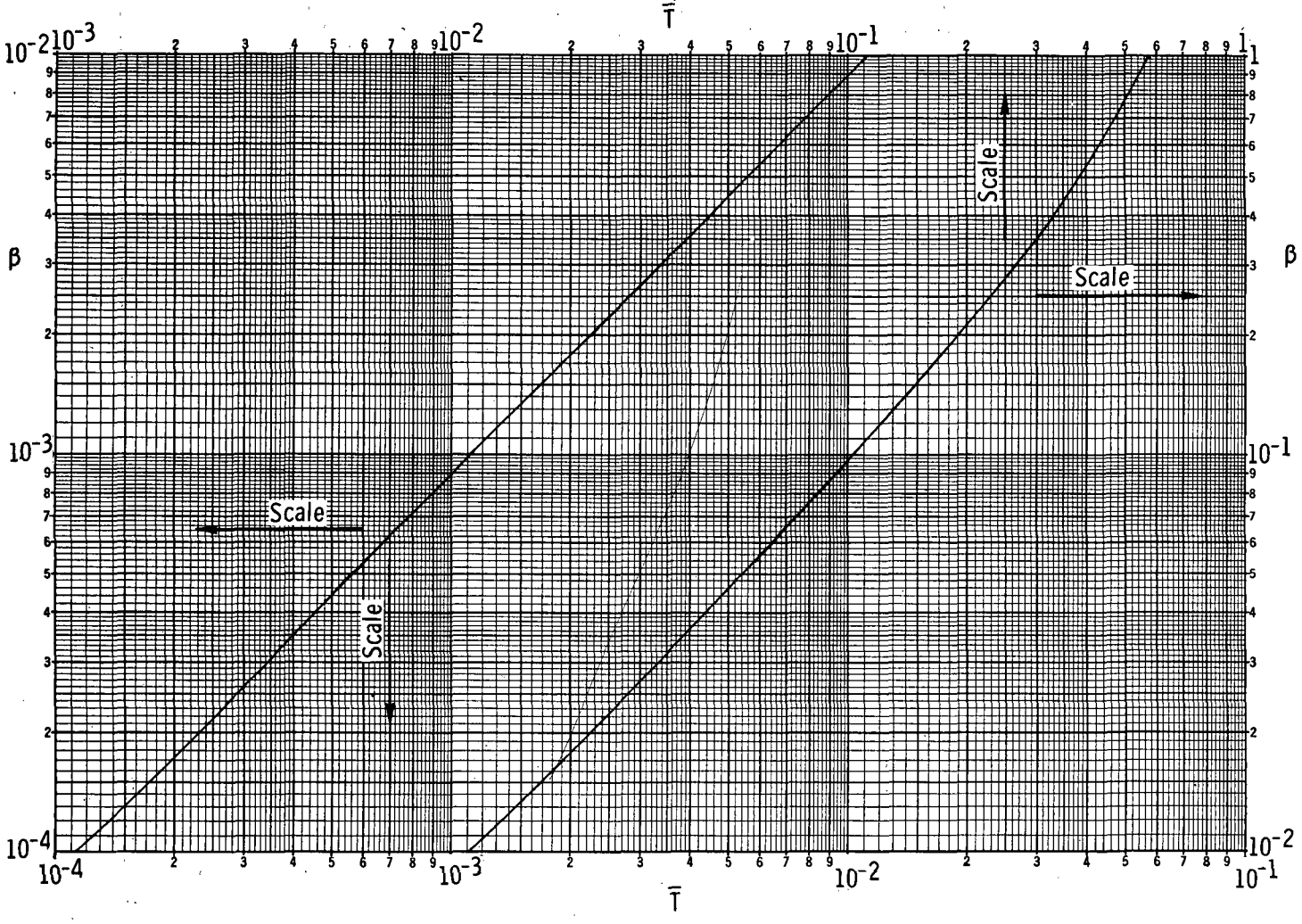

Figure 15.- Solution of heat-conduction equations (plot of eq. (B5)).

NATIONAL AERONAUTICS AND SPACE ADMINISTRATION
WASHINGTON, D.C. 20546

OFFICIAL BUSINESS
PENALTY FOR PRIVATE USE $300

SPECIAL FOURTH-CLASS RATE
BOOK

POSTAGE AND FEES PAID
NATIONAL AERONAUTICS AND
SPACE ADMINISTRATION
451

U.S.MAIL

POSTMASTER: If Undeliverable (Section 158 Postal Manual) Do Not Return

"The aeronautical and space activities of the United States shall be conducted so as to contribute . . . to the expansion of human knowledge of phenomena in the atmosphere and space. The Administration shall provide for the widest practicable and appropriate dissemination of information concerning its activities and the results thereof."

—NATIONAL AERONAUTICS AND SPACE ACT OF 1958

NASA SCIENTIFIC AND TECHNICAL PUBLICATIONS

TECHNICAL REPORTS: Scientific and technical information considered important, complete, and a lasting contribution to existing knowledge.

TECHNICAL NOTES: Information less broad in scope but nevertheless of importance as a contribution to existing knowledge.

TECHNICAL MEMORANDUMS: Information receiving limited distribution because of preliminary data, security classification, or other reasons. Also includes conference proceedings with either limited or unlimited distribution.

CONTRACTOR REPORTS: Scientific and technical information generated under a NASA contract or grant and considered an important contribution to existing knowledge.

TECHNICAL TRANSLATIONS: Information published in a foreign language considered to merit NASA distribution in English.

SPECIAL PUBLICATIONS: Information derived from or of value to NASA activities. Publications include final reports of major projects, monographs, data compilations, handbooks, sourcebooks, and special bibliographies.

TECHNOLOGY UTILIZATION PUBLICATIONS: Information on technology used by NASA that may be of particular interest in commercial and other non-aerospace applications. Publications include Tech Briefs, Technology Utilization Reports and Technology Surveys.

Details on the availability of these publications may be obtained from:

SCIENTIFIC AND TECHNICAL INFORMATION OFFICE

NATIONAL AERONAUTICS AND SPACE ADMINISTRATION

Washington, D.C. 20546